Expression of the mouse odorant receptor genes *Olfr1507*, *Olfr1508*, and *Olfr1509* in gene-targeted strains

Inaugural dissertation

Zur Erlangung des Grades
Doktor der Naturwissenschaften
Dr. rer. nat.
Des Fachbereiches Biologie und Chemie
Der Justus-Liebig-Universität Giessen

Vorgelegt von
Paola Luz Eréndida Segoviano Arias
Frankfurt am Main, 2024

Die vorliegende Arbeit wurde an der Max-Planck-Forschungsstelle für Neurogenetik in der Zeit von 02.2019 bis 04.2024 unter der Leitung von Peter Mombaerts, M.D., Ph.D. durchgeführt.

Erstgutachter: Peter Mombaerts, M.D., Ph.D.
Max Planck Research Unit for Neurogenetics
Max-von-Laue-Straße 4
60438 Frankfurt am Main

Zweitgutachterin: Mona Khan, Ph.D.
Max Planck Research Unit for Neurogenetics
Max-von-Laue-Straße 4
60438 Frankfurt am Main

Drittgutachter: Prof. Dr. Ivan Manzini
Institut für Tierphysiologie, FB 08
Justus-Liebig-Universität
Heinrich-Buff-Ring 38
35392 Giessen

Certificate of originality

I declare that I have completed this dissertation single-handedly without the unauthorized help of a second party and only with the assistance acknowledged therein. I have appropriately acknowledged and cited all text passages that are derived verbatim from or are based on the content of published work of others, and all information relating to verbal communications. I consent to the use of an anti-plagiarism software to check my thesis. I have abided by the principles of good scientific conduct laid down in the charter of the Justus Liebig University Giessen „Satzung der Justus-Liebig-Universität Gießen zur Sicherung guter wissenschaftlicher Praxis“ in carrying out the investigations described in the dissertation.

Frankfurt am Main, _____

Manuscripts don't burn

Mikhail Bulgakov

Acknowledgements

I would like to express my sincere gratitude to Peter Mombaerts for providing me with the opportunity to work on this fascinating olfaction project and for granting me the freedom and flexibility to conduct research throughout the years in my Ph.D. project.

I wish to extend my appreciation to Mona Khan for being an excellent mentor in terms of quality and an amazing supervisor, proving me with valuable guidance throughout my Ph.D. project.

I am grateful to Ivan Manzini for accepting me as his student at the JLU and for his supervision throughout my Ph.D. project.

I would like to extend special thanks to my parents for their 30 years of dedication, support and presence.

A part of this work was also motivated by my grandma, who encouraged me spiritually to persevere and achieve this goal.

I am grateful to Pompon, my furry companion for the last eight years, who gave me emotional support on this journey.

I would like to express my gratitude to Florian Lindenblatt for his assistance in navigating the German bureaucratic system as a newcomer to the country.

I would like to express my sincere appreciation to all of the individuals who have played a role in my Ph.D. journey for their companionship and support.

Lastly, my deepest gratitude goes to Radzabs, who accompanied me through the everyday challenges of Ph.D. life. Despite the uncertainties of this path, his support and encouragement have been instrumental in bringing me to where I am today.

List of abbreviations

Abbreviation	Full name
AC	adenylyl cyclase
AOB	accessory olfactory bulb
ATP	adenosine triphosphate
bp	base pairs
CNGC	cyclic nucleotide-gated-ion channel
DNA	deoxyribonucleic acid
EDTA	ethylenediaminetetraacetic acid
EPL	external plexiform layer
ES	embryonic stem
gap	growth associated protein
GCL	granule cell layer
GFP	green fluorescent protein
GG	Grueneberg ganglion
GL	glomerular layer
GPCR	G-protein-coupled receptor
IHC	immunohistochemistry
IPL	internal plexiform layer
IRES	internal ribosome entry site
ISH	*in situ* hybridization
kb	kilobase
lacZ	ß-galactosidase
MCL	mitral cell layer
MOE	main olfactory epithelium
NQO1	NAD(P)H quinone dehydrogenase
OMP	olfactory marker protein
ON	olfactory nerve
ONL	olfactory nerve layer
OR	odorant receptor
OB	olfactory bulb
OCAM	olfactory cell adhesion molecule
OSN	olfactory sensory neuron

PBS	phosphate buffer saline
PCR	polymerase chain reaction
PD	postnatal day
PFA	paraformaldehyde
PGC	periglomerular cell
RFP	red fluorescent protein
RNA	ribonucleic acid
SO	septal organ
TCR	T-cell antigen receptor locus
TGV	total glomerular volume
VGLUT2	vesicular glutamate transporter 2
VNO	vomeronasal organ
VR	vomeronasal receptor
VSN	vomeronasal sensory neuron
YAC	yeast artificial chromosome

List of figures

Figure 1.1. Schematic representation of the mouse olfactory system.
Figure 1.2. Schematic representation of the mouse olfactory mucosa.
Figure 1.3. Olfactory signal transduction.
Figure 1.4. Anatomy of the mouse olfactory bulb.
Figure 1.5. Diagram of OSN axons projecting to glomeruli in the olfactory bulb.
Figure 1.6. Genetic manipulation of the MOR28/Olfr1507 locus.
Figure 1.7. IHC of the main olfactory epithelium of homozygous MOR28-IRES-gap-GFP mice with antibodies for Olfr1507/MOR28.
Figure 1.8. Numbers of fluorescent cells in OR-IRES-marker strains.
Figure 1.9. Number of Olfr1507-expressing cells in the MOR28-IRES-gap-GFP strain.
Figure 2.1. Targeting vectors.
Figure 2.2. Perfusion protocol for mice at PD21 and PD56.
Figure 2.3. Cryoprotection and embedding of the samples.
Figure 2.4. The reference end points for the collection of cryosections.
Figure 2.5. OSN counting.
Figure 2.6. Comparison of nucleus diameters.
Figure 2.7. Acquisition of a Z-stack of GFP-immunoreactive glomeruli.
Figure 3.1. Gene targeting.
Figure 3.2. Location of GFP-immunoreactive cells in the main olfactory epithelium of mice at PD21.
Figure 3.3. Olfr1507-immunoreactivity in the main olfactory epithelium of homozygous Olfr1507-IRES-tauGFP, Olfr1507-IRES-gapGFP, Olfr1507-IRES-tauLacZ, or MOR28-IRES-gap-GFP mice at PD21.
Figure 3.4. Olfr1507-immunoreactivity in the main olfactory epithelium of homozygous Olfr1508-IRES-tauGFP or Olfr1509-IRES-tauGFP mice at PD21.
Figure 3.5. Cell counts for Olfr1507, Olfr1508, or Olfr1509 in gene-targeted strains.
Figure 3.6. Cell counts for Olfr1507, Olfr1508, or Olfr1509 in gene-targeted strains after Abercrombie correction.
Figure 3.7. The Olfr1507 glomerulus in the medial half-olfactory bulb of homozygous Olfr1507-IRES-tauGFP, Olfr1507-IRES-gapGFP, or Olfr1507-IRES-tauLacZ mice at PD21.

Figure 3.8. The Olfr1507 glomerulus in the lateral half-olfactory bulb of homozygous Olfr1507-IRES-tauGFP, Olfr1507-IRES-gapGFP, or Olfr1507-IRES-tauLacZ mice at PD21.
Figure 3.9. GFP-immunoreactive glomeruli in the medial half-olfactory bulb of homozygous Olfr1508-IRES-tauGFP or Olfr1509-IRES-tauGFP mice at PD21.
Figure 3.10. GFP-immunoreactive glomeruli in the lateral half-olfactory bulb of homozygous Olfr1508-IRES-tauGFP or Olfr1509-IRES-tauGFP mice at PD21.
Figure 3.11. GFP-immunoreactive glomeruli in the medial and lateral half-olfactory bulb of homozygous Olfr1507-IRES-tauGFP, Olfr1508-IRES-tauGFP, or Olfr1509-IRES-tauGFP mice at PD56.
Figure 3.12. Olfr1507 glomeruli in the medial and lateral half-olfactory bulb of homozygous MOR28-IRES-gap-GFP mice at PD21.
Figure 3.13. CellProfiler overview and features.
Figure 3.14. Rescale Intensity module applied to both the GFP and VGLUT2 channels.
Figure 3.15. Threshold module applied to both the GFP and VGLUT2 channels.
Figure 3.16. Object identification of GFP and VGLUT2 after processing using the Identify Primary Objects module.
Figure 3.17. The process of removing objects based on their measurements to filter the GFP glomerulus.
Figure 3.18. Total glomerular volume per mouse.
Figure 3.19. Relative positions of the GFP-immunoreactive glomeruli in relation to the Olfr1507-immunoreactive glomeruli in the olfactory bulb of mice double heterozygous for Olfr1508-IRES-tauGFP and Olfr1509-IRES-tauGFP at PD21.
Figure 3.20. GFP-immunoreactive axons follow different routes in the lateral half-olfactory bulb of mice double heterozygous for Olfr1508-IRES-tauGFP and Olfr1509-IRES-tauGFP at PD21.
Figure 3.21. Olfr1507-immunoreactivity in homozygous ∆Olfr1507-GFP mice at PD21.
Figure 3.22. Location and axonal projections of ∆Olfr1507 OSNs in homozygous ∆Olfr1507-GFP mice at PD21.

Figure 3.23. Different degrees of apparent innervation by GFP-immunoreactive axons in the olfactory bulbs of a homozygous ΔOlfr1507-GFP mouse at PD21.
Figure 3.24. GFP-immunoreactive OSNs in the septal organ of homozygous Olfr1509-IRES-tauGFP mice at PD21.
Figure 3.25. Atypical trajectories of GFP-immunoreactive axons in the olfactory bulb of homozygous Olfr1508-IRES-tauGFP mice at PD21.
Figure 3.26. GFP-immunoreactive axons follow different routes in the lateral half-olfactory bulb of homozygous Olfr1508-IRES-tauGFP mice at PD56.

Summary

In mice, odorants are detected in the olfactory epithelium by olfactory sensory neurons (OSNs) via 1141 odorant receptors (ORs), which are G-protein-coupled seven-transmembrane proteins. The position of an OSN in the olfactory epithelium restricts gene choice to a subset of the repertoire of OR genes. A mature OSN expresses RNA of only one OR gene. Counts of OSNs expressing a given OR gene in mouse can vary greatly from gene to gene.

One of the most frequently chosen OR genes is *Olfr1507*, previously referred to as MOR28. This gene is located on Chromosome 14 in a cluster that includes the highly homologous OR genes *Olfr1508* and *Olfr1509*.

In my Ph.D. thesis, I studied novel inbred C57BL/6 gene-targeted mouse strains carrying mutations of the OR-IRES-marker type in *Olfr1507*, *Olfr1508*, or *Olfr1509*. This genetic approach enables the visualization of OSNs (including the cilia, dendrite, cell body, axon, and axon termini) that express a given OR, by targeted integration of a cassette that leads to cotranslation of the OR with a marker such as taulacZ or tauGFP via an internal ribosome entry site (*IRES*).

I examined the spatial pattern of OSNs that express Olfr1507, Olfr1508, or Olfr1509 in the olfactory epithelium of Olfr1507-IRES-tauGFP, Olfr1508-IRES-tauGFP, and Olfr109-IRES-tauGFP strains. By using immunohistochemistry, I located these OSNs to the dorsolateral and ventromedial regions of the olfactory epithelium. I found that Olfr1507 is expressed in four-fold more OSNs than Olfr1508 and in three-fold more OSNs than Olfr1509.

I applied immunohistochemistry to characterize the positions of the Olfr1507, Olfr1508, or Olfr1509 glomeruli in the olfactory bulb and to test the specificity of a commercially available Olfr1507 antibody in the olfactory bulb.

∆OR strains have been used to study OR gene choice. In this paradigm, the coding region of an OR gene is replaced with that of a reporter such as GFP. The absence of Olfr1507-immunoreactive signal in homozygous ∆Olfr1507 mice is powerful evidence that the commercially available Olfr1507 antibody is specific for Olfr1507. I found that axons of ∆Olfr1507-expressing OSNs project diffusely over the ventral aspect of the olfactory bulb and innervate >100 glomeruli, suggesting there may be >50 OR gene candidates for second choice in these OSNs.

Taken together, my studies have validated the specificity of the Olfr1507 antibody. Working with inbred gene-targeted strains led to a consistent number and positions of the Olfr1507, Olfr1508, or Olfr1509 glomeruli. OSNs expressing ∆Olfr1507 reside in the same area of the main olfactory epithelium as Olfr1507-expressing OSNs and project their axons to >100 glomeruli, with various apparent degrees of innervation.

Zusammenfassung

Geruchsstoffe werden von olfaktorischen sensorischen Neuronen (OSNs) im olfaktorischen Epithel der Maus wahrgenommen. Diese OSNs exprimieren 1141 verschiedene olfaktorische Rezeptorgene (OR). Die Rezeptoren sind G-Protein-gekoppelt und bestehen aus sieben Transmembrandomänen. Die Position des OSN im olfaktorischen Epithel beschränkt die „*gene choice*“ (Genwahl) der OR-Gene auf einen Teil des OR-Genrepertoires. Jedes bestimmte OR-Gen weist ein spezifisches Expressionsmuster auf. Ein reifes OSN exprimiert nur die RNA eines einzigen OR-Gens. Die Anzahl der OSNs, die ein bestimmtes OR-Gen exprimieren, variiert stark zwischen den OR-Genen der Maus.

Eines der am häufigsten exprimierten OR-Gene ist *Olfr1507*, früher bekannt als MOR28. Dieses Gen befindet sich in einem Gencluster auf Chromosom 14. Zu diesem Cluster gehören auch die homologen OR-Gene *Olfr1508* und *Olfr1509*.

In meiner Dissertation werden C57BL/6-Inzuchtstämme untersucht, in denen *Olfr1507*, *Olfr1508*, oder *Olfr1509* mit der OR-IRES-Marker-Strategie mutiert wurden. Dieser genetische Ansatz ermöglicht die Visualisierung von OSNs (einschließlich Zilien, Dendriten, Zellkörper, Axone und Axonterminale), die ein bestimmtes OR exprimieren. Die gezielte Insertion einer Genkassette, die eine interne ribosomale Eintrittsstelle (*IRES*) und ein Markergen wie taulacZ oder tauGFP enthält, resultiert neben der Expression des spezifischen OR in der Kotranslation des Markers.

Das Expressionsmuster von OSNs, die Olfr1507, Olfr1508 oder Olfr1509 exprimieren, wurde in diesen genetisch modifizierten Mausstämmen Olfr1507-IRES-tauGFP, Olfr1508-IRES-tauGFP und Olfr109-IRES-tauGFP untersucht. Mit Hilfe von Immunhistochemie konnte ich diese OSNs in den dorsolateralen und ventromedialen Bereichen des olfaktorischen Epithels nachweisen. Olfr1507 wurde von viermal mehr OSNs als Olfr1508 und von dreimal mehr OSNs als Ofr1509 exprimiert.

Durch Immunohistochemie konnte ich die Positionen der Olfr1507-, Olfr1508- und Olfr1509-Glomeruli in den Riechkolben der genetisch modifizierten Mausstämme charakterisieren und die Spezifität eines kommerziell erhältlichen Olfr1507-Antikörpers im Riechkolben validieren.

∆OR-Stämme wurden verwendet, um die „*gene choice*“ der OSNs zu untersuchen. In diesen Stämmen ist die codierende Region eines OR-Gens durch einen Reporter wie GFP ersetzt. Das Fehlen eines Olfr1507-immunreaktiven Signals im olfaktorischen Epithel und Riechkolben von homozygoten ∆Olfr1507-Mäusen ist ein starker Beweis dafür, dass der Antikörper spezifisch für Olfr1507 ist. Axone von ∆Olfr1507-exprimierende OSNs zerstreuen sich undefiniert über den gesamten ventralen Bereich des Riechkolbens und innervieren mehr als 100 Glomeruli. Dies deutet darauf hin, dass ∆Olfr1507-OSNs möglicherweise mehr als 50 verschiedene OR-Gen-Kandidaten als „*second choice*“ (Zweitwahl) zur Verfügung haben.

Table of contents

Acknowledgments……..I

List of abbreviations……II

List of figures……IV

Summary……...VII

Zusammenfassung……...VIII

1. Introduction……1

1.1. Sensory structures in the mouse olfactory epithelium……..1

1.2. Main olfactory epithelium……...3

1.3. Olfactory sensory neurons and odorant receptors……4

1.4. Olfactory bulb……..6

1.5. Glomeruli in the olfactory bulb……..8

1.6. Axonal convergence……10

1.7. Axonal sorting……11

1.8. The ΔOR paradigm……..12

1.9. The *Olfr1507* gene cluster……..13

1.9.1. Transgenic and gene-targeted *Olfr1507* strains from the Sakano laboratory……14

1.9.2. Gene-targeted *Olfr1507* strains from the Axel laboratory……...15

1.10. Odorant receptor antibodies……...17

1.11. Number of OSNs……..19

1.12. The stability of *Olfr1507* gene choice……21

2. Materials and Methods ……22

2.1 Materials……23

2.1.1 Mice……...23

2.1.2 Targeting vectors……24

2.1.3 Reagents……..25

2.1.3.1 Perfusion and embedding……25

2.1.3.2 Immunohistochemistry……..26

2.1.3.3 Antibodies……...27

2.1.3.4 Genotyping……29

2.1.4 Consumables……30

2.1.4.1 General consumables……...30

2.1.4.2 Dissection……31

2.1.4.3 Cryoprotection and immunohistochemistry……31
2.1.5 Equipment……32
2.1.6 Software……33
2.1.7 Genotyping primers……34
2.2 Methods……35
2.2.1 Perfusion and cryoprotection……35
2.2.2 Sectioning……37
2.2.3 Genotyping……38
2.2.3.1 Genomic DNA extraction……38
2.2.3.2 Genotyping protocols……38
2.2.4 Immunohistochemistry……40
2.2.4.1 Antigen retrieval……40
2.2.4.2 IHC protocol……40
2.2.5 Cell counting ……41
2.2.6 Glomerular volume……44
3 Results……47
3.1 Zonal expression of *Olfr1507*, *Olfr1508*, and *Olfr1509*……48
3.2 Testing a commercially available Olfr1507 antibody in Olfr1507 gene-targeted strains……51
3.3 Testing the specificity of the Olfr1507 antibody in Olfr1508 and Olfr1509 gene-targeted strains……55
3.4 Cell counts of OSNs expressing Olfr1507, Olfr1508, or Olfr1509 ……57
3.5 Abercrombie correction of the numbers of cells expressing Olfr1507, Olfr1508, or Olfr1509……59
3.6 The Olfr1507 antibody in the olfactory bulb of different *Olfr1507* gene-targeted strains……61
3.7 Positions of Olfr1508 and Olfr1509 glomeruli in the olfactory bulb……65
3.8 Olfr1507 glomeruli in MOR28-IRES-gap-GFP mice……70
3.9 Glomerular volume in the Olfr1507, Olfr1508 and Olfr1509 gene-targeted strains……72
3.9.1 Rescale intensity module……72
3.9.2 Threshold module……73
3.9.3 Identify Primary Objects module……73

3.9.4 Convert Objects to Image module……74
3.9.5 Filter Objects module……..74
3.9.6 Mask Objects module……75
3.9.7 Measure Area Occupied module……..75
3.10 The positions of Olfr1508 and Olfr1509 glomeruli relative to the Olfr1507 glomeruli…….83
3.11 Path taken by GFP-expressing axons in double heterozygous mice……86
3.12 The ΔOlfr1507-GFP strain ……..89
3.13 The septal organ of Olfr1509-IRES-tauGFP mice……94
3.14 Atypical trajectories of GFP-immunoreactive axons in Olfr1508-IRES-tauGFP mice……96
4 Discussion……99
4.1 The Olfr1507 antibody is specific for Olfr1507……..102
4.2 *Olfr1507* is the highest expressed OR gene ……104
4.3 Characterization of the positions of the glomeruli for Olfr1507, Olfr1508, or Olfr1509……106
4.4 The Olfr1507 glomeruli in the MOR28-IRES-gap-GFP strain……107
4.5 Total glomerular volume in homozygous OR-IRES-marker mice……..108
4.6 Glomeruli in double heterozygous Olfr1508-IRES-tauGFP x Olfr1509-IRES-tauGFP mice ……..110
4.7 GFP-immunoreactive axons in double heterozygous mice……111
4.8 GFP-immunoreactivity in the main olfactory epithelium of ΔOlfr1507-GFP mice……..112
4.9 GFP-immunoreactivity in the olfactory bulb of ΔOlfr1507-GFP mice……113
4.10 Olfr1509-expressing OSNs in the septal organ……..114
4.11 Olfr1508 axons follow atypical trajectories in Olfr1508-IRES-tauGFP mice……..115
4.12 Concluding remarks……116
5 Literature……117

1 Introduction

The sense of smell has recently received much interest due to the common association of olfactory dysfunction with SARS-CoV-2 infection. For mammals, the sense of smell is crucial as it greatly influences their health and behavior. Critical functions such as prey localization, predator avoidance, food exploration, and identification of suitable mates heavily rely on their olfactory abilities. Olfactory processing is of utmost importance for the survival of the species and the individual.

1.1 Sensory structures in the mouse olfactory system

The olfactory system within the nasal cavity of the mouse comprises four anatomically distinct sensory structures (Figure 1.1).

The first structure, at the tip of the nose, is the Grüneberg or Grueneberg ganglion (GG). It resides in the nasal vestibule near the nasal septum and dorsolateral cartilage, and a small group of OSNs is embedded within connective tissue beneath a dense network of blood vessels (Grueneberg, 1973). More posteriorly, the vomeronasal organ (VNO) is located on the floor of the nasal cavity adjacent to the vomer bone. It consists of a slender cylindrical structure that includes the vomeronasal duct, as well as surrounding glands, blood vessels, nerves, and connective tissue. The VNO contains vomeronasal sensory neurons (VSNs) expressing vomeronasal receptors (VRs), which primarily respond to pheromonal signals and project their axons to glomeruli in the accessory olfactory bulb (AOB) (Døving and Trotier, 1998; Barrios et al., 2014). The bulk of the sensory component of the mouse olfactory system is the MOE, located in the most posterior part of the nasal cavity. Finally, the septal organ (SO) is a small anatomical structure that shares characteristics with the MOE (Ma et al., 2003).

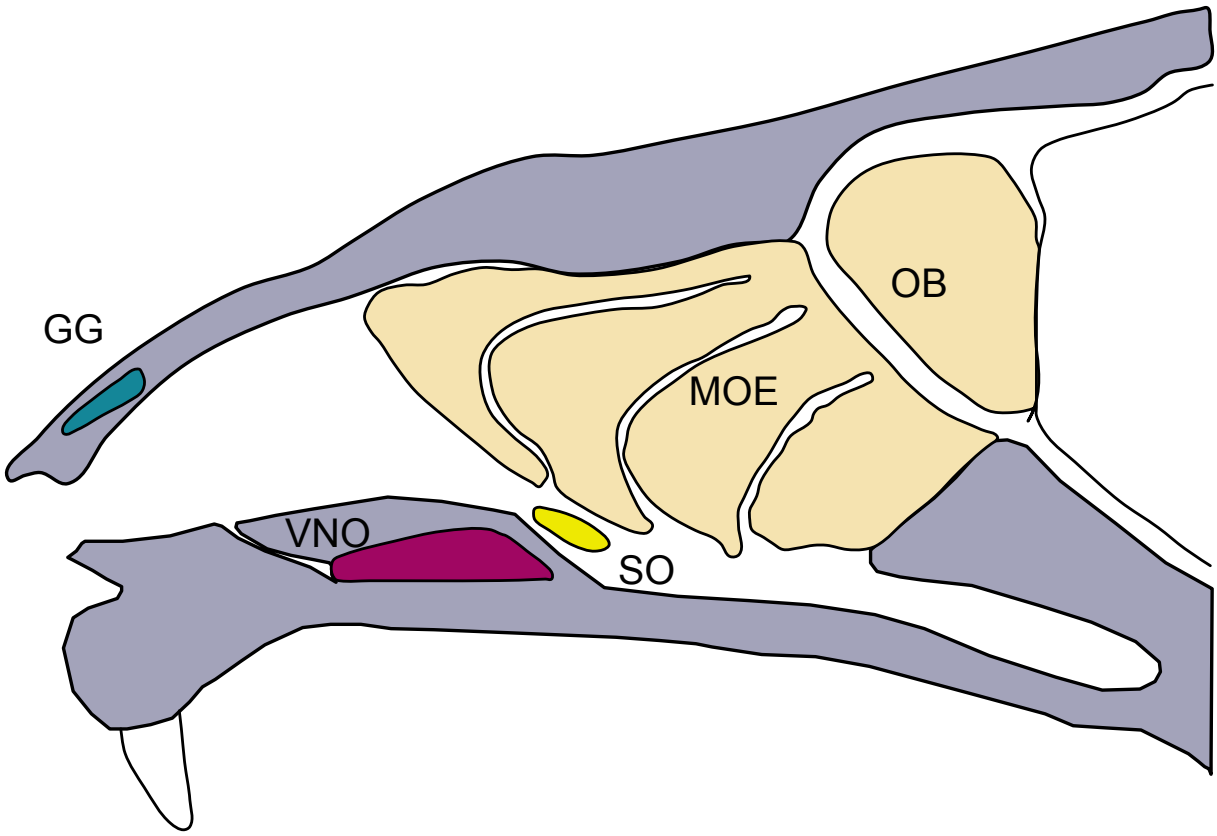


Figure 1.1. Schematic representation of the mouse olfactory system.

GG: Grueneberg ganglion. VNO: vomeronasal organ. MOE: main olfactory epithelium. SO: septal organ. OB: olfactory bulb (BioRender, 2024).

1.2 Main olfactory epithelium

The MOE is a pseudostratified structure containing three main cell types: OSNs, sustentacular cells (serving glia-like, supportive functions), and stem cells (responsible for regenerating OSNs and supporting cells throughout the life of the individual). The basement membrane separates the MOE from the underlying lamina propria, which contains Bowman's glands, olfactory ensheathing cells, and OSN axon bundles (Figure 1.2).

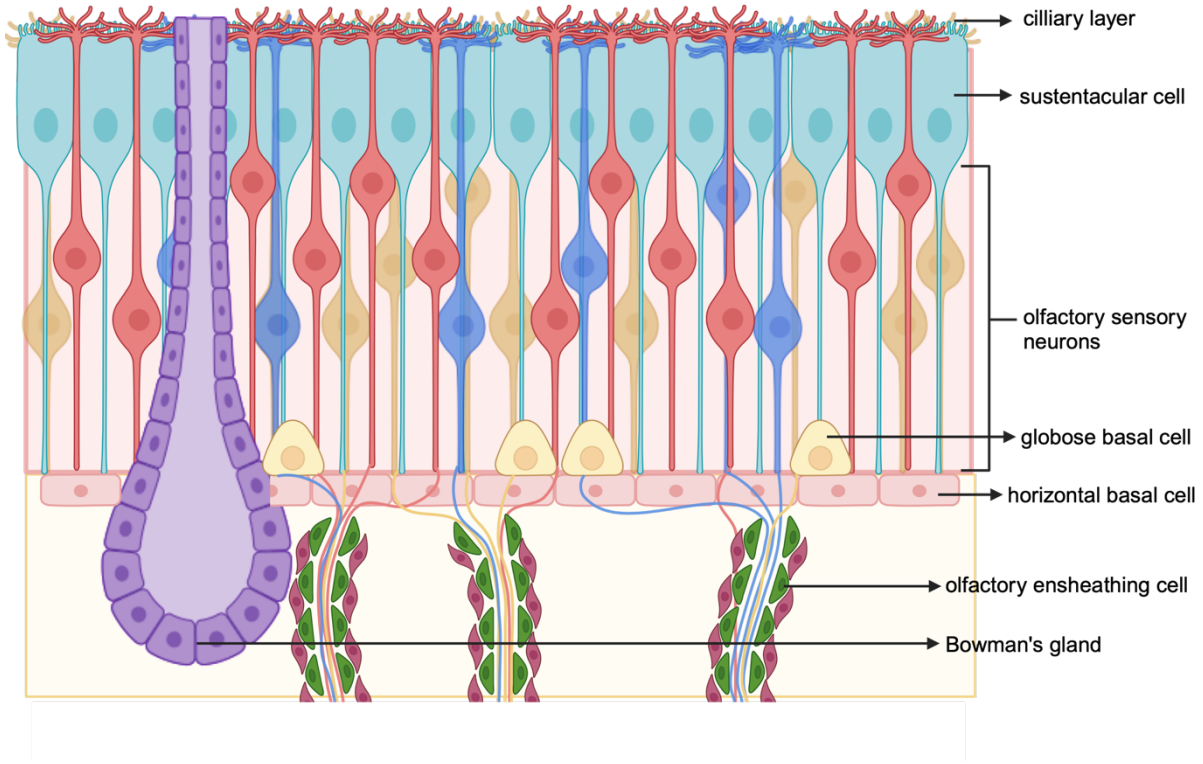


Figure 1.2. Schematic representation of the mouse olfactory mucosa.

The MOE and the lamina propria are separated by a basement membrane (BioRender, 2024).

1.3 Olfactory sensory neurons and odorant receptors

OSNs are bipolar cells, with a single dendrite ending in cilia that protrude into the mucus covering the epithelium, and a single, unbranched, and unmyelinated axon that terminates in the OB (Mombaerts, 1999). A mature OSN typically expresses transcripts of only one OR gene at a high level, a phenomenon known as monogenic expression (Malnic et al., 1999). OSNs expressing a given OR gene are distributed within the MOE. Early studies suggested the existence of four broad areas known as zones (Ressler et al., 1993; Vassar et al.,1993; Sullivan et al., 1996). Another group described a fifth zone called the patch (Strotmann et al., 1992; Strotmann et al., 1994). Subsequent research revealed that subpopulations of OSNs can be located in more than one of the classical zones, indicating that the concept of a small number of discrete zones was not entirely accurate. A continuous numerical index has been implemented by one group in order to represent quantitatively the spatial expression pattern of an OR gene (Miyamichi et al., 2005). Three-dimensional (3D) reconstruction of OR gene expression in the MOE led to the identification of 9 zones, which are overlapping and highly complex in 3D (Zapiec and Mombaerts, 2020). A 3D transcriptomics study utilized an algorithm to reconstruct the topographical expression of 689 OR genes and determined that a minimum of 5 zones represents the diversity of ORs (Ruiz Tejada Segura et al., 2022). Thus far, no direct physiological correlation has been identified for the zonal organization of the MOE. It is plausible that this zonal organization serves as a strategic arrangement for the axonal wiring of the olfactory system.

Odorants interact with OR proteins located on the cilia of the dendrites of OSNs in the MOE. A given odorant activates one to many ORs. The interaction between the odorant and an OR triggers a series of events involving the activation of G proteins and adenylyl cyclase (AC) that result in the opening of cyclic nucleotide-gated-ion channels (CNGC) and membrane depolarization (Figure 1.3).

Buck and Axel discovered the vertebrate OR genes (Buck and Axel, 1991). OR genes encode polypeptides with a seven transmembrane structure, which is a hallmark of G-protein-coupled receptors (GPCRs). The small intronless open reading frames of mammalian OR genes makes them easily identifiable from genomic

sequences. The mouse genome harbors 1141 intact OR genes and a few hundred pseudogenes and forms the largest gene repertoire (Barnes et al., 2020). OR genes are organized in clusters spread across 68 loci scattered among most chromosomes (Zhang and Firestein, 2002; Young et al., 2003).

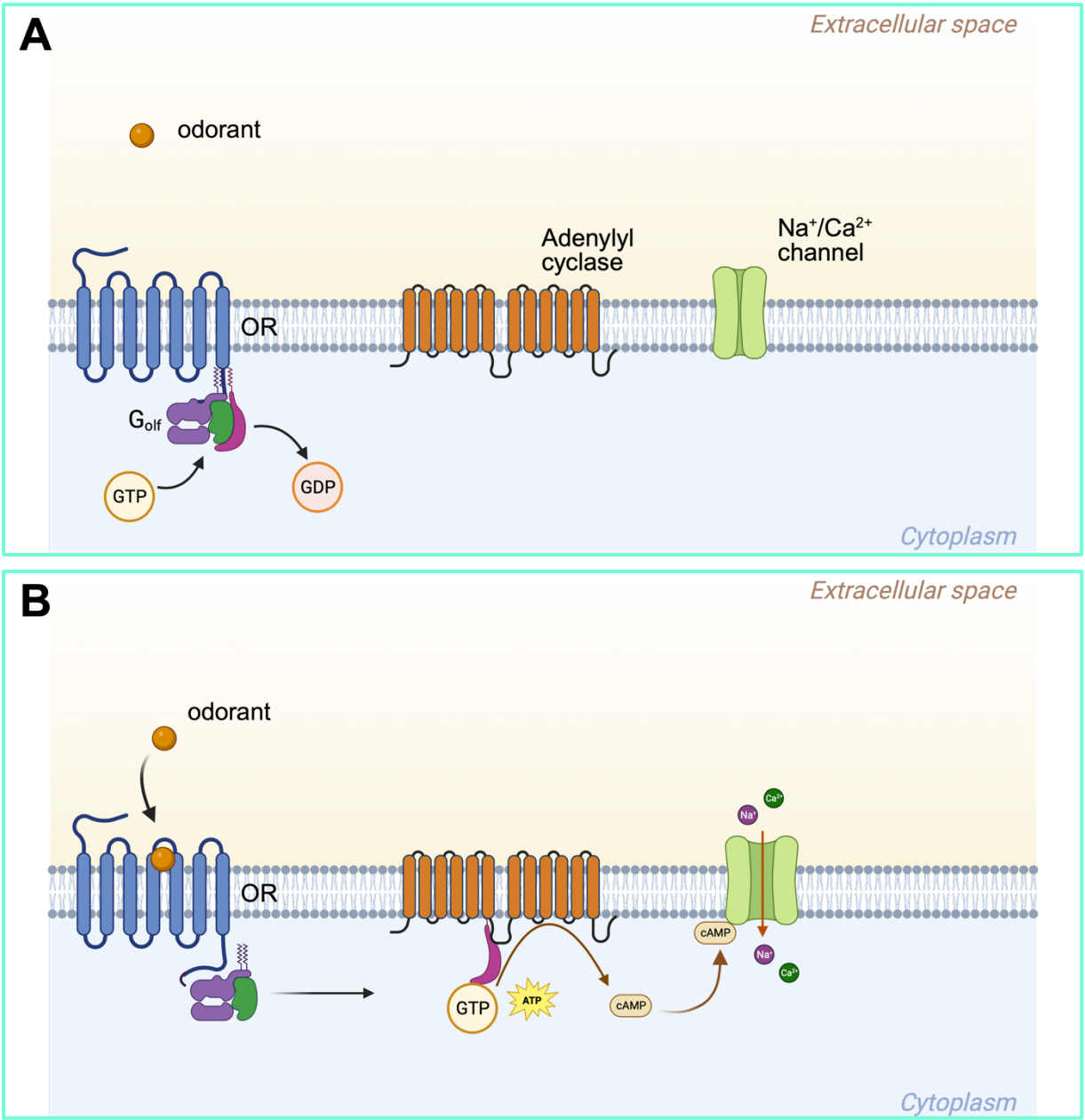


Figure 1.3. Olfactory signal transduction.

(A) The interaction between an odorant and an OR activates adenylyl cyclase producing cyclic AMP. (B) The transient intracellular increase of cyclic AMP opens a cyclic nucleotide-gated-cation channel resulting in a flow of sodium and calcium ions, which in turn depolarizes the membrane. Action potentials are generated and travel along the OSN axon to the OB (BioRender, 2024).

1.4 Olfactory bulb

The OB is an anatomical structure of the brain and processes and relays olfactory information from the nose to higher brain regions. In mouse, the OB is located at the front of the brain, near the base of the skull. The OB receives input from OSNs, which send their axons forming the olfactory nerve (Figure 1.5) (Shepherd, 2004).

The mouse OB, like that of other mammals, consists of several layers (Figure 1.4) (Price and Powell, 1970; Pinching and Powell, 1971). The olfactory nerve layer (ONL) is the closest layer to the nasal cavity and contains axon bundles of OSNs. Neurons surrounding glomeruli are called juxtaglomerular cells and consist of three cell types: periglomerular cells, external tufted cells, and superficial short-axon cells. The second layer is the glomerular layer containing spherical neuropil structures called glomeruli. Each glomerulus receives input from OSNs expressing a given OR gene. The glomerular layer is the first step of odor processing and integration of olfactory information (Lledo et al., 2005). The periglomerular cell layer contains periglomerular cells, a type of inhibitory interneurons. Periglomerular cells are responsible for modulating the activity of glomeruli and help shape the olfactory response (Parrish-Aungst et al., 2007). The external plexiform layer contains the dendrites of mitral cells, which are the principal projection neurons in the OB, and is the layer where the axon terminals of OSNs make synapse with the dendrites of mitral cells. The somata of tufted cells are located in the external plexiform layer (Mori et al., 1983). The mitral cell layer consists primarily of cell bodies of mitral cells, the primary output neurons in the OB (Orona et al., 1983). Mitral cells make synapse with higher brain regions involved in olfactory processing. The internal plexiform layer contains interneurons called granule cells, which receive input from mitral cells (Nagayama et al., 2004). The granule cell layer is occupied mostly by granule cells, a type of inhibitory interneurons with small cell bodies, as well as deep short-axon cells (Price and Powell, 1970).

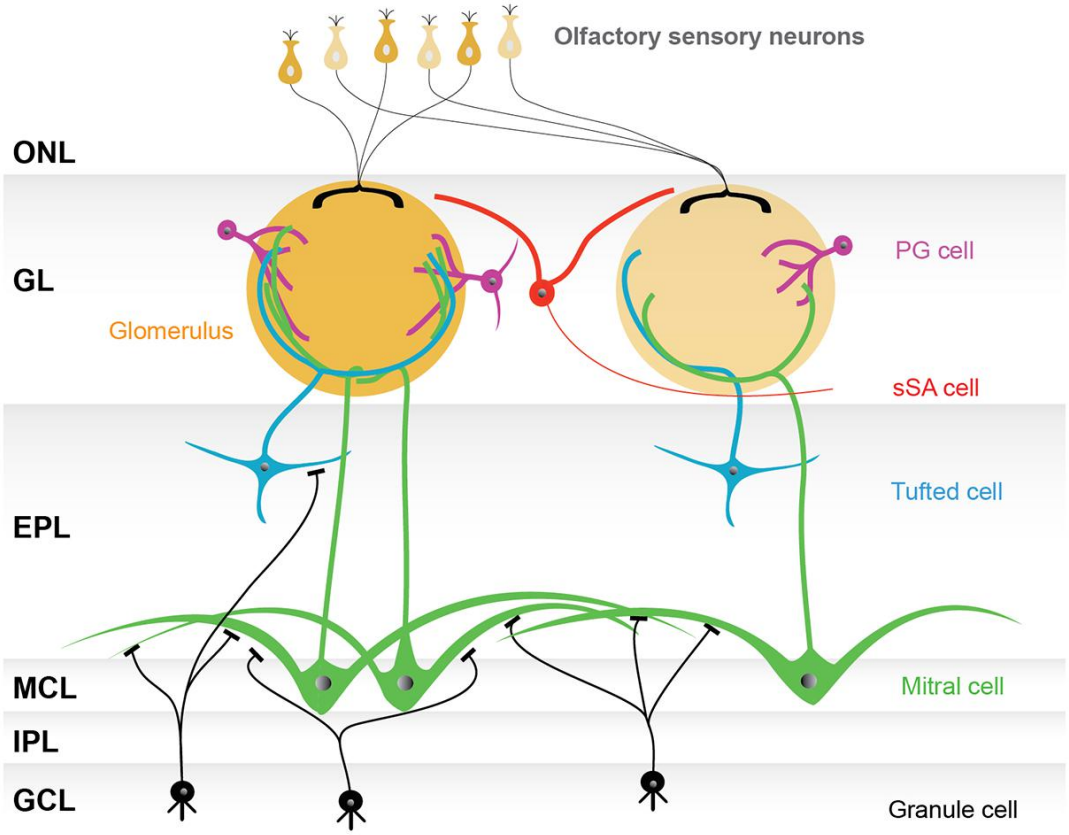


Figure 1.4. Anatomy of the mouse olfactory bulb.

The glomerular layer (GL) is the first step of odorant processing and integration of olfactory information. Two types of juxtaglomerular cells surround glomeruli in the GL: periglomerular (PG) cells and superficial short-axon (sSA) cells. The external plexiform layer (EPL) contains tufted cells. Mitral cells are located in the mitral cell layer (MCL). Both mitral and tufted cells project a single primary dendrite into a single glomerulus. The internal plexiform layer (IPL) comprises axons of mitral cells and axon collaterals of external tufted cells. The granule cell layer (GCL) contains granule cells, which are axon-less interneurons extending dendrites apically into the EPL (Nagayama, 2014, p. 2). Retrieved from https://doi.org/10.3389/fncir.2014.00098.

.

1.5 Glomeruli of the olfactory bulb

OSNs that express a given OR gene send convergent axonal projections to a small area within the medial half-OB and lateral half-OB (Figure 1.5). Within each half-OB, axons coalesce usually into a single homogeneous glomerulus in adult mice. Often two or more glomeruli per half-OB can be formed initially during development (Potter et al., 2001).

Glomeruli are arranged in a recognizable pattern (Mombaerts et al., 1996; Mombaerts 2006; Soucy et al., 2009), which is however not stereotyped (Zapiec and Mombaerts, 2015). The pattern of glomeruli in the medial half-OB and lateral half-OB roughly forms mirror images (Mombaerts 2006; Soucy et al., 2009) such that there is (at least) one glomerulus per OR in each half-OB. A mouse OB is thought to contain ~3600 glomeruli (Richard et al., 2010), which would be sufficient to accommodate two to three glomeruli for the 1141 intact OR genes.

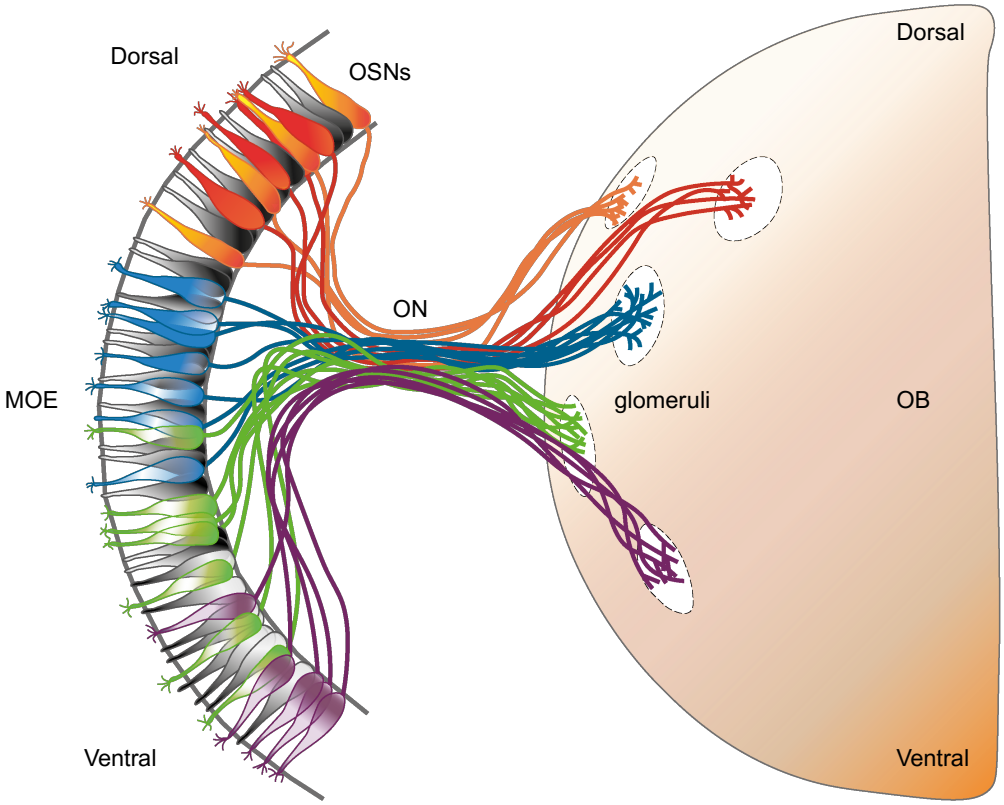


Figure 1.5. Diagram of OSN axons projecting to glomeruli in the olfactory bulb.

Five populations of OSNs, each expressing a different OR, are depicted in various colors. OSNs that express the same OR are scattered in a seemingly random fashion with the MOE, but their axons coalesce into the same glomeruli of the main olfactory bulb. Within a glomerulus, OSNs synapse with the dendrites of the second-order neurons, mitral or tufted cells, which in turn project their axons to the olfactory cortex (BioRender, 2024).

1.6 Axonal convergence

Axonal convergence to glomeruli was first demonstrated by RNA ISH methods in rats (Vassar et al., 1994) and mice (Ressler et al., 1994). These experiments detected minute amounts of OR mRNA within OSN axons and their termini. The convergence of axons expressing the same species of RNA transcripts is sufficient for the detection of signals using highly sensitive methods. But the ISH approach has several limitations: it may not work for every OR gene and cannot reliably distinguish highly related OR genes due to cross-hybridization. Instead, the OR-IRES-marker strategy, first employed for the *P2* gene (Mombaerts et al., 1996), has become the standard approach for characterizing OR-specific glomeruli and studying axonal coalescence into glomeruli. This strategy involves the use of OR-IRES-marker constructs, whereby a marker such as taulacZ or tauGFP is inserted downstream of the stop codon of an OR coding region (Mombaerts et al., 1996).

Several studies with light microscopy have employed the gene-targeted OR-IRES-marker approach to show that axons expressing the same OR gene typically coalesce into a single homogeneous glomerulus per half-OB. The OR-IRES-marker strategy has been applied to numerous OR genes that together are representative of the repertoire of OR genes, including: *M71, M72, P3, P4, M50, I7, MOR23, mOR37A, mOR37B, mOR37C, S50, SR1, MOR256* (Strotmann et al., 2000; Zheng et al., 2000; Potter et al., 2001; Bozza et al., 2002; Vassalli et al., 2002; Feinstein et al., 2004; Feinstein and Mombaerts, 2004; Bozza et al., 2009; Khan et al., 2011; Fuss et al., 2013; Bressel et al., 2016). The OR-IRES-marker strategy has also been applied to *Olfr1507* (Serizawa et al., 2000; Barnea et al., 2004; Shykind et al., 2004). The observations with OR-IRES-marker strains have consistently shown that there are typically two, sometimes three, glomeruli per OR per OB in an adult mouse. The mOR37 gene cluster is an exception to this rule, as they typically exhibit only one glomerulus per OB (Strotmann et al., 2000).

1.7 Axonal sorting

One model proposes that axonal sorting is mediated by homophilic and heterophilic interactions between axons (Feinstein and Mombaerts, 2004). Homophilic interactions would occur between axons of OSNs expressing the same OR. Heterophilic interactions are not referred as repulsive but rather as less attractive between axons expressing dissimilar ORs. Axonal sorting starts when axons transition from the outer to the inner nerve layer (Potter et al., 2001; Au et al., 2002; Treloar et al., 2002). Following the trajectory of single axons showed that in the periphery, the majority of axons course individually or in small fascicles and as axons approach the target glomerulus, they enter the inner olfactory nerve layer as larger fascicles (Treloar et al., 2002). Fascicles of OSN axons follow variable pathways before entering the glomerulus. Diverse and complex trajectories suggest that multiple guidance mechanisms are used for axon targeting (Potter et al., 2001; Treloar et al., 2002). The synapses within the cognate glomeruli are highly precise with a high level of homogeneous composition despite the often-idiosyncratic trajectories of single axons as visualized using the OR-IRES-marker approach (Potter et al., 2001; Treloar et al., 2002).

1.8 The ΔOR paradigm

ORs are determinants of axonal convergence (Mombaerts et al., 1996; Wang et al., 1998; Bozza et al., 2002; Serizawa et al., 2003; Feinstein et al., 2004; Fuss et al., 2013). An experimental model, known as the ΔOR paradigm, has been popular to further explore mechanisms of OR gene choice and the role of ORs in axonal wiring. It consists in deleting or disabling the OR coding region, either at the endogenous locus by gene targeting or by conventional transgenesis at a random position in the genome (Wang et al., 1998; Serizawa et al., 2003; Feinstein et al., 2004; Lewcock and Reed, 2004; Shykind et al., 2004; Imai et al., 2006; Grosmaitre et al., 2009; Bozza et al., 2009; Vassalli et al., 2011; Fuss et al., 2013; Zapiec and Mombaerts, 2020). The ΔOR paradigm has been applied to several OR genes including *Olfr1507* (*MOR28)*. A fraction of OSNs expressing the locus with the deleted OR coding region (ΔOR OSNs) coexpress a second OR locus with an intact coding region. The term "coexpression" refers to the colocalization of marker RNA or protein produced from the ΔOR locus or transgene together with RNA transcribed from another endogenous OR locus in the same OSN. The choice of a second OR gene appears to be restricted to a subset of the OR gene repertoire. The coexpression of one of several other OR genes in ΔOR OSNs corresponds to a variety of odorant response profiles (Feinstein et al., 2004; Grosmaitre et al., 2009). Axons of labeled ΔOR OSNs do not coalesce into a pair of glomeruli but spread diffusely over a wide domain of the OB and enter many glomeruli.

1.9 The *Olfr1507* gene cluster

A mature OSN has the choice of OR gene expression expression among the repertoire of 1141 intact OR genes. OSNs expressing *Olfr1507* are the most prevalent in C57BL/6 and 129 mice (Shykind et al., 2004; Ibarra-Soria et al., 2017). *Olfr1507* is also known by various other gene names, such as *MOR28*, *Or28*, *MOR244-11* in the past, and the latest name is *Or4e5*. Interestingly, there are still no ligands reported for Olfr1507. The *Olfr1507* gene resides in a cluster of seven OR genes on Chromosome 14 (Serizawa et al., 2003). The H element, which serves as regulatory element for this cluster, demarcates the telomeric end of the cluster and acts as a boundary between this cluster and the T-cell antigen receptor (TCR) locus. The *TCR Vα1* gene segment divides the *Olfr1507* cluster into two groups: a proximal group comprising *Olfr1507*, *Olfr1508*, and *Olfr1509*, and a distal group consisting of four related OR genes from the *Olfr168/MOR223* gene family. The expression of *Olfr1507*, *Olfr1508*, and *Olfr1509* genes is dependent on the H element: deletion of the H element from a mouse transgene results in the loss of expression of the proximal group of *Olfr1507*, *Olfr1508*, and *Olfr1509* (Serizawa et al., 2003) and targeted deletion demonstrates that it acts as a cis-acting regulatory element for the expression of *Olfr1507*, *Olfr1508*, and *Olfr1509* (Fuss et al., 2007).

Olfr1507 has a coding region of 939 bp (313 amino acids), *Olfr1508* has a coding region of 930 bp (310 amino acids), and *Olfr1509* has a coding region of 924 bp (308 amino acids). The *Olfr1507* and *Olfr1508* genes are separated by 25 kb and *Olfr1509* gene is 10 kb downstream of *Olfr1508*. The amino acid sequences of Olfr1507, Olfr1508, and Olfr1509 share between 75% and 95% of similarity (Tsuboi et al., 1999). The expression of *Olfr1507*, *Olfr1508*, and *Olfr1509* is restricted to a dorsolateral and ventromedial area of the MOE, corresponding to zone 4 in Buck's initial nomenclature (Sullivan et al., 1996), and Zolfr1507 in the latest nomenclature (Zapiec and Mombaerts, 2020). The ratio of OSNs expressing *Olfr1507*, *Olfr1508*, and *Olfr1509* is approximately 5:2:1 (Tsuboi et al., 1999).

The positions of the respective glomeruli were initially characterized by using radioactive ISH. The Olfr1507 glomeruli are located in the most ventral position, the Olfr1508 glomeruli are located approximately one glomerular width dorsally from

Olfr1507, and the Olfr1509 glomeruli occupy the most dorsal position, situated approximately three to four glomeruli dorsally from Olfr1507 in both the medial half-OB and lateral half-OB (Tsuboi et al., 1999; Serizawa et al., 2000). The glomerular arrangement maintains symmetry between the two halves of an OB.

1.9.1 Transgenic and gene-targeted *Olfr1507* strains from the Sakano laboratory

The Sakano laboratory reported several transgenic or gene-targeted mouse strains to tag *Olfr1507*, building upon the 1996 Mombaerts technique of OR-IRES-marker. Transgenic mouse strains were generated with a yeast artificial chromosome (YAC) clone isolated from the C57BL/6 genome carrying the *Olfr1507* gene cluster. The transgenic mice express the tauLacZ marker in conjunction with Olfr1507 by the IRES strategy and are referred to as MOR28-IRES-tau-LacZ (Figure 1.6). The Sakano laboratory also reported a gene-targeted strain using embryonic stem (ES) cells from the R1 cell line in a 129X1/SvJ x 129S1/Sv genetic background (Serizawa et al., 2000). By homologous recombination, the *Olfr1507* gene was tagged with the gap-green fluorescent protein (GFP) marker and this strain is referred to as MOR28-IRES-gap-GFP (Figure 1.6).

These genetically manipulated mouse strains corroborated that Olfr1507-expressing OSNs are located ventrally the MOE. Puzzlingly, axons of Olfr1507 OSNs in this mixed genetic background segregate and converge onto multiple glomeruli. The formation of multiple glomeruli may be due to the chromosomal location of the OR transgene altering the level or onset of transcription. Another possibility is that accidental deletions or mutations occurred in the constructs (Serizawa et al., 2000).

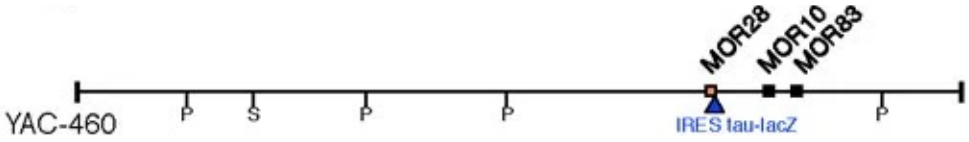
Axonal segregation and projection sites of Olfr1507 OSNs in different strains was further investigated (Ishii et al., 2001). *Olfr1507* transgenic and gene-targeted mice displayed the monoallelic property of OSNs, in that Olfr1507 OSNs express only one reporter. Differences in the genetic background corresponded to glomerular segregation of the differentially labeled Olfr1507 OSN axons. The glomerular positions of Olfr1507 also display differences between different genetic backgrounds: B6 and 129 (Ishii et al., 2001).

The broad distribution of glomerular positions in the MOR28-IRES-gap-GFP strain has been attributed to the mixed genetic background (Zapiec and Mombaerts, 2015). Generating strains in an inbred genetic background may result in a constant number of glomeruli and less variable glomerular positions.

1.9.2 Gene-targeted *Olfr1507* strains from the Axel laboratory

The Axel laboratory also used *Olfr1507* as a model system and reported gene-targeted mouse strains called MOR28-IRES-gap-GFP and MOR28-IRES-tau-lacZ (Barnea et al., 2004; Shykind et al., 2004). These strains were generated in a mixed genetic background by inserting an IRES-marker cassette immediately downstream of the coding region of the *Olfr1507* locus. A home-grown antibody for Olfr1507 gave immunoreactive signal that colocalized with the lacZ-immunoreactive signal in OSNs and in the Olfr1507 glomeruli (Barnea et al., 2004).

MOR28 transgene (C57BL/6) tagged with tauLacZ



MOR28 'knock-in' (129X1/SvJ x 129S1/Sv) tagged with gapGFP

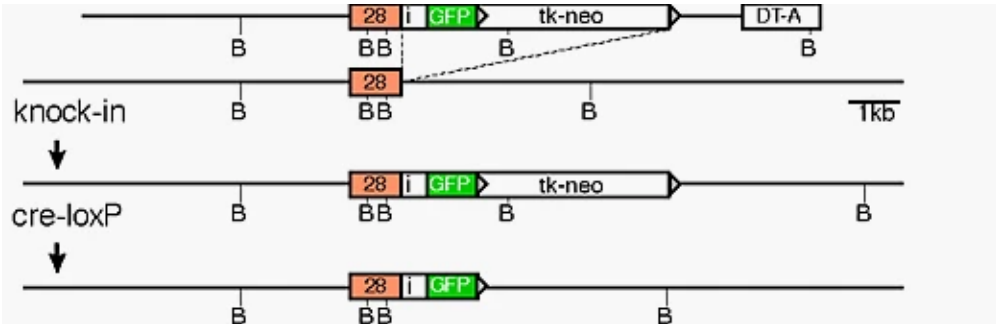


Figure 1.6. Genetic manipulation of the MOR28/Olfr1507 locus.

(Top) A 460-kb YAC clone (YAC-460) was isolated from a mouse genomic library and tagged with an *IRES-tau-LacZ* cassette (triangle) at the 3' end of the MOR28 coding region. (Bottom) The endogenous *MOR28* gene was tagged with gap-GFP by the knock-in method. Homologous recombination between the targeting vector and the endogenous *MOR28* gene resulted in the insertion of the *IRES-gap-GFP-loxP-tk-neo-loxP* cassette downstream region of the stop codon of MOR28. The Cre-loxP system was used to remove the tk-neo cassette. Triangles, *loxP* sequences (Serizawa, 2000, p. 690). Retrieved from https://doi.org/10.1038/76641.

1.10 Odorant receptor antibodies

The literature on IHC of mouse MOE and OB using antibodies for ORs is very limited (Koshimoto et al., 1994; Menco et al., 1997; Barnea et al., 2004; Strotmann et al., 2004; Low and Mombaerts, 2017). Furthermore, commercially available OR antibodies are typically not well characterized by the vendors. Generating antibodies against OR proteins is challenging due to specific features of these G-protein-coupled receptors. These challenges include difficulties in protein expression, the nature of their membrane proteins, their low expression levels, and the need for high specificity with minimal cross-reactivity. Immunofluorescent signals produced by such antibodies can be misleading due to high sequence homology between ORs, post-translational modifications, protein folding, protein-protein interactions, and fixation crosslinking. Nevertheless, the production of antibodies against ORs has been instrumental in visualizing the expression of OR proteins within OSNs. The availability of antibodies against ORs enabled the use of IHC techniques to visualize OR expression at the protein level, supplementing ISH methods.

The first report of a specific OR antibody was Strotmann et al., 2004. Antibodies for mOR256-17 (Olfr15) and mOR37 (Olfr37) were developed in the laboratory. OR proteins were found to be predominantly expressed in the cilia, dendritic knobs, and cell bodies of their respective OSNs types, as well as in the axon termini. The mOR37 antibody displayed immunoreactivity toward all OSNs expressing *mOR37A*, *mOR37B*, or *mOR37C* in the MOE of gene-targeted mice. In sections through the OB of mOR37 gene-targeted mice, the antibody exhibited immunoreactivity in two distinct adjacent glomeruli (Strotmann et al., 2004).

Another study reported an Olfr1507 antibody and applied it to MOR28-IRES-tau-LacZ mice (Barnea et al., 2004). (Note that Olfr1507 was then referred to as MOR28.) All Olfr1507-expressing OSNs in sections of the MOE exhibited immunoreactivity for the antibody. The lacZ-immunoreactive glomeruli were also immunoreactive for the antibody – a single glomerulus in each half-OB.

A comprehensive assessment was conducted with 21 commercial antibodies for mouse ORs, including an Olfr1507 antibody in the gene-targeted MOR28-IRES-gap-

GFP strain from the Sakano laboratory (Low and Mombaerts, 2017). The findings were consistent with previous investigations about Olfr1507 (Figure 1.7). This study did not examine a possible cross-reactivity of the Olfr1507 antibody to the homologous ORs Olfr1508 and Olfr1509.

Combining commercially available antibodies for ORs with inbred OR-IRES-marker strains should be rigorous approach for investigating the expression of an OR gene in the MOE and the convergence of OSN axons in the OB. Such strains allow for the easy quantification of the subpopulation of OSNs expressing a given OR and to compute the size of their corresponding glomeruli in the OB.

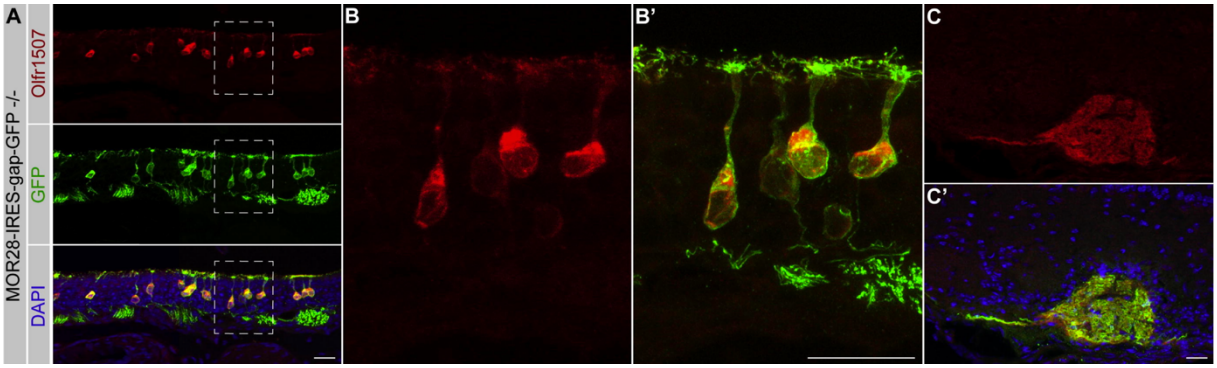


Figure 1.7. IHC of the main olfactory epithelium of homozygous MOR28-IRES-gap-GFP mice with antibodies for Olfr1507/MOR28.

(A) Olfr1507-immunoreactive cells (red) are also GFP-immunoreactive (green). (B) High magnification of insert in A. Olfr1507 immunoreactivity is detected in the cell body, dendrite, and cilia, and colocalizes with GFP immunoreactivity (B'). (C) Olfr1507 immunoreactivity colocalizes with GFP immunoreactivity within a glomerulus (Low and Mombaerts, 2017, p. 174). Retrieved from https://doi.org/10.1016/j.neuroscience.2016.12.044.

1.11 Number of OSNs

There are few studies about the number of OSNs that express a given OR gene (Royal and Key, 1999; Fuss et al., 2013; Bressel et al., 2016; Low and Mombaerts 2017). Counting OSNs in a mouse is time-consuming and must, thus far, be done manually. Only estimates of the total number of OSNs in a mouse have been offered (Kawagishi et al., 2014). One study reported cell counts for 11 OR genes using OR-IRES-marker strains in a mixed 129 x B6 background and found that the average number of OSNs can vary within a wide range across gene-targeted strains (Bressel et al., 2016). This study revealed a strong linear correlation between the number of OSNs and the volume of the corresponding glomeruli (Figure 1.8)

Another study examined the gene-targeted MOR28-IRES-gap-GFP strain of the Sakano laboratory with a commercially available Olfr1507 antibody (Figure 1.7) (Low and Mombaerts, 2017). The Olfr1507-immunoreactive signal colocalizes with the GFP-immunoreactive signal. The numbers of OSNs expressing a gene-targeted or wild-type *Olfr1507* gene were counted. This study confirmed specificity of this Olfr1507 antibody as well as monoallelic expression. The probability of Olfr1507 expression to be chosen was higher for C57BL/6 than for 129, using mice in a mixed background (Figure 1.9).

To date, no studies have reported tests to assess the specificity of the commercial Olfr1507 antibody or have examined glomerular characteristics for the homologous Olfr1508 or Olfr1509 genes.

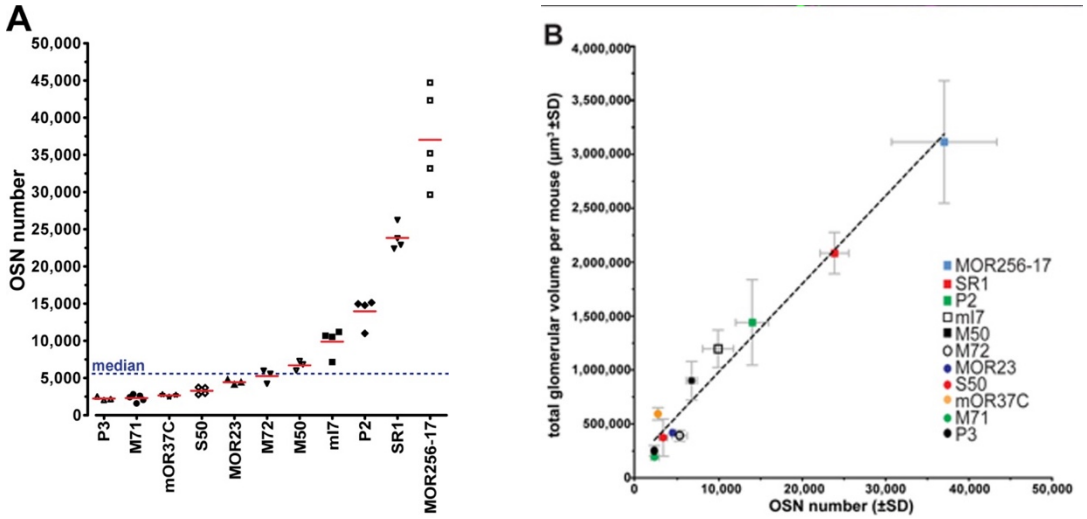


Figure 1.8. Numbers of fluorescent cells in OR-IRES-marker strains.

(Left) Average OSN number in a set of 11 strains at PD21. (Right) Total glomerular volume and correlation with OSN numbers. Total glomerular volume per strain at PD21 correlates strongly and linearly with OSN number (Bressel, 2016, pp. 203, 207). Retrieved from https://doi.org/10.1002/cne.23835

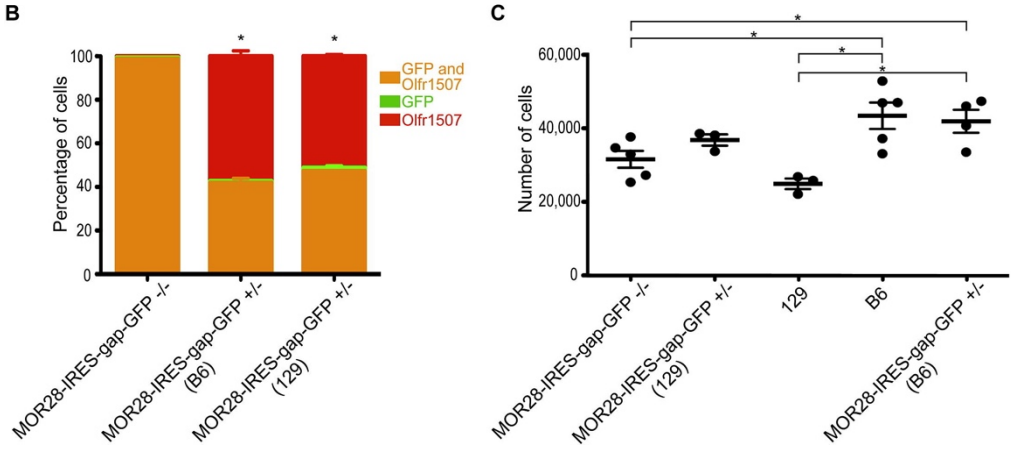


Figure 1.9. Number of Olfr1507-expressing cells in the MOR28-IRES-gap-GFP strain.

(Left) Percentages of cells immunoreactive for the Olfr1507 antibody (red), the GFP antibody (green), and both the Olfr1507 and GFP antibodies (orange) in 3 types of mice: homozygous MOR28-IRES-gap-GFP, heterozygous MOR28-IRES-gap-GFP (B6 background), and heterozygous MOR28-IRES-gap-GFP (129 background). (Right) Comparison of the number of cells counted in homozygous MOR28-IRES-gap-GFP, heterozygous MOR28-IRES-gap-GFP (129 background), wild-type 129 background, wild-type B6 background, and heterozygous MOR28-IRES-gap-GFP (B6 background). Cell counts in every fifth section were multiplied by 5 and subjected to Abercrombie correction (Low and Mombaerts, 2017, p. 175). Retrieved from https://doi.org/10.1016/j.neuroscience.2016.12.044.

1.12 The stability of *Olfr1507* gene choice

The Cre/loxP system has been implemented to study stability of OR gene choice (Shykind et al., 2004; Fuss et al., 2013). Of interest here, Shykind et al. 2004 reported gene-targeted strains MOR28-IRES-Cre-FNF and ΔMOR28-IRES-Cre-FNF. The expression of Olfr1507 and Cre recombinase serves as lineage marker that allows to assess the stability of OR choice and the fate of OSNs initially choosing the modified Olfr1507 allele. Based on the analysis of the MOR28-IRES-Cre-FNF strain, the authors suggested that an OSN expressing a functional OR continues to express this OR for the life of the cell. In contrast, labeled OSNs in ΔMOR28-IRES-Cre-FNF mice switch OR gene choice, possibly via a negative feedback signal that suppresses switching and stabilizes OR expression (Serizawa et al., 2003; Lewcock and Reed, 2004; Shykind et al., 2004). However, the stability of OR gene choice may be misinterpreted when working with Cre-expressing strains. A major caveat is that the threshold for Cre recombinase activity acting on the reporter gene is not known. Retention of the *FNF* cassette in the strain reported by Shykind et al., 2004 may affect the patterns and levels of expression for the Olfr1507 locus. Another possibility is that OR loci may be expressed transiently in bursts in immature or even mature OSNs, a scenario referred to as gene “twitching”, which cannot be distinguished from gene switching (Shykind et al., 2004; Mombaerts, 2006; Fuss et al., 2013). Expression of Cre above a certain level during the lifetime of an OSN may be sufficient for the reporter gene to be activated and the marker to be expressed for the remainder of the life of the cell (Fuss et al., 2013).

2 Materials and Methods

2.1 Materials

2.1.1 Mice

All mouse strains were designed using the gene-targeting strategy of Mombaerts et al., 1996, in which a target OR locus in the mouse genome is modified by homologous recombination in ES cells. The strategy allows for histological markers such as tauGFP, tauLacZ, or gapGFP to be co-expressed with the OR from the mutant allele. The gene-targeted mutation generates a bicistronic message, and the translation of the reporter is controlled by an *IRES* of viral origin.

The novel gene-targeted strains were generated by Ozgene (Perth, Australia) in the B6-derived ES cell line Bruce4 (Figure 2.1). Sperm was cryopreserved at The Jackson Laboratory (Maine, ME, USA) for public distribution after publication.

Mice were maintained in specified pathogen-free conditions in individual ventilated cages of the green line (Tecniplast, Italy). Mice were fed *ad libitum* with ssniff V1124-727 (ssniff, Germany). Nesting, bedding, and enrichment were provided as nestpak, Datesand Grade 6 (Datesand, United Kingdom). Mouse experiments were performed in accordance with the German Animal Welfare Act, European Communities Council Directive 2010/63/EU, and the institutional ethical and animal welfare guidelines of the Max Planck Research Unit for Neurogenetics. Approval came from the *Regierungspräsidium Darmstadt* and the *Veterinäramt* of the city of Frankfurt. All efforts were made to minimize the number of mice used and their suffering.

Table 1 List of unpublished strains

Nickname	Strain name	JAX official strain name	JAX JR#
Tintin	Olfr1507-IRES-tauGFP	B6.Cg-Olfr1507<tm1Mom>/MomJ	27250
Milou	Olfr1507-IRES-gapGFP	B6.Cg-Olfr1507<tm3Mom>/MomJ	30965
Snowy	Olfr1507-IRES-tauLacZ	B6.Cg-Olfr1507<tm2Mom>/MomJ	30516
Loki	Olfr1508-IRES-tauGFP	B6.Cg-Olfr1508<tm1Mom>/MomJ	30966
Shield	Olfr1509-IRES-tauGFP	B6.Cg-Olfr1509<tm1Mom>/MomJ	30967
Maveth	ΔOlfr1507-GFP	B6.Cg-Olfr1507<tm5Mom>/MomJ	35750

2.1.2 Targeting vectors

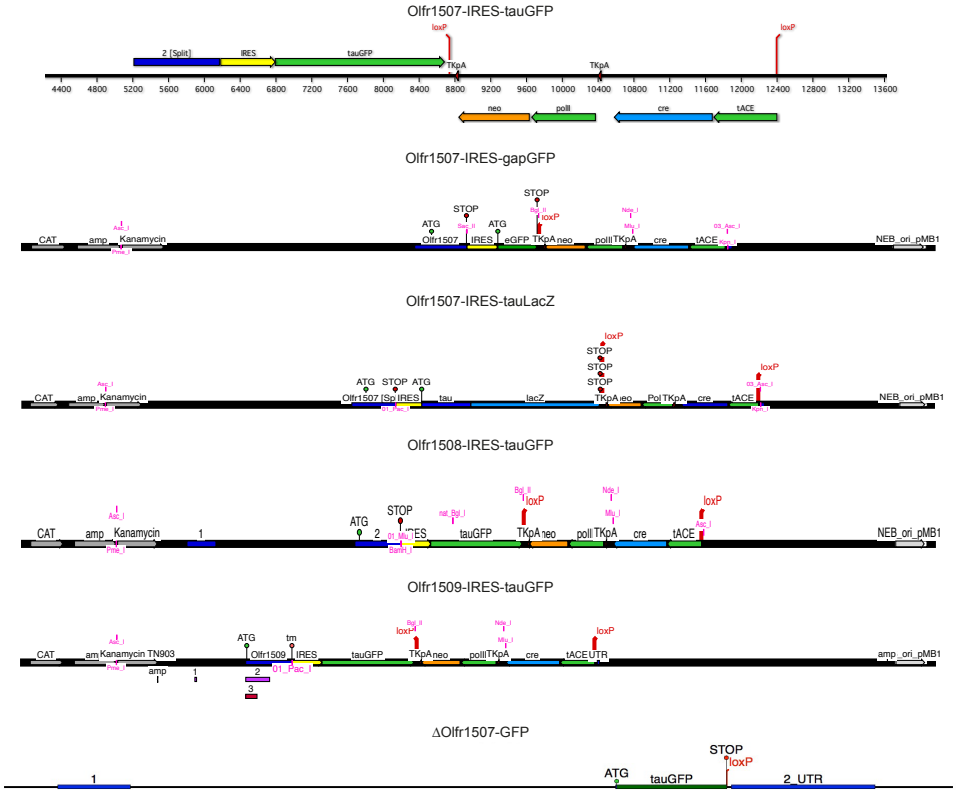


Figure 2.1. Targeting vectors.

Olfr1507 (*Or4e5*), *Olfr1508* (*Or4e1*), and *Olfr1509* (*Or4e2*) loci were modified by homologous recombination in ES cells. The sequence encoding *tauGFP* preceded by an internal ribosome entry site (*IRES*) was inserted after the stop codon of the OR gene. The *neo* cassette is self-excised during transmission through the male germline and is absent in all mice that were analyzed. Strains were generated by Ozgene (Perth, Australia) and sperm was cryopreserved at The Jackson Laboratory (Bar Harbor, ME, USA).

2.1.3 Reagents

2.1.3.1 Perfusion and embedding

Material	**Catalog number**	**Vendor**
Paraformaldehyde	201021-12	Electron Microscope Science
Phosphate Buffered Saline (PBS)	1003441003	Sigma-Aldrich
Ethylenediaminetetra-acetic acid (EDTA)	992156	Invitrogen
MiliQ water	F2HB71325	Biopack polisher
NaCl	16443401	B.Braun, Melsungen
Ketamine 10%	221	Serumwerk
Xylavet	21F235	cp-pharma
Sucrose	SLCG9690	Sigma
O.C.T.	2208109812	Tissue-Tek

2.1.3.2 Immunohistochemistry

Material	**Catalog number**	**Vendor**
RNAscope Target retrieval reagents	2010934	Advanced Cell Diagnostics
Triton X-100	017K00112	Sigma Ultra
Normal Donkey Serum	3286457	Millipore
DAPI	1942278	Invitrogen
Solid antifade	21123PK-3	Abberior
Hybridization oven UVP	HL-2000	Hybrilinker
Steamer	HD9140	Philips

2.1.3.3 Antibodies

Primary antibodies				
Antigen	**Host**	**Catalog number**	**Source**	**Optimal antibody dilution**
Olfr1507	Rabbit	OSR00212W	Osenses	1:2000
GFP	Chicken	GFP-1020	Aves Labs	1:1000
LacZ	Chicken	ab9361	Abcam	1:1000
OMP	Goat	019-22291	Wako	1:1000
VGLUT2	Guinea pig	135404	Synaptic Systems	1:1000
NQO1	Rabbit	ab34173	Abcam	1:500
OCAM	Goat	ECR032004A	R&D Systems	1:500

Secondary antibodies					
Host	**Target**	**Conjugate**	**Catalog number**	**Source**	**Optimal antibody dilution**
Donkey	Chicken	Alexa Fluor 488	703-545-155	Jackson Immunoresearch	1:500
Donkey	Rabbit	Alexa Fluor 555	A-32794	Invitrogen	1:500
Donkey	Guinea pig	Alexa Fluor 647	706-606-148	Jackson Immunoresearch	1:500
Donkey	Goat	Alexa Fluor 647P	A32849	Invitrogen	1:500

2.1.3.4 Genotyping

Material	Catalog number	Vendor
Direct PCR (Tail)	102-T	Biotech Inc.
Proteinase-K (pK)	BIO-37084	Meridian Bioscience
Taq HS, dNTP, 10x Buffer	R007A	Takara Bio Inc.
Nuclease-Free water	AM9937	Invitrogen
Agarose standard	3810.4	Roth
Tris Borate EDTA (TBE) 10x-Buffer	3061.2	Roth
Ethidium Bromide (EtBr)	2218.2	Roth
DNA ladder 100 bp	N3231L	Biolabs

2.1.4 Consumables

2.1.4.1 General consumables

Consumables	**Vendor**
Pipette tips (20 µl, 200 µl, 1000 µl)	RAININ, Mettler toledo
Eppendorf tubes (0.5 ml, 1.5 ml, 2.0 ml, 5.0 ml)	Eppendorf
PCR tubes	Thermo Scientific
Kimtech wipes	Kimberly-Clark
Pipettes (20 µl, 200 µl, 1000 µl)	RAININ
Syringes (1 ml, 12 ml, 20 ml)	B.Braun, Melsungen
Needles	B.Braun, Melsungen
Gloves	Microflex XCEED
Glassware	DURAN, Schott
Aluminum foil	Labor

2.1.4.2 Dissection

Tools	Catalog number	Vendor
Strabismus scissors	14074-09	FST
Hartman hemostats	13003-10	FST
Extra fine grief forceps	11150-10	FST
Dumont #5 fine forceps	11254-20	FST
Vannas spring scissors - 2.5 mm cutting edge	15000-08	FST
Extra fine grief forceps	11152-10	FST
Noyes spring scissors	15011-12	FST
Vannas spring scissors – 3 mm cutting edge	15000-10	FST
Extra fine micro dissecting scissors	RS-5882	Roboz Surgical Store
Large ring scissors 3.75” straight	RS-5850	Roboz Surgical Store
Double edge razor blades		PERSONNA

2.1.4.3 Cryoprotection and Immunohistochemistry

Material	Catalog number	Vendor
Multiwells	353046	Falcon
Granulated dry ice	DE31715140	Linde AG
Microtome blades Leica 818	121392117	Leica
Slides Super Frost Plus	121392117	Avantor, VWR
Parafilm	PM-996	Amcor
Coverslips 20 x 50 mm	48983	Avantor VWR

2.1.5 Equipment

Instrument	Model	Vendor
Scale	CS200	Ohaus
Shaker	Rotamax120	Heidolph
Vacuum pump	5305XK408525	Eppendorf
Stereomicroscope	Stemi 2000-C	Zeiss
Cryostat	CM3050S	Leica
Epi-fluorescent microscope Axioplan 2	HAL00	Zeiss
Hybridization oven	HL-2000	UVP Hybrilinker
Steamer	HD9140	Philips
Panoramic MIDI II	PMIDI-048909	3D Histech
Confocal microscope	LSM 800	Zeiss
Thermomixer	Compak 535	Eppendorf
Mini centrifuge	SN 1311 0714	VWR
Thermal cycler Simpli Amp	Life prof	Applied Biosystems
Gel electrophoresis	Power Pac Basic	BIO-RAD

Gel documentation	QUANTUM-ST4-1100	Peqlab
Fridge		Liebherr
Frezzer		Liebherr

2.1.6 Software

Software	Provider
Prism 9	Graphpad Software Inc., USA
Excel	Microsoft
Word	Microsoft
ZEN	Carl Zeiss GmBH, Jena
Fiji	Open-source software
Cell Profiler 4.1.3	Broad Institute, USA
Slide Viewer 2.5	3DHistech Ltd., USA
Zotero	Open-source software

2.1.7 Genotyping primers

Primer Name	**Sequence**	**Length (bp)**
MK1140-F	*CAT CTC ACC GTA GTC ACT CTG TTT*	24
MK1141-R	*GCT CAG CGT GAG TTT TTG TTC*	21
MK1142-F	*CTT CAA GGA GGA CGG CAA CAT C*	22
MK1271-F	*TTC TCC TTT GAT GCC TGT GTG*	21
MK1278-R	*GCA GGG TTA ATG TTC AGC ATG G*	22
MK1273	*TCG ACA AGG TGG TAT CGG TT*	20
MK1274	*CAG CCA AAA CTC TTT GAG GC*	20
MK99	*TAC ACA GTA AGA GTC AAG ATA AGG*	23
797	*TGG AGC CCG TCA GTA TCG GC*	20
819	*GAG AAG CGC GAT CAC ATG GTC CT*	23

2.2 Methods

2.2.1 Perfusion and cryoprotection

Tissue fixation is a key factor of processing of tissue samples. Overfixation prevents antibodies from reaching target antigens and underfixation results in the tissue continuing to degrade. Adequate cryoprotection impedes tissue damage and keeps the anatomical structure intact.

Mice were anesthetized with intraperitoneal injection of ketamine HCl and xylazine (120 mg/kg and 5 mg/kg body weight, respectively) and, after the onset of anesthesia, weighted and fixed under a stereomicroscope on a bench. Alcopads were used to mildly sterilize the fur. The skin was removed from the mouse thoracic cage. The ribcage was removed from the sternum to the throat and held with hemostats close to the mouse head. Once the thoracic organs were exposed, the left ventricle was pierced with the perfusion needle in a parallel direction to the heart and a snip with fine spring scissors (CAT# 15000-08 FST) was made at the right atrium. Care was taken not to pierce the needle through the interventricular septum of the heart. For 21 days old mice, 15 ml of ice-cold PBS were injected through the needle to wash out the blood, followed by 12 ml perfusion of ice-cold 4% PFA in 1 x PBS. For 56 day- old mice, 30 ml and 20 ml were used respectively (Figure 2.2).

After perfusion, a tail biopsy was collected for genotyping and the head was decapitated with scissors (CAT#RS-5882 Roboz Surgical Store). The skin, eyes, lower jaw, and palatine bone were removed for a better diffusion of buffers during incubation. The head was immersed for decalcification in 0.45 M EDTA in PBS and placed in a vacuum pump to remove the trapped air. Decalcification was performed at 4˚C on a shaker, overnight for PD21 mice and two overnights for PD56 mice. Samples were cryprotected in successive incubation of 15%, 25%, and 30% sucrose in PBS on a shaker at 4˚C overnight.

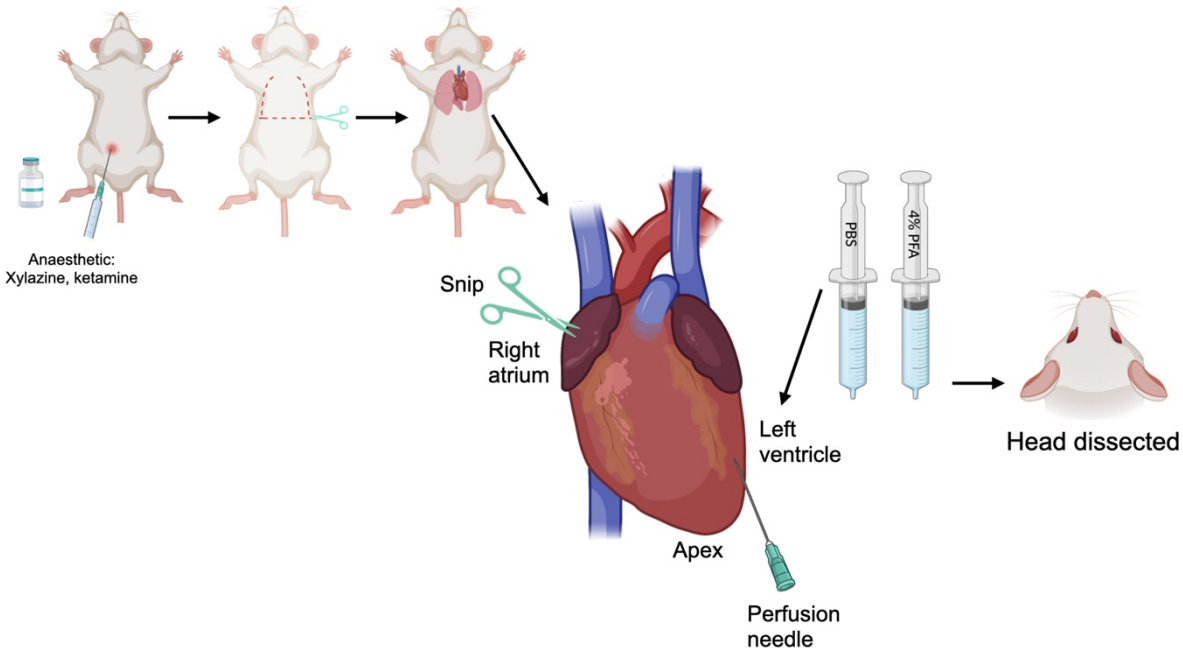


Figure 2.2. Perfusion protocol for mice at PD21 and PD56 (BioRender, 2024).

After cryoprotection, samples were trimmed to remove excess tissue and teeth. The caudal part of the brain was cut coronally and serves as a base for the positioning of the head during freezing. The prepared sample was immersed in a cylinder of aluminum foil filled with O.C.T. A precise positioning of the samples is critical for the collection of sections. Therefore, the samples were positioned consistently. The most rostral part, the tip of the nose, was oriented to point to the center of the cylinder and the coronal base, the most caudal part, of the head was lowered to the bottom (Figure 2.3). Afterwards the cylinder was placed in granulated dry ice until the O.C.T. was frozen. The frozen blocks were stored at -20˚C for sectioning.

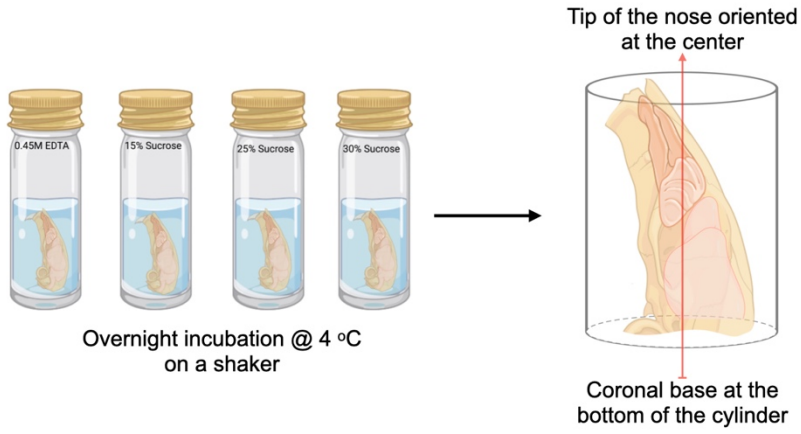


Figure 2.3. Cryoprotection and embedding of the samples (BioRender, 2024).

2.2.2 Sectioning

A consistent and reproducible method for sectioning is crucial for comparing and analyzing images among strains. Two sectioning methods were followed: one method to collect sections of the nasal cavity comprising olfactory mucosa for cell counting and another method for collecting sections of the OB to measure the glomerular area/volume. Frozen samples were sectioned with a Leica CM3050 S cryostat at 6 µm thickness and -21˚C. To begin collecting the sections, the septal organ was taken as the reference anatomical landmark in every sample. Sections of the MOE were collected one in every third and in sets of twelve in consecutive slides. The reference point to terminate the collection of sections was chosen according to the glomerular positions of the gene-targeted glomeruli in all strains. The reference end points were the end of the MOB left on the medial sides and the beginning of the brain cortex (Figure 2.4).

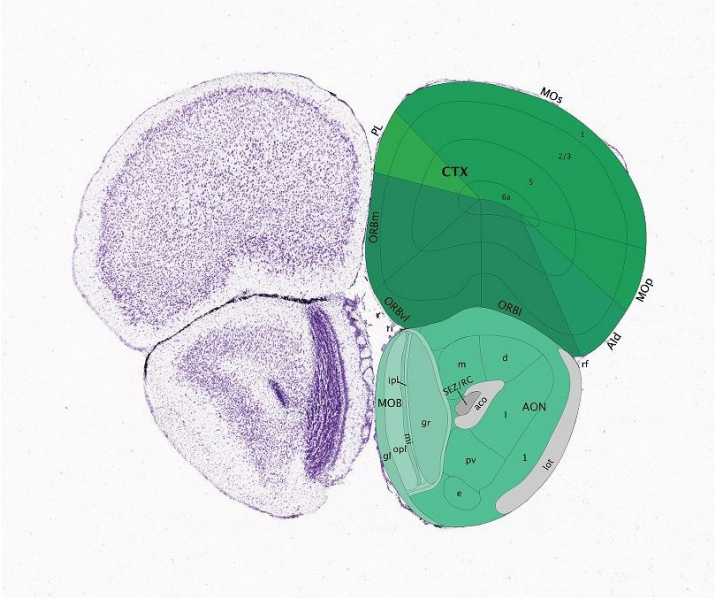


Figure 2.4. The reference end points for the collection of cryosections.

The first point is the cortex and the second point is the end of the MOB on the medial sides of the sample (Allen Institute from Brain Science, 2008). Retrieved from https://mouse.brain-map.org/static/atlas.

The OB sections were collected consecutively in sets of 18 in non-alternating slides starting from the ethmoturbinate III until the same anatomical point as described in the MOE part (Figure 2.3). Slides were stored at -20˚C for subsequent experiments.

2.2.3 Genotyping

2.2.3.1 Genomic DNA extraction

This method was used to extract genomic DNA from tail biopsies. Approximately 5 mm of tail biopsy obtained after perfusion from mice at PD21 was placed in screw capped tail tubes. The tail biopsy was kept at -20˚C until lysis. Before genotyping, tails were digested in a 202 µl mix of 1:100 Proteinase K (20 mg/ml) (Meridian Bioscience) in digestion buffer Direct PCR (tail) (Biotech Inc). Tails were incubated in a Thermomixer overnight at 55˚C, 300 rpm. The next day, tails were incubated to deactivate the Proteinase K at 85˚C, 300 rpm for 1 h. Lysed tails were stored at 4˚C until genotyping.

2.2.3.2 Genotyping protocols

The gene-targeted strains are unpublished and each strain targets highly homologous OR genes. Therefore, reliable and accurate genotyping is essential. To achieve a high level of confidence, specific primers for each strain were used to amplify specific DNA sequences of known length using PCR. The table below lists the pair of primers (Sigma-Aldrich) and the PCR program chosen for every gene-targeted strain (Table 2.1). For every strain, a primer pair for the wildtype (WT) allele and the mutated (MUT) allele were used. Negative (water) controls were used as well.

Table 2.1. List of primers for genotyping

Strain	**Oligo wildtype**	**WT band**	**Oligo mutant**	**MUT band**	**PCR**
Olfr1507-IRES-tauGFP	MK1140-F/MK1141-R	450 bp	MK1141-R/MK1142-F	706 bp	PCR1
Olfr1507-IRES-gapGFP	MK1140-F/MK1141-R	450 bp	819/MK1141-R	416 bp	PCR1
Olfr1507-IRES-tauLacZ	MK1140-F/MK1141-R	450 bp	797/MK1141-R	472 bp	PCR1
Olfr1508-IRES-tauGFP	MK1271/MK1278	919 bp	MK99/MK1278	477 bp	PCR1
Olfr1509-IRES-tauGFP	MK1273/MK1274	380 bp	MK99/MK1274	452 bp	PCR1

A standard reaction mix was used. For each reaction, 0.2 µl of each primer at 20 µM concentration was used (Table 2.2). Buffer, dNTPs, and Taq were provided by Takara Bio Inc. Protocol PCR 1 was used (Table 2.3).

Table 2.2. Reaction mix

Water	14.8 µl
10X Buffer	2.0 µl
dNTP	1.6 µl
Primer 1	0.2 µl
Primer 2	0.2 µl
Taq	0.2 µl

Table 2.3. PCR protocol for genotyping

Steps	**PCR1**
Initial denaturation	95˚C
DNA denaturation	95˚C
	60˚C
DNA polymerization	72˚C
Final polymerization	72˚C
Holding	4˚C

After PCR amplification, the DNA fragments were stained with loading dye (Life Technologies) and loaded on a 1.5% agarose (Roth) in TBE gel, and the NEB ladder was added. The gel was run at 120V in TBE buffer for approximately 30 min. Gel pictures were taken with PeqLab Geldoc. The preparation for the TBE buffer consists in diluting 10X concentrated TBE buffer 10-fold with MiliQ water.

2.2.4 Immunohistochemistry

Most PFA-fixed samples require an antigen retrieval step before IHC. Methylene bridges formed during fixation cross-link proteins and mask antigen sites. Antigen retrieval methods break these bonds and expose antigen site, allowing antibodies to bind. The method used was heat-induced epitope retrieval.

2.2.4.1 Antigen retrieval

Various antigen retrieval steps were tested to optimize visualization of the target protein. Prior to IHC, the frozen slides were taken out from the -20˚C freezer, put in the cryostat chamber, and dried individually with a hairdryer. Slides were placed on a slide staining rack for 20 samples and dried in the oven at 55˚C for 1.5 h. The preparation for the target retrieval buffer consisted in diluting 10X Target retrieval reagents 10-fold with MiliQ water. After heating for 7 min in a steamer, slides were left to cool for 20 min in 1x PBS solution. Additionally, slides were washed 2 times in 1x PBS/0.1 % Triton X-100 (PBS-T) for 7 min each.

2.2.4.2 IHC protocol

IHC was performed after the final step of antigen retrieval. Slides were blocked in 10% normal donkey serum (Sigma-Aldrich) in 0.1% Triton/PBS at room temperature for 2 h. The following primary antibodies were diluted in 2% donkey serum in 0.1% Triton/PBS and incubated at 4˚C overnight: to detect the Olfr1507 protein commercial rabbit antibodies against Olfr1507 were used at 1:1000 from Osenses. Green fluorescent protein (GFP) was detected with chicken GFP antibodies (1:500; Aves Labs). Mature OSNs were visualized with goat OMP antibody (olfactory marker

protein; 1:1000; Wako). Guinea pig VGLUT2 antibody (1:1000, Synaptic systems) labeled glomeruli. After incubation with primary antibodies, slides were then washed with 0.1% Triton/ PBS 3x5 min each followed by incubation with secondary antibodies at 1:500 in 2% normal donkey serum in 0.1% Triton/PBS: Alexa488 donkey anti-chicken (Jackson Immunoresearch), Alexa 555 donkey anti-rabbit (Invitrogen), Alexa 647P donkey anti-goat (Invitrogen), Alexa 647 donkey anti-guinea pig (Jackson Immunoresearch). Slides were washed in 0.1% Triton/PBS 3x5 min each followed by DAPI (Thermo Fisher Scientific) application for nuclei staining. Slides were mounted in Mount Solid antifade (abberior).

2.2.5 Cell counting

Following labeling with IHC, slides were scanned under a Panoramic MIDI Scanner II. Slides were analyzed offline and the counting of OSNs was done manually using the Slide Viewer Software (3D Histech Ltd.). All sections that contained mouse MOE were examined to obtain the number of GFP-immunoreactive cells. Gene-targeted strains expressing the same histological marker, tauGFP, were considered for comparative outcomes. GFP-immunoreactive OSNs of which the entire cell soma was visualized in a section were counted by visual inspection (Figure 2.5). Sampling methods were not used due to the spatial expression patterns of the trio of OR genes studied (Tsuboi et al. 1999; Zapiec and Mombaerts 2020). As a result of the collection of sections, the number of counted cells was relative. To obtain a better approximation of the number of labeled OSNs, the relative number of GFP-immunoreactive OSNs was multiplied by three, assuming there is a constant distribution of OSNs across sections.

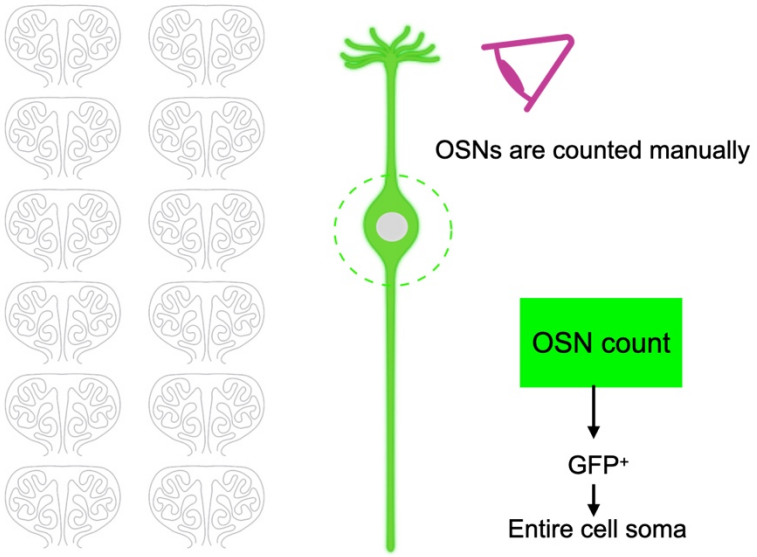


Figure 2.5. OSN counting.

Mice of gene-targeted strains expressing the tauGFP marker were manually analyzed offline. Each GFP-immunoreactive cell was counted when the entire cell soma could be viewed (BioRender, 2024).

To prevent overcounting of cells, the Abercrombie formula was performed on the counted cell number. This method is the most commonly used in biology for correcting the cell number. Counts are adjusted by a factor based on the section thickness (20 – 100 µm) and the average diameter of the particles being counted (Abercrombie 1946). The average nucleus diameter of 30 cells for each gene-targeted strain was measured in the X and Y dimensions using Slide Viewer Software (Figure 2.6 A) (3D Histech Ltd.) and ZEN blue only from the DAPI signal (Figure 2.6 B) (Carl Zeiss) for comparative results (Tables 2.4 – 2.5). For each gene-targeted strain, the correction factor was calculated using the formula:

$$C_f = \frac{section\ thickness}{nucleus\ diameter + section\ thickness}$$

Table 2.4. Correction factor using Slide Viewer Software

Strain	Nuclear diameter (µm)	Correction factor
Olfr1507-IRES-tauGFP	6.206	0.49
Olfr1508-IRES-tauGFP	6.23	0.49
Olfr1509-IRES-tauGFP	5.924	0.503

Table 2.5. Correction factor using Zen BLUE Software

Strain	Nuclear diameter (µm)	Correction factor
Olfr1507-IRES-tauGFP	6.789	0.47
Olfr1508-IRES-tauGFP	6.46	0.48
Olfr1509-IRES-tauGFP	6.59	0.47

The final estimated cell number for each strain was obtained by multiplying the counted cell number times the respective correction factor:

$$Estimated\ cell\ number = (Counted\ cell\ number) * (C_f)$$

Statistical analysis was performed using Graphpad Prism 9. Values are shown as the mean $\pm$ standard error of the mean. For multiple comparisons, the one-way ANOVA Newman-Keuls multiple comparison test was used to test for significance. Significance was set at $P \leq 0.05$.

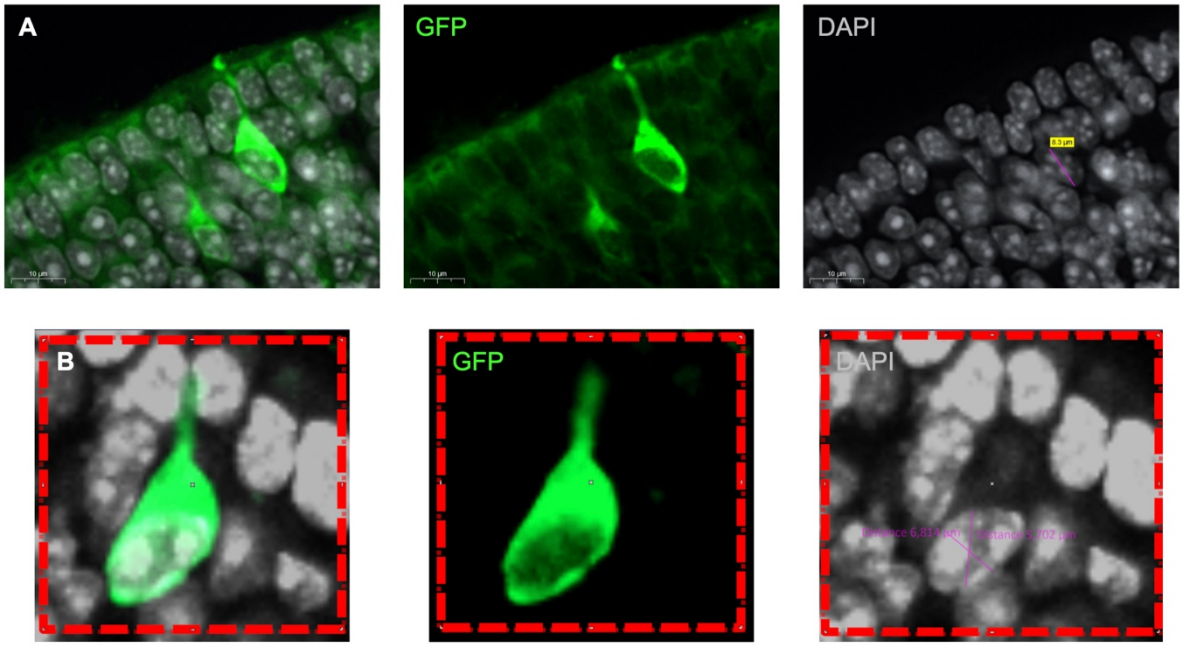


Figure 2.6. Comparison of nucleus diameters.

(A) Nucleus diameter measured with Slide Viewer. (B) Nucleus diameter measured with ZEN blue.

2.2.6 Glomerular volume

After immunostaining of OB sections, slides were scanned with a Panoramic MIDI Scanner II. OB coronal sections were examined with the Slide Viewer Software to select the sections that contained GFP-positive glomeruli. Images of fluorescent glomerular sections were taken with the Zeiss LSM 800 confocal microscope (Figure 2.7). Glomerular volume was measured using Microsoft Excel, Cell Profiler 4.1.3, and Graphpad Prism 9 was used for statistical analyses and graphs.

Glomeruli are spread over five sections on average but can span more than ten sections. In the Olfr1507-IRES-tauGFP, Olfr1508-IRES-tauGFP, and Olfr1509-IRES-tauGFP strains, the fluorescent glomeruli were distributed between 14 and 20 consecutive sections. An important factor to approximate the glomerular volume is the shape because glomeruli are not perfect spherical structures. The confocal images were acquired taking Z-stacks. Glomeruli were reconstructed by taking z-stack images with the confocal microscope within a range of 6 µm thickness in 1 µm

intervals throughout the OB sections that contained labeled GFP axons within the glomerular layer (Figure 2.7) (Bressel et al., 2016).

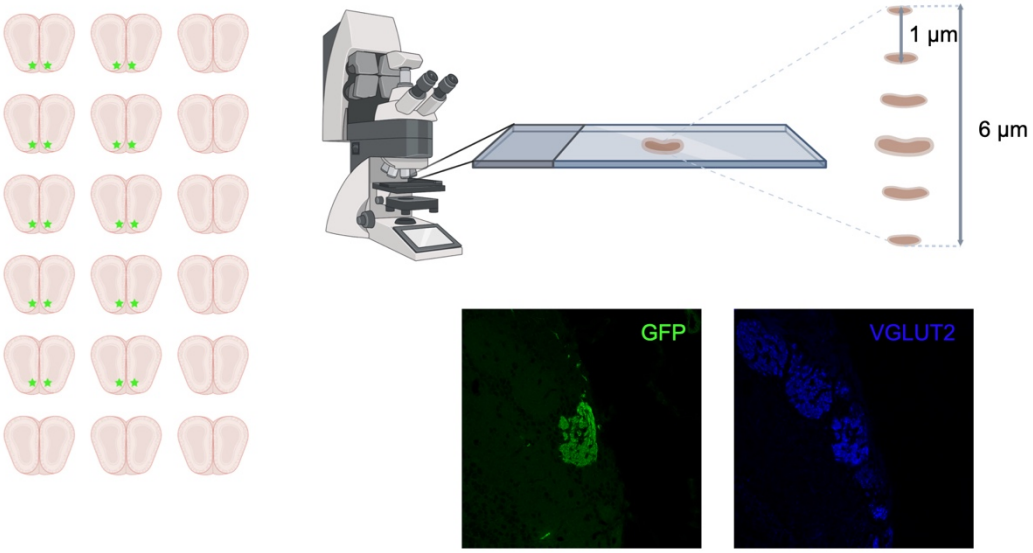


Figure 2.7. Acquisition of a Z-stack of GFP-immunoreactive glomeruli.

Co-staining with an antibody for vesicular glutamate transporter 2 (VGLUT2) allows to define the glomerular structures (BioRender, 2024).

Another factor to increase the efficiency of volume reconstruction was obtained by colabeling the OB sections with an antibody for vesicular glutamate transporter 2 (VGLUT2), a robust marker of glomeruli that labels only OSN axon termini within glomeruli (Greer et al., 2010) and GFP that labels OR-specific glomeruli but it also labels axons in the olfactory nerve layer. The VGLUT2 signal was used to define the glomerular structure excluding the axonal layer by thresholding this signal to perform semi-automated image segmentation (Figure 2.7). Each Z-stack confocal image was processed using a custom pipeline that we developed specifically for these studies. The surface area was measured using a CellProfiler pipeline programmed to segment VGLUT2-stained glomeruli on OB sections. In each optical section from the Z-stack with GFP and VGLUT2 positive signal, the glomerular contour was delimited as the overlapping region of the GFP and VGLUT2 staining. These areas were added and multiplied by the optical section thickness (1 µm) to get the total glomerular volume:

$$Total\ glomerular\ volume = (\sum overlapping\ region\ \ GFP^{+}/VGLUT2^{+}) * 1\ \mu m$$

The glomerular volume was calculated as three different measurements: total medial glomerular volume, total lateral glomerular volume, and total glomerular volume per mouse (TGV) for each of the tauGFP gene-targeted strains (Bressel et al., 2016).

3 Results

3.1 Zonal expression of *Olfr1507*, *Olfr1508*, and *Olfr1509*

Olfr1507, *Olfr1508*, and *Olfr1509* were reported to be expressed in the most dorsolateral and ventromedial areas of the MOE, by using ISH (Tsuboi et al., 1999). The mouse MOE can be divided into two broad regions, with a well-demarcated boundary. OSNs in the dorsal region express quinone oxidoreductase (NQO1) and olfactory-specific medium-chain acyl coenzyme A (CoA) synthetase (OMACS). OSNs in the ventral region express olfactory cell adhesion molecule (OCAM, also known as NCAM2) (Yoshihara et al., 1997; Gussing et al., 2004; Oka et al., 2006; Bozza et al., 2009; Zapiec and Mombaerts, 2020).

I performed IHC in MOE sections of homozygous Olfr1507-IRES-tauGFP, Olfr1508-IRES-tauGFP, or Olfr1509-IRES-tauGFP mice at PD21 (Figure 3.1) with a GFP antibody to visualize the GFP-immunoreactive cells. Additionally, I used NQO1 and OCAM antibodies to demarcate the dorsal vs. ventral region of the MOE. My results revealed that GFP-immunoreactive OSNs are indeed located in the OCAM-immunoreactive region of the MOE (Figure 3.2).

The expression pattern of these three OR genes correspond roughly to zone 1 according to the nomenclature of the Axel laboratory for rats (Vassar et al., 1993) and zone 4 according to the nomenclature of the Buck laboratory for mice (Ressler et al., 1993; Sullivan et al., 1996). *Olfr1507* defines the Zolfr1507 zone (Zapiec and Mombaerts, 2020). The GFP-immunoreactive cells in the 3 strains are located within the most dorsolateral area (Figure 3.2 A – C) and ventromedial area (Figure 3.2 D – F) of the MOE, consistent with ISH data (Tsuboi et al., 1999). The GFP-immunoreactive cells reside within OCAM-immunoreactive region and not in the NQO1-immunoreactive region of the MOE.

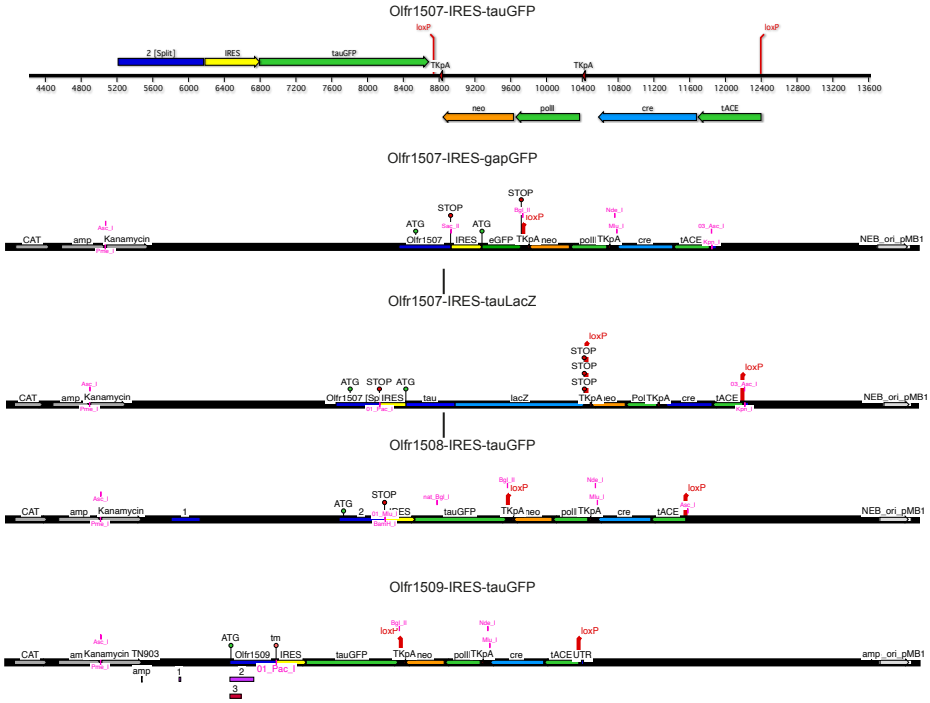


Figure 3.1. Gene targeting.

Olfr1507 (*Or4e5*), *Olfr1508* (*Or4e1*), *Olfr1509* (*Or4e2*) loci were modified by homologous recombination in ES cells. The sequence encoding *tauGFP* preceded by an internal ribosome entry site (*IRES*) was inserted after the stop codon of the OR gene. The *neo* cassette is self-excised during transmission through the male germline and is absent in the mice that were analyzed. Strains were generated by Ozgene (Perth, Australia) and sperm was cryopreserved at The Jackson Laboratory (Bar Harbor, ME, USA).

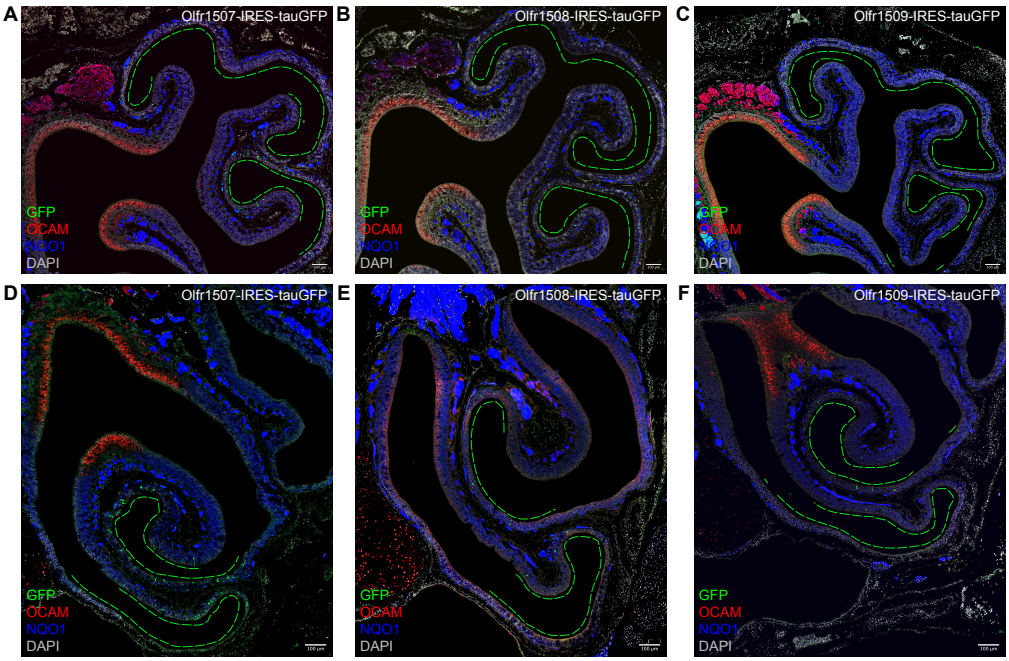


Figure 3.2. Location of GFP-immunoreactive cells in the main olfactory epithelium of mice at PD21.

(A – C) Confocal images at low magnification of coronal sections showing the dorsolateral area of the MOE of a homozygous Olfr1507-IRES-tauGFP mouse (A), homozygous Olfr1508-IRES-tauGFP mouse (B), and homozygous Olfr1509-IRES-tauGFP mouse (C). (D – F) Confocal images at low magnification of coronal sections showing the ventromedial area of the MOE of a homozygous Olfr1507-IRES-tauGFP mouse (D), a homozygous Olfr1508-IRES-tauGFP mouse (E), and a homozygous Olfr1509-IRES-tauGFP mouse (F). The green-dashed lines indicate the areas of the MOE in which GFP-immunoreactive OSNs (green) reside. These OSNs are located in the OCAM-immunoreactive region (blue) but not in the NQO1-immunoreactive region (red). Data were obtained from nine mice.

3.2 Testing a commercially available Olfr1507 antibody in Olfr1507 gene-targeted strains

Of 21 commercially available antibodies raised for mouse ORs, 6 were reported to yield reproducible immunoreactive signal in the mouse MOE (Low and Mombaerts, 2017). Factors that can affect the specificity of OR antibody signal are the high sequence homology between ORs, post-translational modifications, protein folding, protein-protein interactions, and fixation crosslinking. Additionally, antigen retrieval can be performed to unmask the epitope in order to improve the detection (Shi et al., 2001; Emoto et al., 2005; Low and Mombaerts, 2017). The commercially available antibody for Olfr1507, called OSR00212W (Osenses), was raised in New Zealand white rabbits immunized with a synthetic peptide from mouse Olfr1507 conjugated to blue carrier protein. The Olfr1507 antibody has been tested in the MOR28-IRES-gap-GFP strain by Low and Mombaerts, 2017 (Figure 1.7 of the Introduction).

I subjected MOE sections of homozygous Olfr1507-IRES-tauGFP mice at PD21 to triple IHC (Figure 3.3). OMP is a marker for mature OSNs (Figure 3.3 A1 – A3). The GFP-immunoreactive signal is observed in dendrites, somata, and axons of Olfr1507-GFP OSNs (Figure 3.3 A1). The Olfr1507 antibody produces strong immunoreactivity in the dendritic knobs and cilia, along the dendritic processes, and within the somata of Olfr1507-immunoreactive OSNs (Figure 3.3 A2). Importantly, the Olfr1507-immunoreactive cells colocalize with the GFP-immunoreactive cells (Figure 3.3 A3), thereby validating the specificity of the Olfr1507 antibody at the level of the MOE.

Next, I performed the same combination of triple IHC on MOE sections of homozygous Olfr1507-IRES-gapGFP mice at PD21 with antibodies for OMP, Olfr1507, and GFP (Figure 3.3 B1 – B3). The GFP-immunoreactive signal (Figure 3.3 B1) and the Olfr1507-immunoreactive signal (Figure 3.3 B2) colocalize within the same, OMP-immunoreactive cells (Figure 3.3 B3).

I analyzed a third gene-targeted strain, Olfr1507-IRES-taulacZ, to further test the specificity of the Olfr1507 and compare the signals. I performed triple IHC on MOE sections of homozygous Olfr1507-IRES-taulacZ mice at PD21 using antibodies for OMP, Olfr1507, and LacZ/beta-galactosidase (Figure 3.3 C1 – C3). The staining

pattern in Olfr1507-IRES-tauLacZ mice is similar to that in Olfr1507-IRES-tauGFP mice and Olfr1507-IRES-gapGFP mice. LacZ immunoreactivity occurs along the dendritic processes and within the somata of Olfr1507-immunoreactive OSNs (Figure 3.3 C1). Olfr1507 immunoreactivity is within the somata of OSNs (Figure 3.3 C2). The LacZ-immunoreactive cells colocalize with the Olfr1507-immunoreactive OSNs (Figure 3.3 C3). The number of LacZ-immunoreactive OSNs is lower compared to the numbers in strains expressing the GFP reporter. The reason for this difference is unclear.

Finally, I performed triple IHC on MOE sections of MOR28-IRES-gap-GFP mice at PD21, the non-inbred strain from the Sakano laboratory (Figure 3.3 D1 – D3). GFP-immunoreactive signal is observed in dendrites, somata, and axons of Olfr1507-GFP OSNs (Figure 3.3 D1). There is strong Olfr1507 immunoreactivity in the dendritic knobs and cilia, along the dendritic processes, and within the somata of Olfr1507-immunoreactive OSNs (Figure 3.3 D2). The Olfr1507-immunoreactive cells colocalize with the GFP-immunoreactive cells (Figure 3.3 D3).

Taken together, the commercially available rabbit antibody raised against an Olfr1507 peptide yields a specific immunoreactive signal in the MOE of three inbred gene-targeted strains: Olfr1507-IRES-tauGFP, Olfr1507-IRES-gapGFP, or Olfr1507-IRES-tauLacZ mice. The Olfr1507 immunoreactive signal is also specific in the MOE of the non-inbred MOR28-IRES-gap-GFP strain.

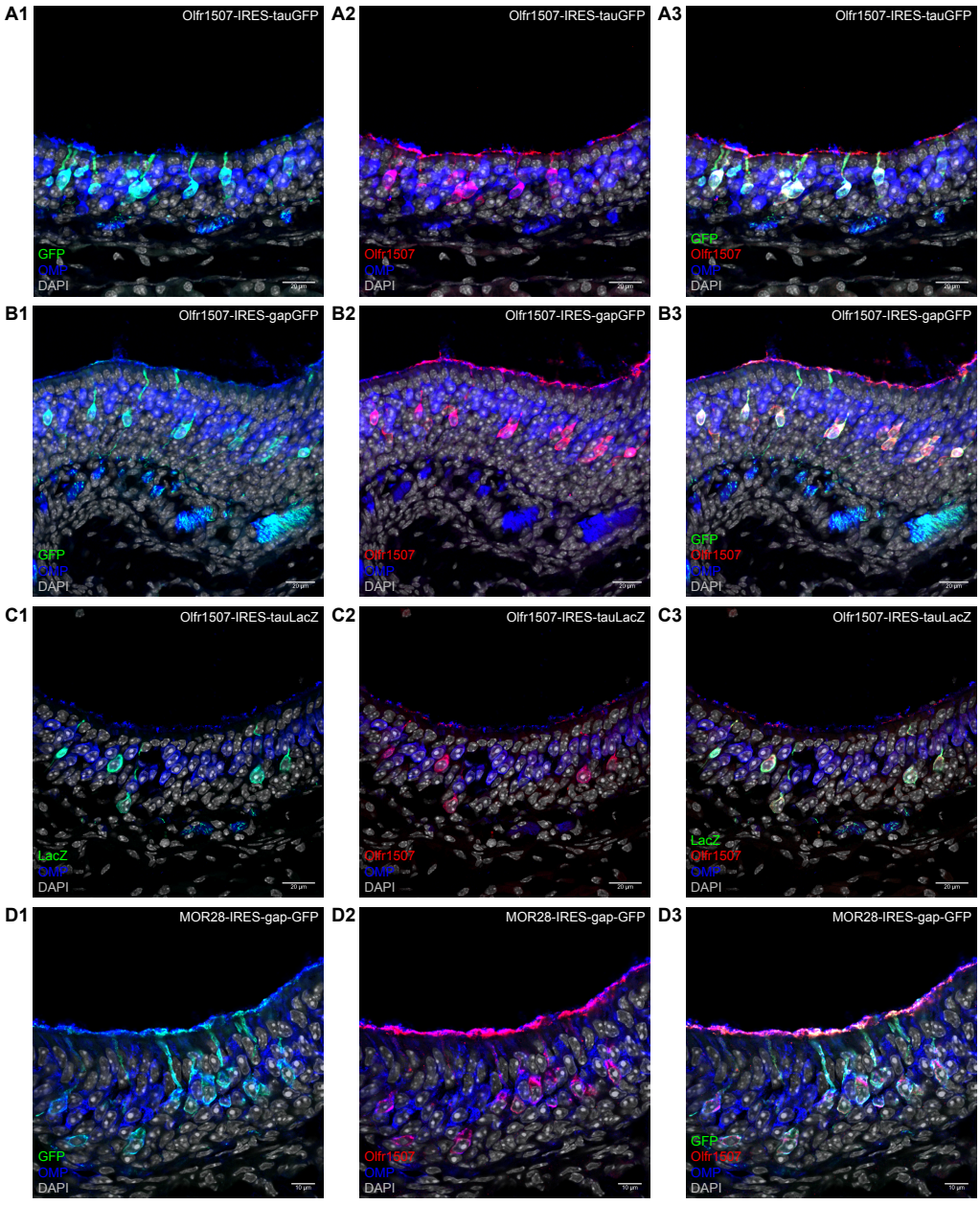


Figure 3.3. Olfr1507-immunoreactivity in the main olfactory epithelium of homozygous Olfr1507-IRES-tauGFP, Olfr1507-IRES-gapGFP, Olfr1507-IRES-tauLacZ, or MOR28-IRES-gap-GFP mice at PD21.

Confocal images of coronal sections of the MOE subjected to triple IHC for OMP (blue), Olfr1507 (red), and either GFP or LacZ (green). (A1 – A3) Homozygous Olfr1507-IRES-tauGFP mouse. (B1 – B3) Homozygous Olfr1507-IRES-gapGFP mouse. (C1- C3) Homozygous Olfr1507-IRES-tauLacZ mouse. (D1 – D3) Homozygous MOR28-IRES-gap-GFP mouse. GFP-immunoreactivity is detectable in the dendritic knobs, the dendrite, somata and axons. LacZ-immunoreactivity is detectable in somata and along axons. Strong Olfr1507-immunoreactivity is detectable in the dendritic knobs, cilia, and somata. The Olfr1507-immunoreactive OSNs show complete concordance with the GFP-

immunoreactive cells or LacZ-immunoreactive cells. DAPI served as nuclear stain. Data were obtained from 15 mice.

3.3 Testing the specificity of the Olfr1507 antibody in Olfr1508 and Olfr1509 gene-targeted strains

The OR gene cluster containing *Olfr1507*, *Olfr1508*, and *Olfr1509* has been studied for a quarter of a century to examine how OSNs expressing highly homologous OR genes project their axons to the OB. These OR genes share 75-95% similarities in their predicted amino acid sequence.

To further test the specificity of the commercially available Olfr1507 antibody, I examined whether OSNs expressing Olfr1508 or Olfr1509 might also be labeled, perhaps weakly. I subjected MOE sections of homozygous Olfr1508-IRES-tauGFP mice (Figure 3.4 A1 – A3) and homozygous Olfr1509-IRES-tauGFP mice (Figure 3.4 B1 – B3) at PD21 to triple IHC with antibodies for OMP, Olfr1507, and GFP. I found that Olfr1507-immunoreactive cells do not colocalize with GFP-immunoreactive cells in either strain. In other words, the staining patterns for GFP and Olfr1507 are mutually exclusive in these two strains.

Taken together, there is no crossreactivity of the Olfr1507 antibody at the level of the MOE. These results are a further validation of the specificity of the Olfr1507 antibody.

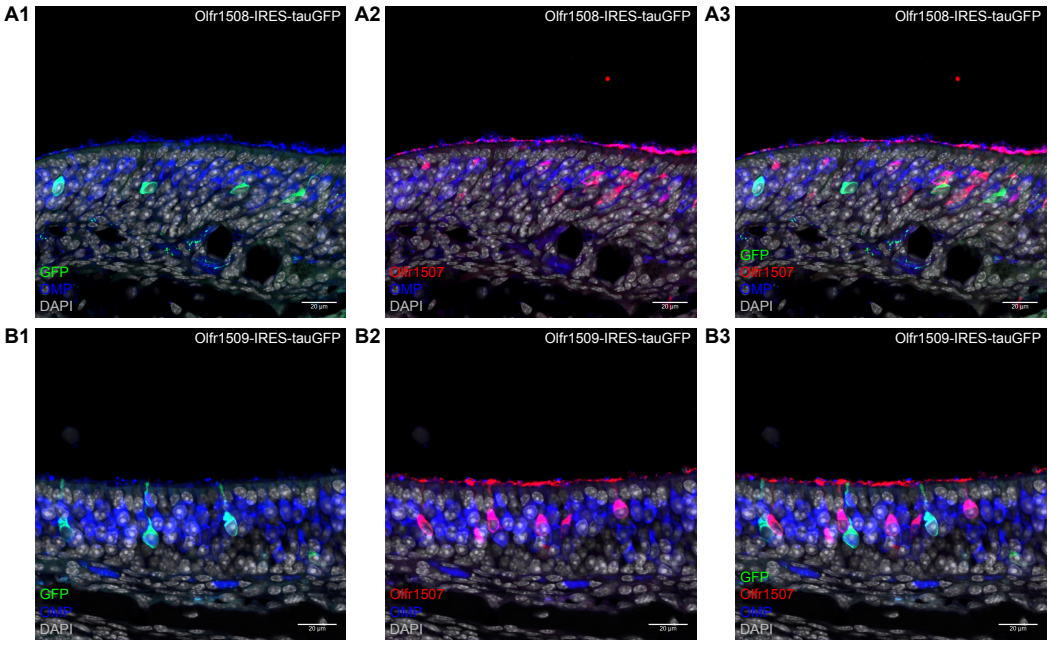


Figure 3.4. Olfr1507-immunoreactivity in the main olfactory epithelium of homozygous Olfr1508-IRES-tauGFP or Olfr1509-IRES-tauGFP mice at PD21.

Confocal images of coronal sections of the MOE of subjected to triple IHC for OMP (blue), Olfr1507 (red), and GFP (green). (A1 – A3) Homozygous Olfr1508-IRES-tauGFP mouse. (B1 – B3) Homozygous Olfr1509-IRES-tauGFP mouse. GFP-immunoreactivity is detectable in the dendrites, somata and axons. Strong Olfr1507-immunoreactivity is detectable in the dendritic knobs, cilia, and somata. GFP-immunoreactive OSNs are not immunoreactive for Olfr1507 and vice versa. DAPI served as nuclear stain. Data were obtained from 10 mice.

3.4 Cell counts of OSNs expressing Olfr1507, Olfr1508, or Olfr1509

There is a limited body of literature with quantification of the numbers of OSNs expressing a given OR in individual mice (Fuss et al., 2007; Rodriguez-Gil et al., 2010; Khan et al., 2011; Bressel et al., 2016; Low and Mombaerts, 2017).

I counted the number of GFP-immunoreactive cells per mouse in coronal sections of the MOE of homozygous Olfr1507-IRES-tauGFP mice (n = 5), homozygous Olfr1508-IRES-tauGFP mice (n = 5), and homozygous Olfr1509-IRES-tauGFP mice (n = 5) at PD21. The total cell numbers obtained are, from high to low: Olfr1507 (55,474 $\pm$ 8352), Olfr1509 (22,368 $\pm$ 6868), and Olfr1508 (14,306 $\pm$ 5218) (Figure 3.5). There is a significant difference in the number of GFP-immunoreactive cells between Olfr1507-IRES-tauGFP mice and Olfr1508-IRES-tauGFP mice ($P = 0.0013$, one-way ANOVA), and between Olfr1507-IRES-tauGFP mice and Olfr1509-IRES-tauGFP mice ($P = 0.0052$, one-way ANOVA) (double asterisks in Figure 3.5). The numbers of GFP-immunoreactive cells in Olfr1508-IRES-tauGFP mice and Olfr1509-IRES-tauGFP mice do not differ significantly ($P = 0.0772$, one-way ANOVA).

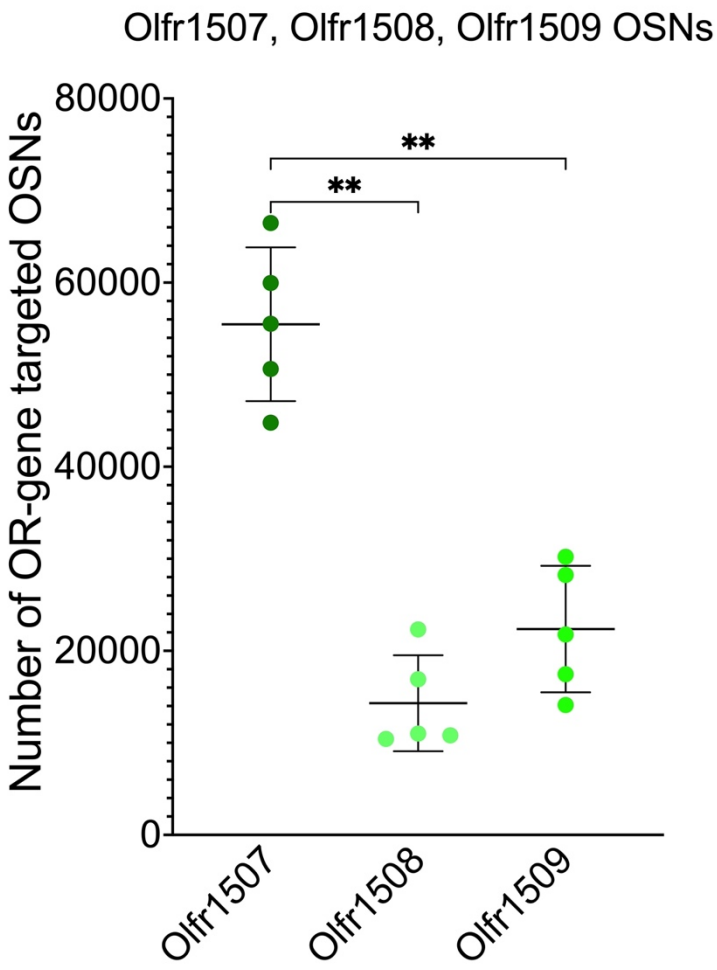


Figure 3.5. Cell counts for Olfr1507, Olfr1508, or Olfr1509 in gene-targeted strains.

Number of GFP-immunoreactive cells in homozygous Olfr1507-IRES-tauGFP mice (n=5), homozygous Olfr1508-IRES-tauGFP mice (n=5), or homozygous Olfr1509-IRES-tauGFP mice (n=5) mice at PD21. The horizontal lines indicate the median and standard deviation (SD). Olfr1507 is statistically different from Olfr1508 and Olfr1509 (double asterisks). There is no significant difference between Olfr1508 and Olfr1509. Data represent results from 15 mice.

3.5 Abercrombie correction of the numbers of cells expressing Olfr1507, Olfr1508, or Olfr1509

A commonly used formula in biology and neuroscience is the Abercrombie formula for estimating the number of cells in a tissue or structure of interest (Abercrombie, 1946). I applied the Abercrombie correction to cope with overcounting of cells in the sections. I employed two software programs, Slide Viewer and ZEN BLUE, to determine the average nuclear diameter of the GFP-immunoreactive cells (see Methods). I then calculated two distinct correction factors for each of the 3 strains, which I subsequently applied to my cell counts (Figure 3.6).

After applying the Abercrombie factor obtained from measuring the nuclear diameter in the Slide Viewer software program, the counts of GFP-immunoreactive OSNs, arranged in descending order, are as follows: Olfr1507-IRES-tauGFP (27,269 $\pm$ 4106), Olfr1509-IRES-tauGFP (11,255 $\pm$ 3456), or Olfr1508-IRES-tauGFP (7,019 $\pm$ 2560) (Figure 3.6 left). Similarly, the cell counts when corrected with Abercrombie factors obtained using the ZEN BLUE software program, are as follows: Olfr1507-IRES-tauGFP (26,026 $\pm$ 3918), Olfr1509-IRES-tauGFP (10,653 $\pm$ 3271), or Olfr1508-IRES-tauGFP (6,889 $\pm$ 2513) (Figure 3.6 right). Thus, applying the Abercrombie correction halves the cell counts and does not affect the ranking pattern of the raw cell counts. Statistical comparison of GFP-immunoreactive OSNs using the Slide Viewer software program does not show a significant difference between the counts for Olfr1508 and Olfr1509 ($P = 0.0626$, one-way ANOVA) but a significant difference between the counts for Olfr1507 vs. the counts for Olfr1508 ($P = 0.0013$) and Olfr1509 ($P = 0.0058$) (double asterisks in Figure 3.6). The OSN numbers yielded similar P values in the statistical analysis conducted after corrections based on the ZEN BLUE software program: $P = 0.0770$ between Olfr1508 and Olfr1509 (no significant difference), $P = 0.0014$ between Olfr1507 and Olfr1508 and $P = 0.0056$ between Olfr1507 and Olfr1509 (Figure 3.6).

A caveat of the Abercrombie correction is that it makes several assumptions about the geometry and distribution of the objects being counted. It may not always provide accurate estimates. Careful sample preparation, adequate imaging, and systematic counting techniques are also important for obtaining reliable results.

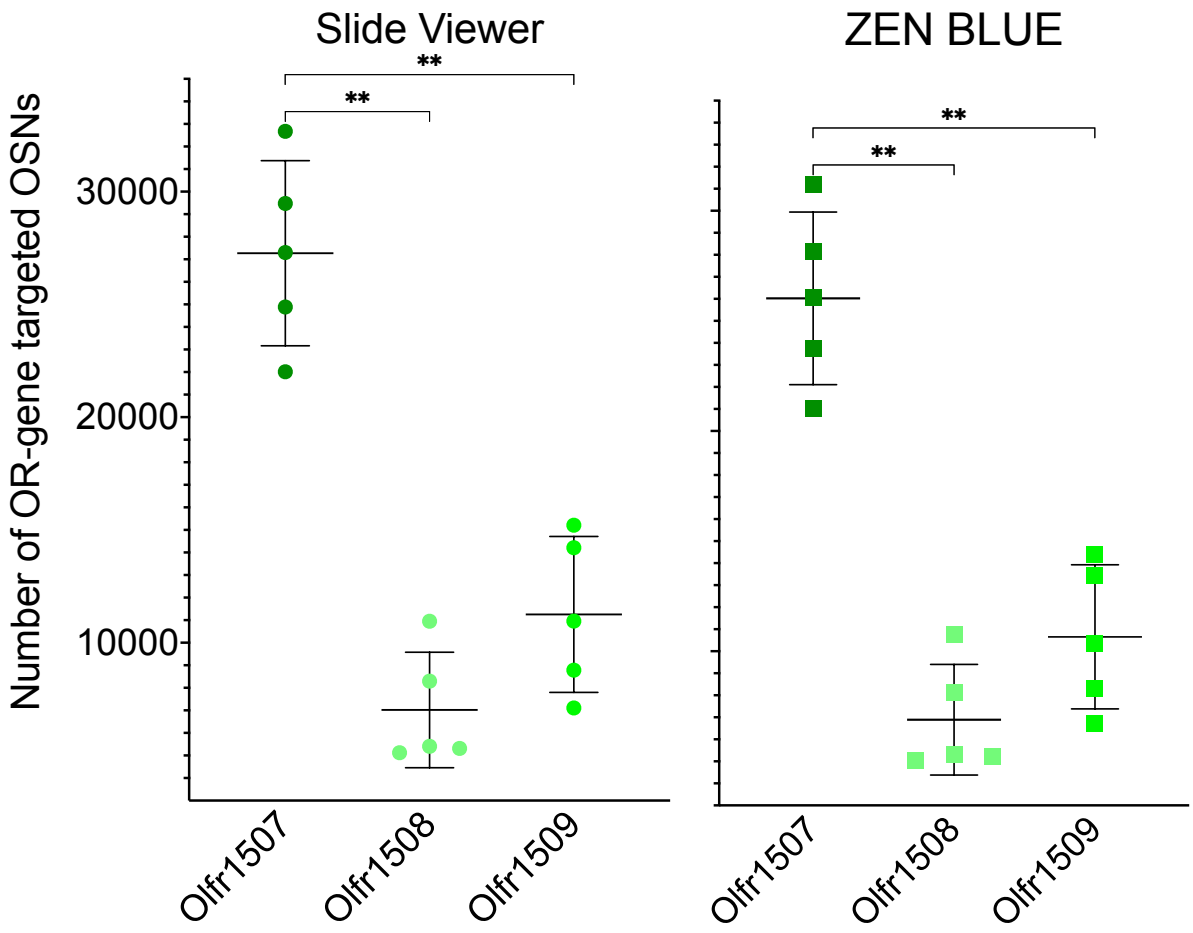


Figure 3.6. Cell counts for Olfr1507, Olfr1508, or Olfr1509 in gene-targeted strains after Abercrombie correction.

Number of GFP-immunoreactive cells in homozygous Olfr1507-IRES-tauGFP mice (n=5), homozygous Olfr1508-IRES-tauGFP mice (n=5), or homozygous Olfr1509-IRES-tauGFP mice (n=5) at PD21 using Slide Viewer and ZEN BLUE software programs. The horizontal lines indicate the median and standard deviation (SD). Statistically significant differences are indicated with double asterisks. Data represent results from 15 mice.

3.6 The Olfr1507 antibody in the olfactory bulb of different *Olfr1507* gene-targeted strains

OSNs that express a given OR gene send convergent axonal projections to a small area within the medial and lateral half-OB. Within each half-OB, axons coalesce usually into a single homogeneous glomerulus in adult mice (Treloar et al., 2002). Axonal coalescence was first demonstrated by methods of RNA ISH in rat (Vassar et al., 1994) and mouse (Ressler et al., 1994). These experiments detected mRNA for ORs within OSN axons and axon terminals. But the radioactive ISH technique is difficult to perform, relies on the presence of mRNA transcripts of ORs in axon termini, works only for a subset of OR genes, and cannot always distinguish with certainty between highly related OR genes.

The OR-IRES-marker strategy has become the standard approach for the characterization of OR-specific glomeruli (Mombaerts et al., 1996). This strategy is based on homologous integration of axonal marker genes such as tauLacZ or tauGFP at OR loci by gene targeting in embryonic stem cells. Coexpression of the OR and the axonal histological marker occurs at the level of translation by virtue of an IRES. In my project, the OR-IRES-tauGFP strategy enables the specific labeling of not only dendrites and cell bodies but also axons and axon termini of OSNs expressing Olfr1507, Olfr1508, or Olfr1509.

I analyzed homozygous Olfr1507-IRES-tauGFP, Olfr1507-IRES-gapGFP, or Olfr1507-IRES-tauLacZ mice at PD21 to verify the specificity of the Olfr1507 antibody and to characterize the glomerular phenotype. I conducted triple IHC for VGLUT2 or OMP, Olfr1507, and GFP or LacZ on consecutive 6 µm coronal sections of the OB. I used an antibody for GFP and for Olfr1507 to identify the positions of the Olfr1507 glomeruli. The Olfr1507 antibody enables the detection of Olfr1507 at the protein level, including in OSN axon termini. I employed a VGLUT2 antibody in the Olfr1507-IRES-tauGFP strain to label OSN axon termini and thereby outline the glomerular structures within the OB to use for further analysis. The OMP antibody labels OSN axons within the olfactory nerve layer in the OB (Treloar et al., 2002). I scanned OB sections using a MIDI Slide scanner and carried out more detailed observations under a confocal microscope.

I observed a single homogeneous Olfr1507-immunoreactive glomerulus per medial half-OB and lateral half-OB (Figure 3.7, 3.8 A1 – A3). GFP-immunoreactive axons in the Olfr1507-IRES-tauGFP or Olfr1507-IRES-gapGFP strains consistently coalesce into a single homogeneous glomerulus per medial half-OB and lateral half-OB (Figure 3.7, 3.8 A1, B1). In homozygous Olfr1507-IRES-tauGFP mice, as expected, the Olfr1507-immunoreactive signal shows complete concordance with the GFP-immunoreactive signal in both halves-OB (Figure 3.7, 3.8 A3). The Olfr1507-immunoreactive and GFP-immunoreactive signals visualize a single homogeneous glomerulus in the medial half-OB (Figure 3.7 B3) and lateral half-OB (Figure 3.8 B3) of homozygous Olfr1507-IRES-gapGFP mice. The glomerular phenotype of Olfr1507-IRES-gapGFP mice is comparable to that of Olfr1507-IRES-tauGFP mice. Finally, I performed triple IHC on OB sections of homozygous Olfr1507-IRES-tauLacZ mice using antibodies for OMP, Olfr1507, and LacZ. I found that LacZ-immunoreactive axons in the Olfr1507-IRES-tauLacZ strain consistently coalesce into a single homogeneous glomerulus per medial half-OB (Figure 3.7 C1) and lateral half-OB (Figure 3.8 C1). There is one Olfr1507-immunoreactive glomerulus per medial half-OB (Figure 3.7 C2) and lateral half-OB (Figure 3.8 C2). I observed complete concordance with the LacZ-immunoreactive signal (Figure 3.7, 3.8 C3). Based on observations under a confocal microscope, Olfr1507-immunoreactive and LacZ-immunoreactive glomeruli occupy 8 to 10 OB consecutive sections, which is fewer sections than in Olfr1507-IRES-tauGFP or Olfr1507-IRES-gapGFP mice, which are in a range between 14 to 20 sections. The lower number of OB sections containing a LacZ-immunoreactive glomerulus is consistent with a lower number of LacZ-immunoreactive OSNs.

Taken together, my IHC results indicate that homozygous Olfr1507-IRES-tauGFP, Olfr1507-IRES-gapGFP, or Olfr1507-IRES-tauLacZ mice consistently exhibit one medial and one lateral homogeneous Olfr1507-immunoreactive glomerulus and one GFP-immunoreactive or LacZ-immunoreactive glomerulus per half-OB. The OSNs of mice expressing the gapGFP axonal marker are comparable to those expressing the tauGFP axonal marker. There are fewer OSNs in mice expressing the taulacZ axonal marker.

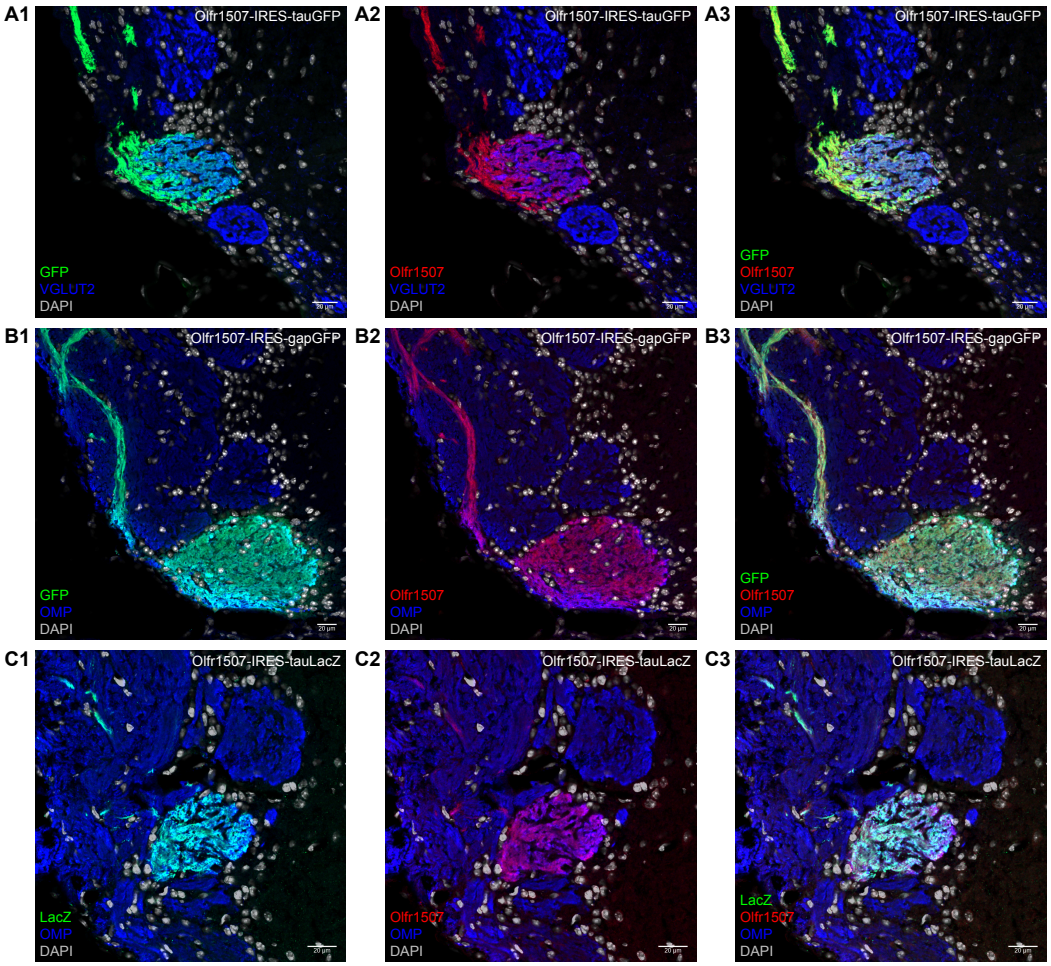


Figure 3.7. The Olfr1507 glomerulus in the medial half-olfactory bulb of homozygous Olfr1507-IRES-tauGFP, Olfr1507-IRES-gapGFP or Olfr1507-IRES-tauLacZ mice at PD21.

Confocal images of coronal sections showing the medial half-OB subjected to triple IHC for either VLGUT2 or OMP (blue), Olfr1507 (red), and either GFP or lacZ (green). (A1 – A3) Homozygous Olfr1507-IRES-tauGFP mouse. (B1 – B3) Homozygous Olfr1507-IRES-gapGFP mouse. (C1 – C3) Homozygous Olfr1507-IRES-tauLacZ mouse. A single homogeneous glomerulus is strongly immunoreactive for GFP or lacZ. One glomerulus is immunoreactive for Olfr1507. A single homogeneous glomerulus is immunoreactive for both GFP and Olfr1507 (A3 and B3) or for both LacZ and Olfr1507 (C3). DAPI served as nuclear stain. Data were obtained from nine mice.

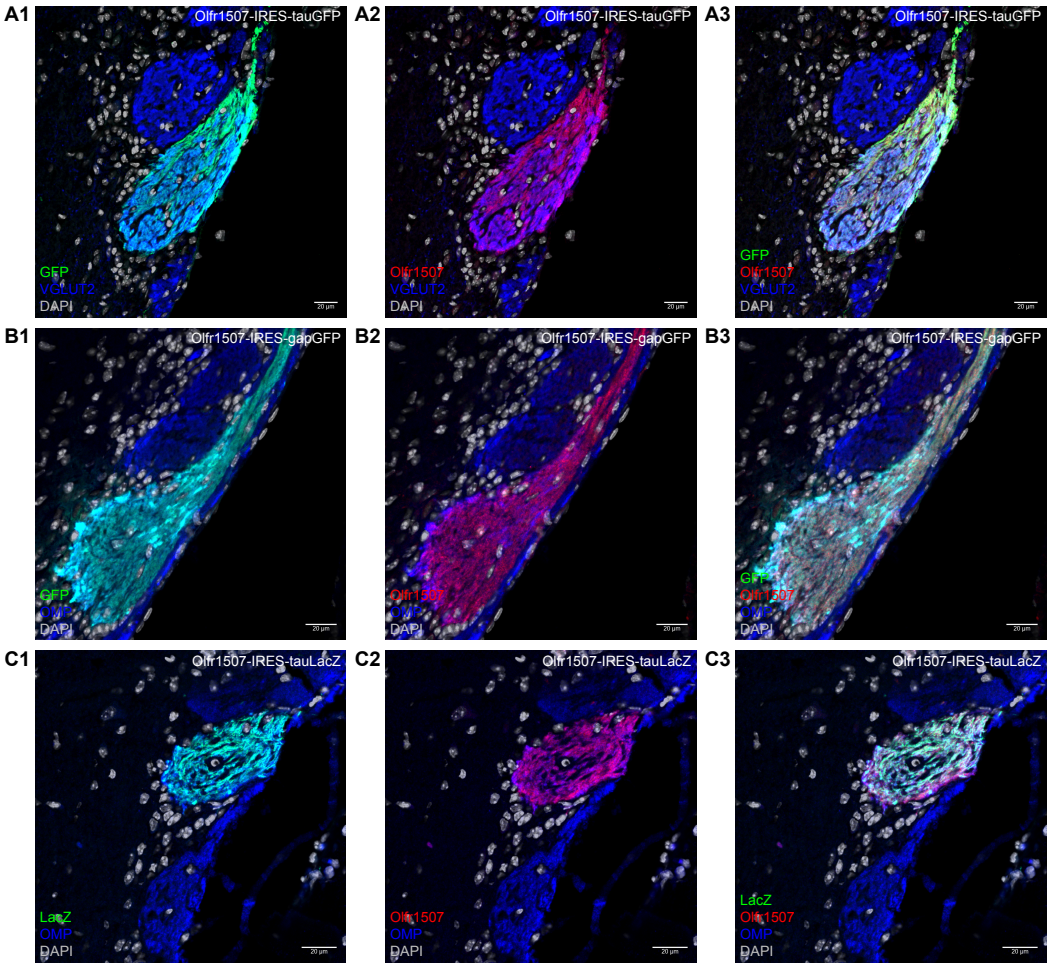


Figure 3.8. The Olfr1507 glomerulus in the lateral half-olfactory bulb of homozygous Olfr1507-IRES-tauGFP, Olfr1507-IRES-gapGFP, or Olfr1507-IRES-tauLacZ mice at PD21.

Confocal images of coronal sections showing the lateral half-OB subjected to triple IHC for either VGLUT2 or OMP (blue), Olfr1507 (red), and GFP or LacZ (green) (A1 – A3) Homozygous Olfr1507-IRES-tauGFP mouse. (B1 – B3) Homozygous Olfr1507-IRES-gapGFP mouse. (C1 – C3) Homozygous Olfr1507-IRES-tauLacZ mouse. A single homogeneous glomerulus is immunoreactive for GFP or lacZ. One glomerulus is immunoreactive for Olfr1507. A single homogeneous glomerulus is strongly immunoreactive for both GFP and Olfr1507 (A3 and B3) or for both lacZ and Olfr1507 (C3). DAPI served as nuclear stain. Data were obtained from nine mice.

3.7 Positions of Olfr1508 and Olfr1509 glomeruli in the olfactory bulb

Using a radioactive ISH technique, OSNs expressing Olfr1507, Olfr1508, and Olfr1509 were reported to coalesce into two sets of very close but distinct glomeruli within the medial and lateral half-OB (Tsuboi et al., 1999). However, using the MOR28-IRES-gap-GFP mouse strain, Zapiec and Mombaerts 2015 showed that axons of Olfr1507-expressing OSNs project to multiple glomeruli and that the positions of Olfr1507 glomeruli present substantial variability from mouse to mouse and even between the left and right OBs of an individual mouse. Note that this strain is not inbred.

To characterize glomerular positions of interest in homozygous Olfr1508-IRES-tauGFP or Olfr1509-IRES-tauGFP mice at PD21, I conducted triple IHC for VGLUT2, Olfr1507, and GFP antibodies on consecutive 6 µm coronal sections of the OBs of mice. I used an antibody for GFP to identify the positions of the Olfr1508 and Olfr1509 glomeruli. The Olfr1507 antibody enables the detection of Olfr1507 at the protein level, including in OSN axon termini. This precise demarcation enabled me to identify unambiguously the glomeruli of Olfr1507, Olfr1508, and Olfr1509 in these strains. I scanned OB sections using a MIDI Slide scanner and carried out more detailed observations under a confocal microscope.

I observed a single homogeneous GFP-immunoreactive glomerulus per medial half - OB (Figure 3.9 A1) and lateral half-OB (Figure 3.10 A1) in homozygous Olfr1508-IRES-tauGFP mice. GFP-immunoreactive axons in the Olfr1509-IRES-tauGFP strain consistently coalesce into a single homogeneous glomerulus per medial half-OB (Figure 3.9 B1) and lateral half-OB (Figure 3.10 B1). Olfr1507-immunoreactive axons in the respective strains consistently coalesce into a single homogeneous glomerulus per medial and lateral half-OB (Figure 3.9, 3.10 A2 – B2). In homozygous Olfr1508-IRES-tauGFP mice, the medial and lateral GFP-immunoreactive glomeruli are located dorsally and at a distance of one glomerular width from the Olfr1507-immunoreactive glomerulus (Figure 3.9, 3.10 A3). In homozygous Olfr1509-IRES-tauGFP mice, the medial and lateral GFP-immunoreactive glomeruli are located dorsally and at a distance of three glomerular widths from the Olfr1507-immunoreactive glomerulus (Figure 3.9, 3.10 B3). In the lateral half-OB, the relative

positions of the Olfr1508 and Olfr1509 glomeruli are similar to those in the medial half-OB (Figure 3.9, 3.10). The Olfr1507 medial and lateral glomeruli occupy the most ventral position compared to the GFP-immunoreactive glomeruli in Olfr1508-IRES-tauGFP mice (Figure 3.9, 3.10 A3) and in Olfr1509-IRES-tauGFP mice (Figure 3.9, 3.10 B3).

To examine whether the relative glomerular positions of Olfr1507, Olfr1508, and Olfr1509 remain consistent with age, I performed triple IHC on serial coronal sections of the OBs of mice at PD56. This age is commonly used in neuroanatomical studies and corresponds to young adulthood. I observed that the relative positions of the three types of glomeruli are conserved in the medial half-OB (Figure 3.11 A – C) and lateral half-OB (Figure 3.11 D – F). In homozygous Olfr1507-IRES-tauGFP mice, Olfr1507-immunoreactive glomeruli are also GFP-immunoreactive, and vice versa (Figures 3.11 A, D). In homozygous Olfr1508-IRES-tauGFP mice, the GFP-immunoreactive glomerulus (representing the Olfr1508 glomerulus) is dorsal to the Olfr1507-immunoreactive glomerulus (Figures 3.11 B, E). Similarly, in homozygous Olf1509-IRES-tauGFP mice, the GFP-immunoreactive glomerulus (representing the Olfr1509 glomerulus) is the most dorsal glomerulus (Figures 3.11 C, F).

Taken together, my IHC experiments indicate that axons of OSNs expressing Olfr1507, Olfr1508, or Olfr1509 coalesce into glomeruli at the same relative locations in the OB at PD21 and PD56. Homozygous mice of the three gene-targeted strains consistently exhibit one pair of GFP-immunoreactive glomeruli per OB. The relative positions of the Olfr1507, Olfr1508, and Olfr1509 glomeruli in the medial and lateral half-OB are consistent. There is one pair of Olfr1507-immunoreactive glomeruli per OB of Olfr1507-tagged mice.

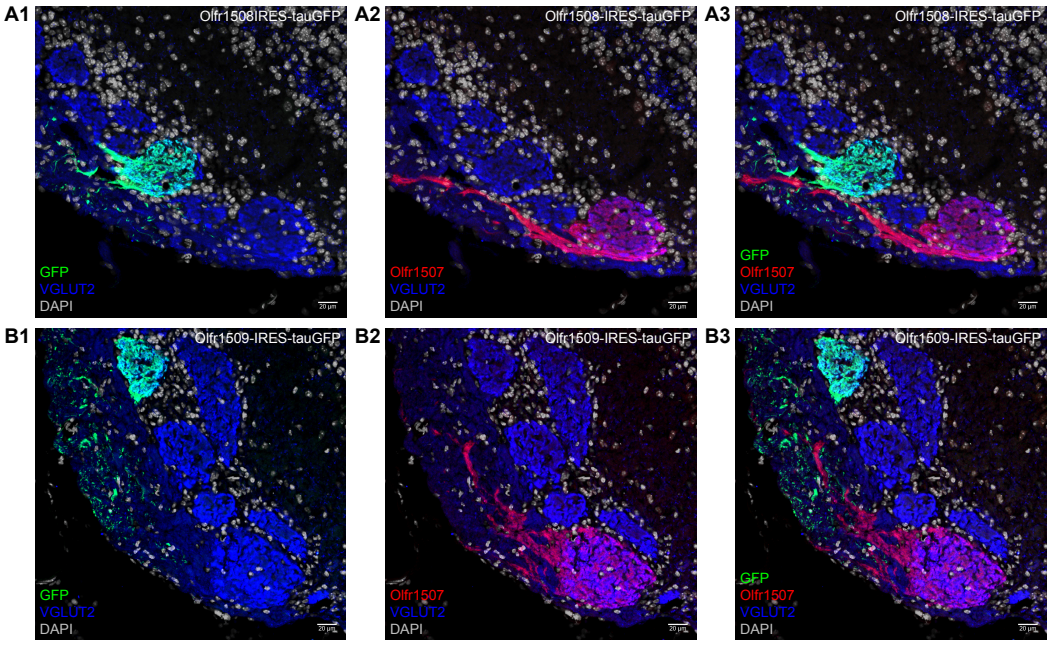


Figure 3.9. GFP-immunoreactive glomeruli in the medial half-olfactory bulb of homozygous Olfr1508-IRES-tauGFP or Olfr1509-IRES-tauGFP mice at PD21.

Confocal images of coronal sections showing the medial half-OB subjected to triple IHC for VGLUT2 (blue), Olfr1507 (red), and GFP (green). (A1 – A3) Homozygous Olfr1508-IRES-tauGFP mouse. (B1 – B3) Homozygous Olfr1509-IRES-tauGFP mouse. A single homogeneous glomerulus is immunoreactive for GFP. A single glomerulus is immunoreactive for Olfr1507. Two distinct labeled glomeruli are visible, one immunoreactive for Olfr1507 and the other for GFP. The number of GFP-immunoreactive medial glomeruli is consistently one per half-OB, for a total of two per mouse. DAPI served as nuclear stain. Data were obtained from 10 mice.

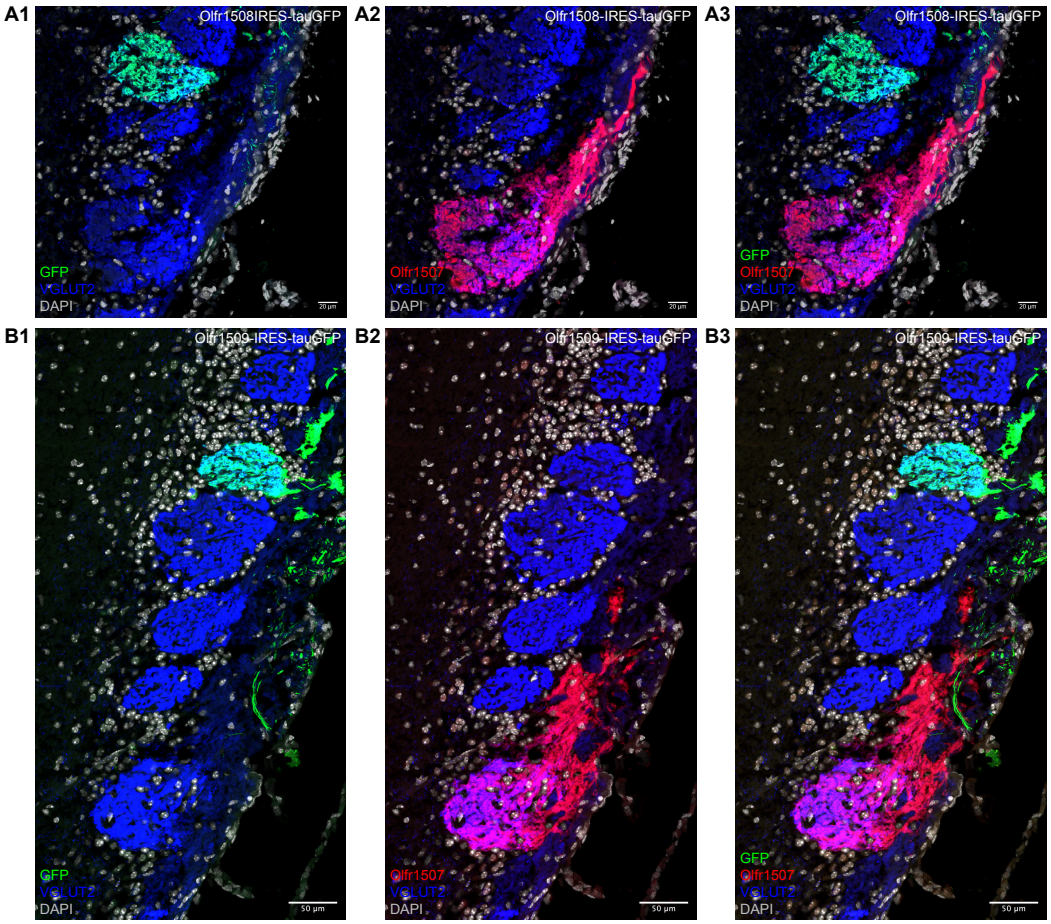


Figure 3.10. GFP-immunoreactive glomeruli in the lateral half-olfactory bulb of homozygous Olfr1508-IRES-tauGFP or Olfr1509-IRES-tauGFP mice at PD21.

Confocal images of coronal sections showing the lateral half-OB subjected to triple IHC for VGLUT2 (blue), Olfr1507 (red), and GFP (green). (A1 – A3) Homozygous Olfr1508-IRES-tauGFP mouse. (B1 – B3) Homozygous Olfr1509-IRES-tauGFP mouse. A single homogeneous glomerulus is immunoreactive for GFP. A single glomerulus is immunoreactive for Olfr1507. Two distinct labeled glomeruli are visible, one immunoreactive for Olfr1507 and the other for GFP. The number of GFP-immunoreactive lateral glomeruli is consistently one per half-OB, for a total of two per mouse. DAPI served as nuclear stain. Data were obtained from 10 mice.

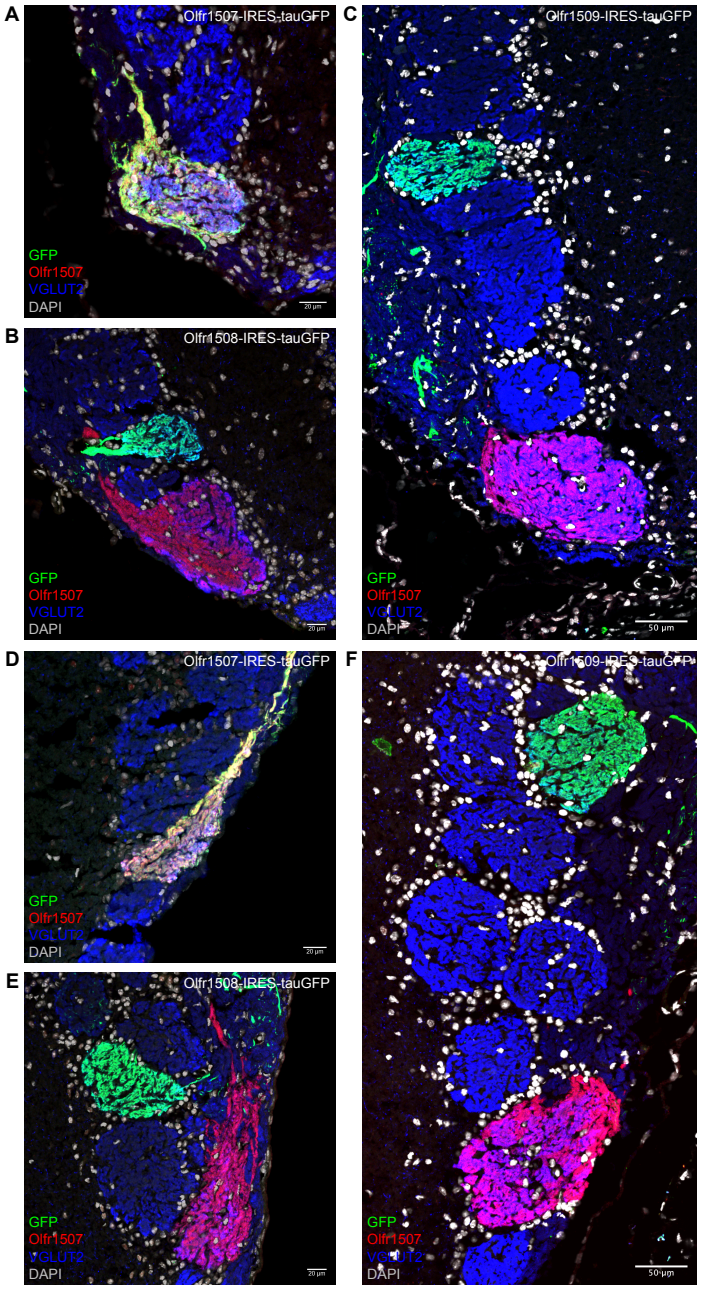


Figure 3.11. GFP-immunoreactive glomeruli in the medial and lateral half-olfactory bulb of homozygous Olfr1507-IRES-tauGFP, Olfr1508-IRES-tauGFP, or Olfr1509-IRES-tauGFP mice at PD56.

Confocal images of coronal sections subjected to triple IHC for VLUT2 (blue), Olfr1507 (red), and GFP (green). A single homogeneous glomerulus is immunoreactive for both Olfr1507 and GFP in an Olfr1507-IRES-tauGFP mouse in the medial half-OB (A) and lateral half-OB (D). Two distinctly labeled glomeruli are visible, one immunoreactive for Olfr1507 and the other for GFP in an Olfr1508-IRES-tauGFP mouse in the medial half-OB (B) and in lateral half-OB (E). Two distinctly labeled glomeruli are visible, one immunoreactive for Olfr1507 and the other for GFP in an Olfr1509-IRES-tauGFP mouse in the medial half-OB (C) and lateral half-OB (F). DAPI served as nuclear stain. Data were obtained from three mice.

3.8 Olfr1507 glomeruli in MOR28-IRES-gap-GFP mice

To conclude with the glomerular characterization of Olfr1507, I examined the MOR28-IRES-gap-GFP strain from the Sakano laboratory, as it constitutes a popular model for studies of OSN axon wiring (Tsuboi et al., 1999; Serizawa et al., 2000; Ishii et al., 2001; Serizawa et al., 2003; Takahashi et al., 2010). This strain displays multiple Olfr1507 glomeruli with high positional variability (Ishii et al., 2001; Zapiec and Mombaerts, 2015).

I analyzed homozygous MOR28-IRES-gap-GFP mice at PD21 to visualize the Olfr1507 glomeruli. I conducted IHC on OB sections using antibodies for OMP, Olfr1507, and GFP. The Olfr1507-immunoreactive signal shows complete concordance with the GFP-immunoreactive signal, forming homogeneous Olfr1507 glomeruli in the medial and lateral half-OB (Figure 3.12). There are four Olfr1507 glomeruli in one mouse (one glomerulus per half-OB) and six Olfr1507 glomeruli in three mice. These three mice have one or two Olfr1507 glomeruli in the medial half-OB (Figure 3.12 A1 – A4, E) and in the lateral half-OB (Figure 3.12 B – D, F). In one of these mice, the two Olfr1507 glomeruli in the medial half-OB are located in different sections, with one glomerulus appearing more anteriorly compared to the other (Figure 3.12 A1 – A4). The variation in the number of Olfr1507 glomeruli in the MOR28-IRES-gap-GFP strain may be associated with the mixed genetic background.

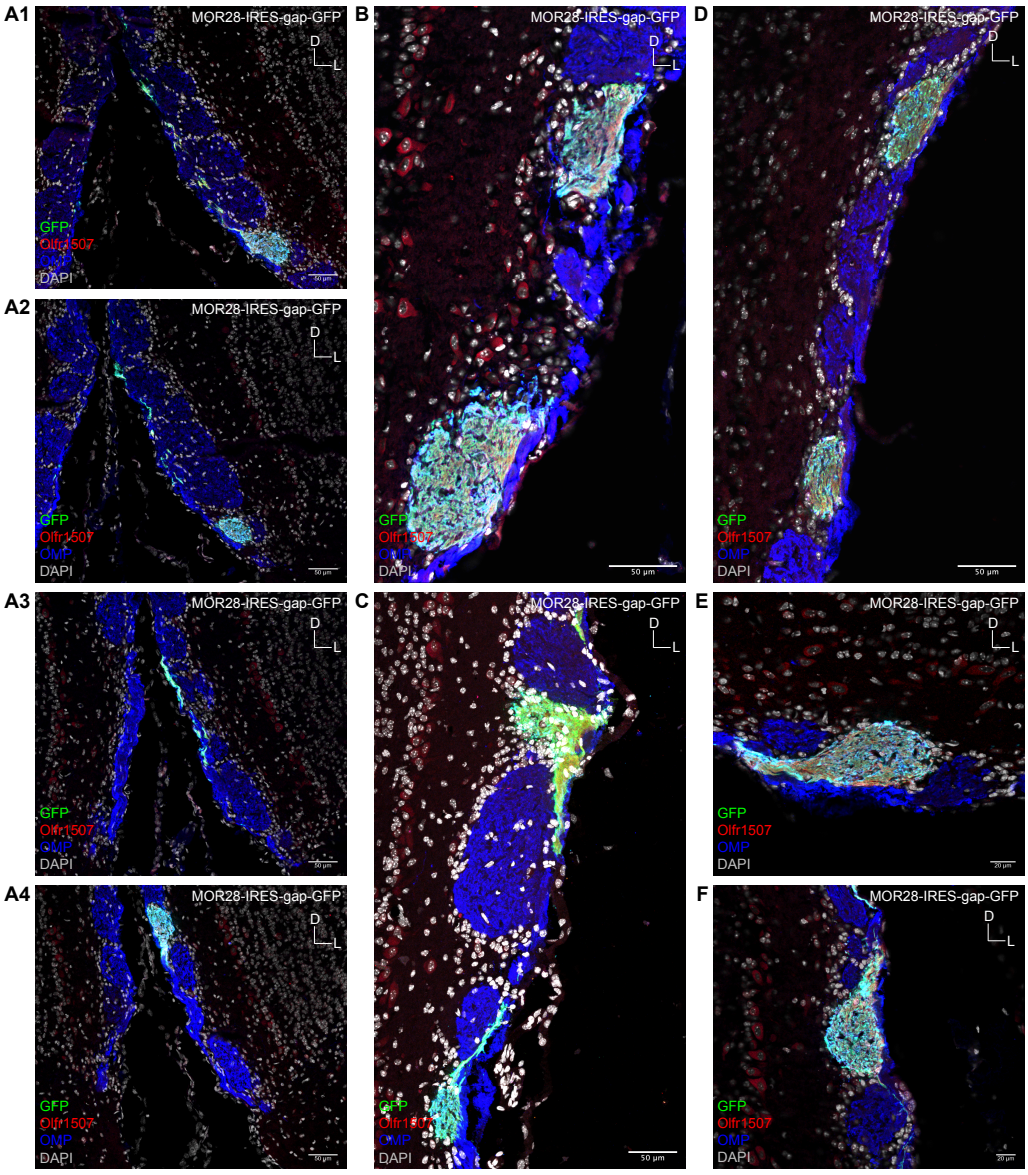


Figure 3.12. Olfr1507 glomeruli in the medial and lateral half-olfactory bulb of homozygous MOR28-IRES-gap-GFP mice at PD21.

(A1 – A4) Confocal images of consecutive coronal sections showing the medial half-OB subjected to triple IHC for OMP (blue), Olfr1507 (red), and GFP (green). Olfr1507 glomeruli are tracked by comparison of consecutive sections. A homogeneous glomerulus is immunoreactive for both Olfr1507 and GFP (A1, A2). In a section immediately following A2, GFP-immunoreactive axons are visualized (A3). In a section immediately following A3, a second glomerulus is immunoreactive for both Olfr1507 and GFP (A4). (B – D) Confocal images of coronal sections showing the lateral half-OB. Two distinct labeled glomeruli are visible, both immunoreactive for Olfr1507 and GFP. One glomerulus immunoreactive for both Olfr1507 and GFP is visible in the medial half-OB (E) and lateral half-OB (F). DAPI served as nuclear stain. Panels A1-A4, B, and F are from one mouse. Panels C, D, and E are from another mouse. Data were obtained from four mice.

3.9 Glomerular volume in the Olfr1507, Olfr1508 and Olfr1509 gene-targeted strains

Next, I conducted a quantitative analysis of glomerular volume using a Zeiss LSM 800 confocal microscope. I captured 6 µm z-stack images with the LSM 800 in 1 µm intervals through consecutive coronal sections that contained GFP-immunoreactive axons in the OB of homozygous Olfr1507-IRES-tauGFP, Olfr1508-IRES-tauGFP, or Olfr1509-IRES-tauGFP mice at PD21. While DAPI counterstaining allows to outline the glomerular shape in a section, it is not an ideal marker for precisely demarcating the glomerular boundaries. To accurately delimit the glomerular layer and visualize the glomeruli, I performed IHC with VGLUT2. I devised a pipeline in collaboration with Yu Weng (at that time, a Ph.D. student in the lab), utilizing CellProfiler. This pipeline segments glomeruli based on the GFP-immunoreactive and VGLUT2-immunoreactive signals. By superimposing the segmented GFP-immunoreactive and VGLUT2-immunoreactive signals, I determined in each optical section the surface area representing the region where GFP-immunoreactive and VGLUT2-immunoreactive signals colocalize.

Image analysis was conducted using the user-friendly graphical interface of CellProfiler (Carpenters et al., 2006) (Figure 3.13 A). The software operates as a modular system, with each module performing specific tasks (Figure 3.13 B). These modules are arranged sequentially to form a pipeline. The modules were configured to work automatically. When the analysis was initiated, a series of images passed through the pipeline, being processed by each module in the designated order. The pipeline modules and their settings are saved and can be used to repeat the analysis for every confocal image.

3.9.1 Rescale intensity module

A critical step in image analysis is illumination correction, as using raw images degrades intensity measurements and can preclude accurate cell identification, thereby affecting area and shape-based measurements. To address this problem, I employed the “Rescale Intensity” module as a first step for the GFP-immunoreactive image (Figure 3.14 A) and the VGLUT2-immunoreactive image (Figure 3.14 B). This module adjusts the intensity of the images by dividing each pixel's intensity value by

the maximum intensity value of the respective image. As a result, an output image is displayed with normalized pixel intensities ranging from 0 to ≤1. The output image is a grey-scale GFP-immunoreactive glomerulus. In all output images, the x, y axes represent the size of the image in pixels (1024 x 1024 px).

3.9.2 Threshold module

The next steps are related to image segmentation. I used the threshold module in the previously rescaled images for GFP (Figure 3.15 A) and VGLUT2 (Figure 3.15 B). First, I pre-selected the Global method that calculates a single threshold value based on the unmasked pixels of the input image. After determining this value, the threshold module sets pixel intensities below the value to zero (black) and above the value to one (white).

3.9.3 Identify Primary Objects module

Following the thresholding step, the resulting image becomes a binary image, which then proceeds to undergo primary object recognition. This module performs primary object recognition from both the GFP-immunoreactive channel (Figure 3.16 A – C) and the VGLUT2-immunoreactive channel (Figure 3.16 D – F). The GFP-immunoreactive glomerulus is easily identified by its uniform morphology and high contrast relative to the background when stained and therefore recognized as a primary object. The VGLUT2-immunoreactive glomeruli are identified by its staining pattern, high contrast relative to the background when stained, and good inter-glomerular separation identifying them as objects. The module applies a set of sequential parameters to the GFP and VGLUT2 channels, as described below:

1. Select the input image: the GFP (Figure 3.16 A) and VGLUT2 (Figure 3.16 D) thresholded images previously calculated.
2. Name the primary objects: enter the name that we want to call the objects, “GFPglom” (Figure 3.16 B) for the GFP object recognition and “Gloms” (Figure 3.16 E) for the VGLUT2 glomeruli recognition.

3. Diameter of objects (pixel unit): give a Min pixel size value and Max pixel size value to recognize the GFP glomerulus (60 – 500) and the VGLUT2 glomeruli 90 – 1000).
4. Discard objects outside diameter range: select “Yes” to discard objects outside the range specified in the previous step.
5. Discard objects touching the border of the image: choose “Yes” to discard objects that touch the border. This point is useful if there are GFP-positive axons touching the borders of the image.
6. Threshold strategy: select “Global” to calculate a new threshold value for the GFP channel based on the GFP sub-regions and a new threshold value for the VGLUT2 channel based on the VGLUT2 sub-regions
7. Thresholding method: select the “Otsu-Two Classes” thresholding method in both images to calculate a threshold value to separate two classes of pixels: foreground and background. This method minimizes the variance between each pixel class.
8. Thresholding smoothing scale: choose a value 0.3 - 0.6 for the GFP channel and a value 0.8 - 1.5 for the VGLUT2 channel to improve homogenization of the resulting objects by removing holes and jagged edges.
9. Method to distinguish clumped objects: select ‘Shape’ to separate large, merged objects into individual objects

The resulting images are then a GFP-object or a set of VGLUT2-objects that will be used for further measurements (Figure 3.16 C, F).

3.9.4 Convert Objects to Image module

This module allows to take the previously identified GFP and VGLUT2 objects and convert them into images that then are be saved with the “SaveImages” module.

3.9.5 Filter Objects module

In addition to object recognition for the GFP images, I employed the “Filter Objects” module to manually remove unwanted objects – these are objects that were mistakenly identified as non-GFP-positive glomeruli. This module allowed me to refine the results and ensure that only truly GFP-positive glomeruli were included in

the analysis. The parameters for this module varied depending on the number of GFP objects identified in the previous step. The general approach involved selecting the “Measurements” filter mode and using “Limits” as the filtering method. The minimum and maximum values for the filtering were determined based on the total number of GFP objects detected in the image. This allowed for precise control over which objects were retained and which ones were filtered out during the analysis (Figure 3.17).

3.9.6 Mask Objects module

To achieve the desired quantitative measurements, I utilized the “Mask Objects” module to combine and filter the recognized objects from Figure 3.16 A – F. This module removes any objects that fall outside of a specified region. In this case, the region of interest is the overlapping signal between the GFP and VGLUT2 in the confocal image. The module takes the identified objects as input, overlaps them, and eliminates any objects that do not exhibit colocalization. The resulting output image is the overlay of the GFP and VGLUT2 images (Figure 3.16 G – I).

3.9.7 Measure Area Occupied module

Finally, to obtain measurements for the region of colocalization between the GFP and VGLUT2 channels, the area occupied by this object must be measured. This module takes the masked image as input and provides the area of the foreground object as output. The area measurement obtained from this module is given in pixels.

After processing the confocal images of the GFP-immunoreactive glomerular sections and obtaining the area occupied by analyzing each optical section from the z-stacks, I calculated the total volume of glomeruli in the medial and lateral half-OB for each mouse in the Olfr1507-IRES-tauGFP, Olfr1508-IRES-tauGFP, and Olfr1509-IRES-tauGFP groups. The sum of the reconstructed areas of all overlapping regions labeled against GFP and VGLUT2 markers is the total glomerular volume (TGV) per mouse (Figure 3.18).

The TGV for the three different gene-targeted strains is as follows: Olfr1507-IRES-tauGFP mice exhibited the largest TGV (15,557,579 + 2,100,135 μm³), Olfr1509-IRES-tauGFP mice showed a slightly smaller glomerular volume (14,629,870 + 1,961,236 μm³), and the smallest glomerular volume was observed in Olfr1508-IRES-tauGFP mice (9,172,490 + 1,739,452 μm³). Statistical analysis revealed no significant difference in TGV between the Olfr1507-IRES-tauGFP and Olfr1509-IRES-tauGFP groups (P = 0.8325, one-way ANOVA) (Figure 3.18). A significant difference in TGV was observed between the Olfr1507-IRES-tauGFP and Olfr1508-IRES-tauGFP groups (P = 0.0161) and between the Olfr1508-IRES-tauGFP and Olfr1509-IRES-tauGFP groups (P = 0.0316) (Figure 3.18).

Taken together, the glomerular volumes in Olfr1507-IRES-tauGFP, Olfr1508-IRES-tauGFP, or Olfr1509-IRES-tauGFP were measured in a semi-automated fashion and using VGLUT2 as a marker to define the glomerular profiles. The methodology is time-consuming but provides a more accurate estimation of the TGV for two reasons: the collection of the OB sections is consecutive and the cross-sectional area is measured from every optical section in the z-stack.



Figure 3.13. CellProfiler overview and features.

(A) Main CellProfiler interface displaying a series of confocal images that were loaded and divided into two categories according to the wavelengths taken in the confocal microscope: GFP-immunoreactive corresponds to the 488 wavelength and VGLUT2 corresponds to a 647 wavelength. (B) Pipeline used to measure the glomerular surface area from every image previously loaded.

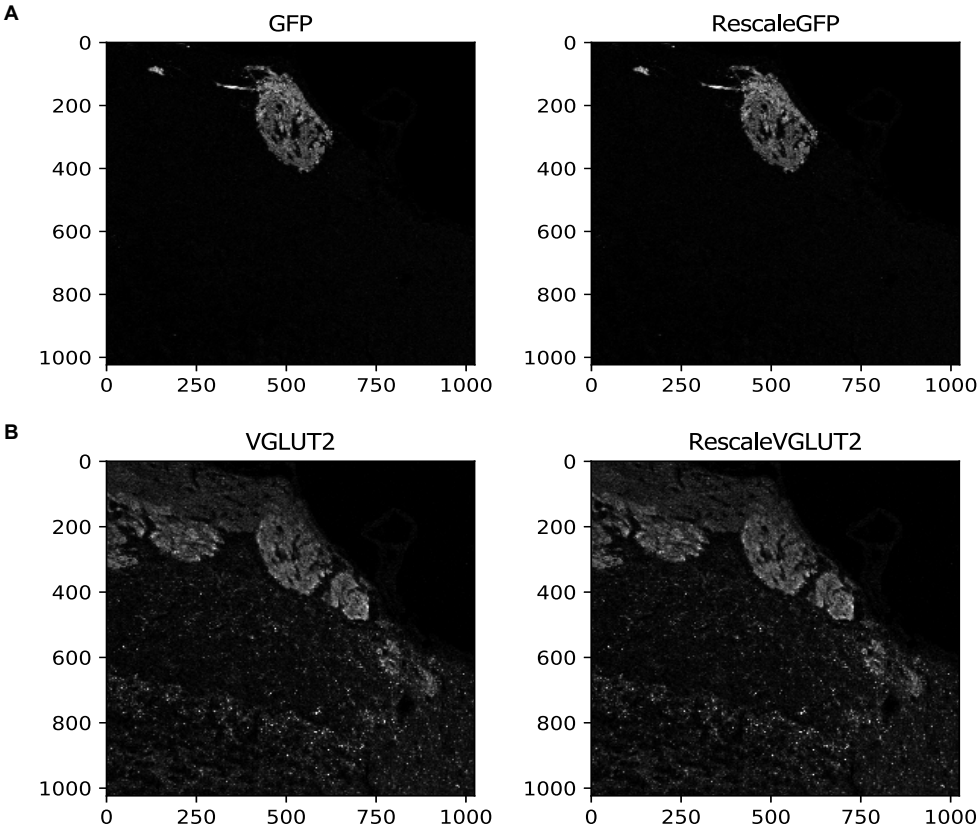


Figure 3.14. Rescale Intensity module applied to both the GFP and VGLUT2 channels.

The acquired wavelengths for these channels were 488 and 647, respectively. (A) The left image displays the raw 488 confocal image of a coronal OB section from a gene-targeted mouse. The right image shows the result after the pixel intensities have been rescaled. (B) The left image shows the raw confocal image in the 647 channel. The right image shows the result after rescaling.

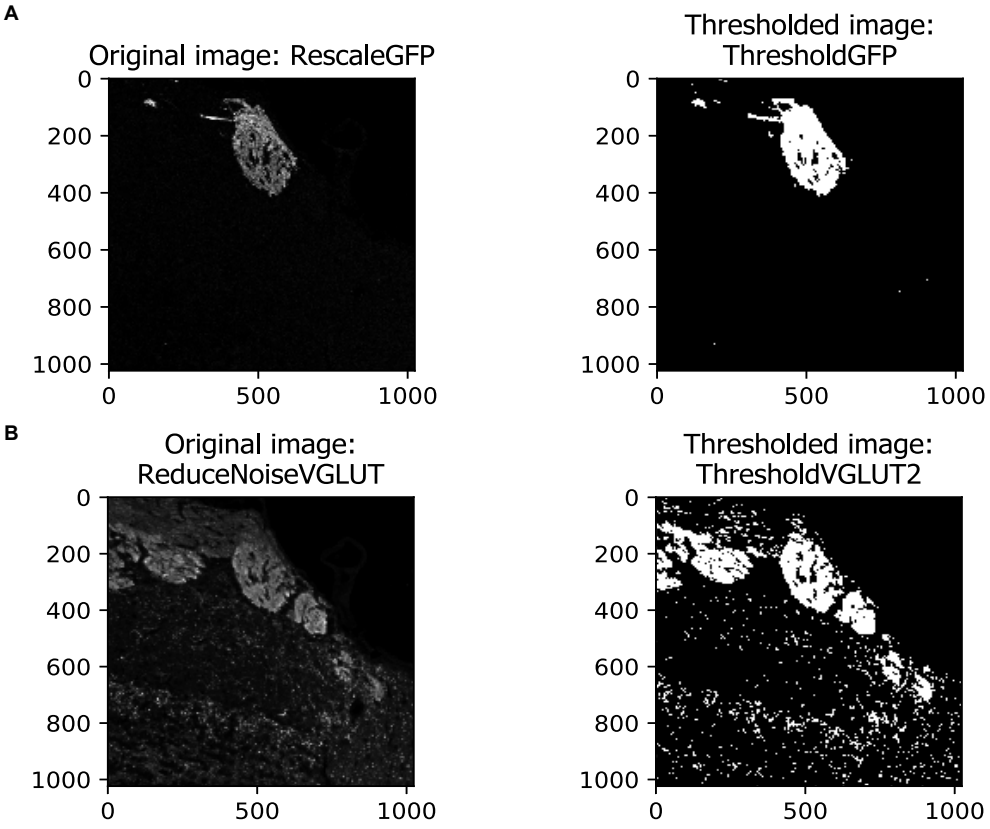


Figure 3.15. Threshold module applied to both the GFP and VGLUT2 channels.

(A) The left image displays the raw confocal image of the GFP glomerulus before determining the threshold value for this channel. The right image shows the resulting image after applying the threshold value, where pixels below the threshold are counted as background (black). (B) The left image represents the raw confocal image of VGLUT2 before thresholding. The right image shows the output VGLUT2 image after selecting the threshold value, which sets pixels above this value as foreground (white).

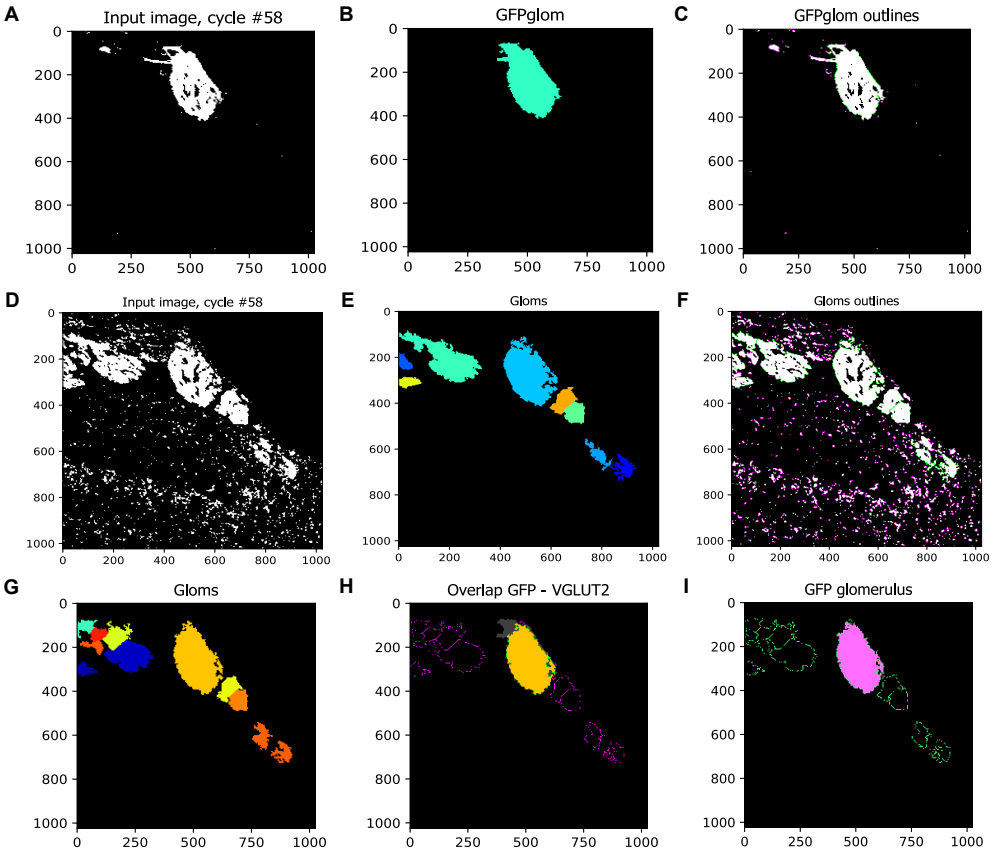


Figure 3.16. Object identification of GFP and VGLUT2 after processing using the Identify Primary Objects module.

(A) The original binary GFP image. (B) The identified GFP object shown as a color image in which connected pixels that belong to the same object are assigned the same color. (C) Image A overlaid with the colored outlines of the identified GFP objects. Green outline: acceptable; passed all criteria. Magenta outline: discarded based on size. Yellow: discarded due to touching the border. (D) The original binary VGLUT2 image. (E) The identified VGLUT2 objects shown as a color image in which connected pixels that belong to the same object are assigned the same color. (F) Image D overlaid with the colored outlines of the identified VGLUT2 objects. Green outline: acceptable; passed all criteria. Magenta outline: discarded based on size. (G) The VGLUT2-identified objects from E. (H) The GFP-identified object from B. (I) The “Mask Objects” module removes objects outside this specified region and gives a resulting image that corresponds only to the colocalizing region of the two input images.

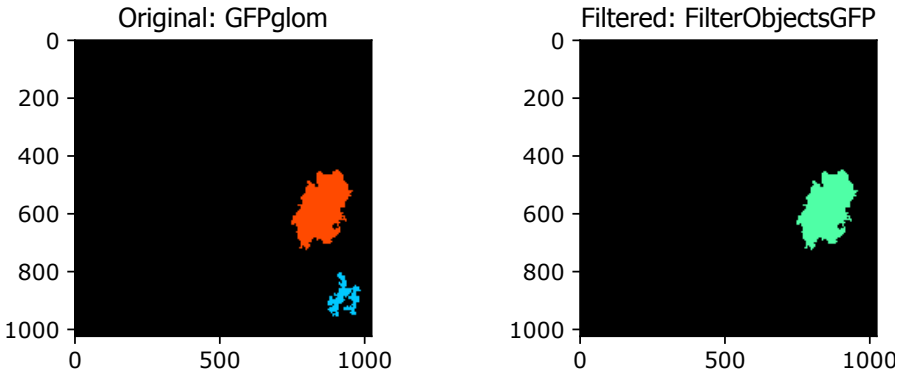


Figure 3.17. The process of removing objects based on their measurements to filter the GFP glomerulus.

(Left) the image prior to filtering is displayed, in which a blue object is clearly not part of the GFP glomerulus. (Right) the filtered image is shown, in which only the GFP-immunoreactive glomerulus remains recognized and can be utilized for subsequent measurements.

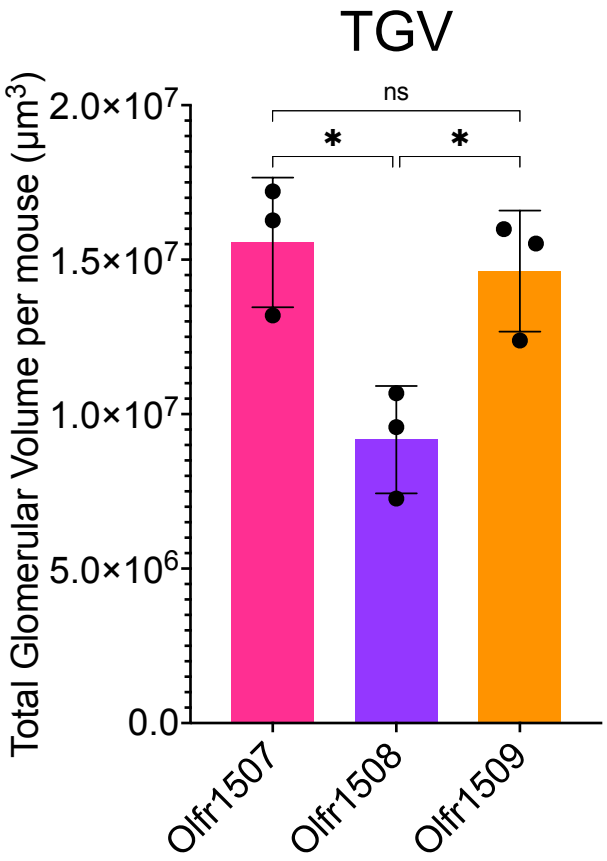


Figure 3.18. Total glomerular volume per mouse.

ns, not significant; one asterisk, significant. The P-value threshold for one-way ANOVA was set at $P < 0.05$. Data represents results obtained from nine mice.

3.10 The positions of Olfr1508 and Olfr1509 glomeruli relative to the Olfr1507 glomeruli

I have thus far described that homozygous Olfr1508-IRES-tauGFP or Olfr1509-IRES-tauGFP mice display each a single homogeneous GFP-immunoreactive glomerulus in the medial and lateral half-OB. At the level of light microscopy, there are no GFP-immunoreactive axons projecting to other glomeruli than to this single homogeneous glomerulus. The Olfr1507-immunoreactive glomerulus does not overlap with the GFP-immunoreactive glomerulus in Olfr1508-IRES-tauGFP or Olfr1509-IRES-tauGFP mice. However, from the data that I have presented thus far, I cannot completely exclude that OSNs expressing Olfr1508 or Olfr1509 might project to the same glomeruli or show variations in the glomerular positions in relation to the Olfr1507 glomeruli.

To investigate the variability in the positions of the Olfr1507, Olfr1508, or Olfr1509 glomeruli, I examined mice that are double heterozygous for the Olfr1508-IRES-tauGFP and Olfr1509-IRES-tauGFP mutations at PD21. I determined the positions of the Olfr1508 and Olfr1509 glomeruli (by virtue of their GFP-immunoreactivity) relative to the Olfr1507 glomerulus (by virtue of its Olfr1507-immunoreactivity). I used an OMP antibody to outline the outer nerve layer and glomerular layer. I employed a VGLUT2 antibody to label OSN axon termini and thereby outline the glomerular structures. I unambiguously identified the Olfr1507 glomerulus in the medial half-OB (Figure 3.19 A) and lateral half-OB (Figure 3.19 B) with the Olfr1507 antibody.

I consistently observed two GFP-immunoreactive glomeruli per half-OB, indicating that, indeed, OSNs expressing Olfr1508 and Olfr1509 coalesce into distinct glomeruli (Figure 3.19). The identity of the GFP-immunoreactive glomeruli in the Olfr1508-IRES-tauGFP x Olfr1509-IRES-tauGFP mice can be inferred based on the glomerular positions observed in homozygous Olfr1508-IRES-tauGFP or Olfr1509-IRES-tauGFP mice.

It is noteworthy that due to monoallelic expression, in double heterozygous Olfr1508-IRES-tauGFP x Olfr1509-IRES-tauGFP mice, only half of the Olfr1508-expressing OSNs and half the Olfr1509-expressing OSNs express the gene-targeted GFP allele.

The other half of these subsets of OSNs express the wild-type allele and are not detectable in these analyses. As a result, the GFP-immunoreactive glomeruli are not homogeneously filled with GFP-immunoreactive OSN axons.

Taken together, the identity of the two distinct GFP-immunoreactive glomeruli can be assumed because of the GFP tagging of the two alleles, Olfr1508 or Olfr1509, and based on the positions of the GFP-immunoreactive glomeruli when compared with homozygous Olfr1508-IRES-tauGFP and Olfr1509-IRES-tauGFP mice.

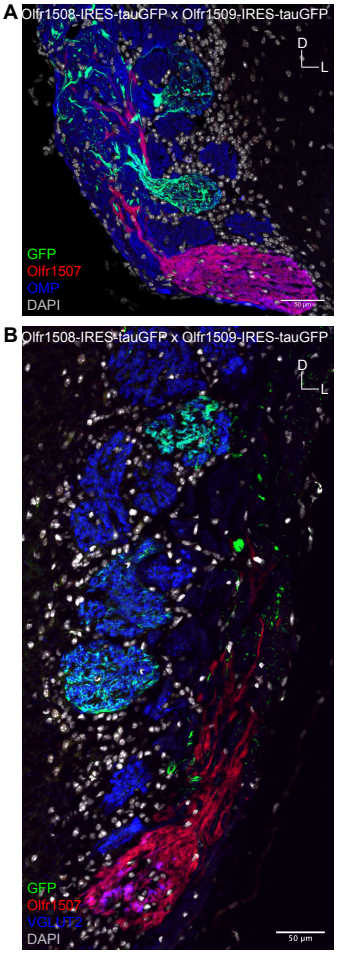


Figure 3.19. Relative positions of the GFP-immunoreactive glomeruli in relation to the Olfr1507-immunoreactive glomeruli in the olfactory bulb of mice double heterozygous for Olfr1508-IRES-tauGFP and Olfr1509-IRES-tauGFP at PD21.

(A – B) Confocal images of coronal sections showing the medial half-OB and lateral half-OB subjected to triple IHC for VGLUT2 or OMP (blue), Olfr1507 (red) and GFP (green). In the medial half-OB, three distinct glomeruli are visualized by immunoreactive signal for Olfr1507 or GFP. The Olfr1507-immunoreactive glomerulus is located at the most ventral position (A). In the lateral half-OB, three distinct glomeruli are visualized by immunoreactive signal for Olfr1507 and GFP. The Olfr1507-immunoreactive glomerulus is located at the most ventral position. DAPI served as nuclear stain. Data were obtained from three mice.

3.11 Path taken by GFP-expressing axons in double heterozygous mice

In mice double heterozygous for Olfr1508-IRES-tauGFP and Olfr1509-IRES-tauGFP at PD21, I observed GFP-immunoreactive axons following distinct courses around one of the GFP-immunoreactive glomeruli in the lateral half-OB before terminating in the target glomerulus (Figure 3.20). Individual GFP-immunoreactive axons are only observed in the lateral half-OB but not the medial half-OB (Figure 3.20 A2 – A5). GFP-immunoreactive axons travel alongside with one of the two GFP-immunoreactive glomeruli and are present in multiple interleaved sections of the lateral half-OB (Figure 3.20 A2 – A5, arrows). The lateral Olfr1507 glomerulus is unambiguously identified with the Olfr1507 antibody and occupies the most ventral position (Figure 3.20). The two GFP-immunoreactive glomeruli in the lateral half-OB correspond to the Olfr1508 glomeruli (Figure 3.20 A1 – A4) and Olfr1509 glomeruli (Figure 3.20 A2 – A5). After extended examination, I did not observe an additional third GFP-immunoreactive glomerulus in the medial half-OB or lateral half-OB. It remains unclear whether GFP-immunoreactive axons can take divergent routes to reach their target glomerulus or if they terminate their path in neighboring glomeruli. By observing the location of GFP-immunoreactive axons positioned near one GFP-immunoreactive glomerulus, I infer that these axons likely are of OSNs that express *Olfr1508*.

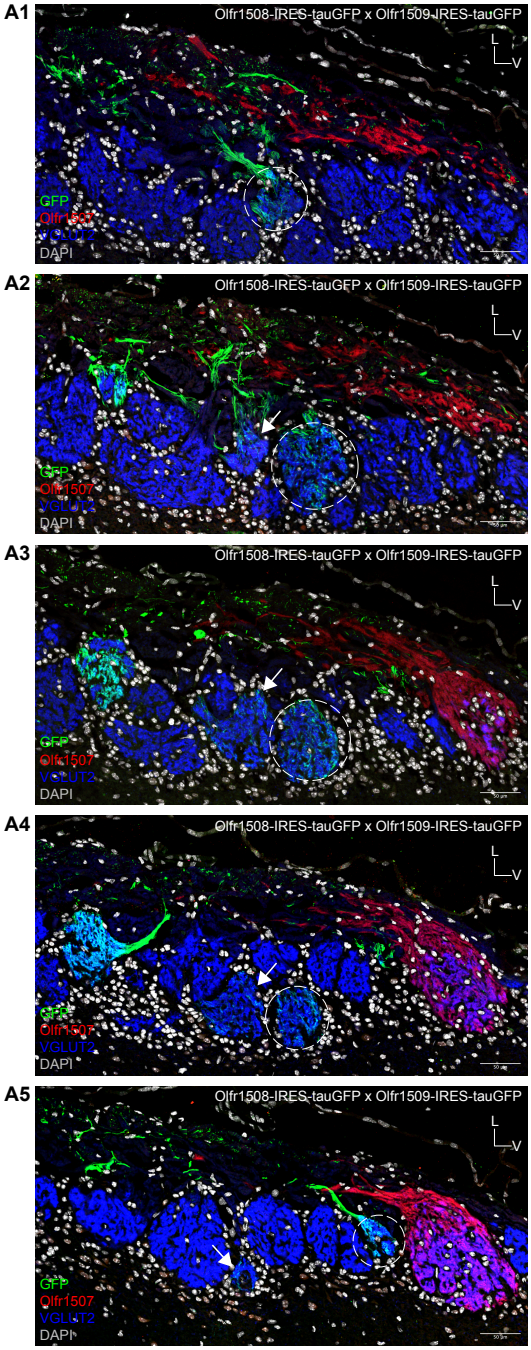


Figure 3.20. GFP-immunoreactive axons follow different routes in the lateral half-olfactory bulb of mice double heterozygous for Olfr1508-IRES-tauGFP and Olfr1509-IRES-tauGFP at PD21.

(A1 – A5) Confocal images of five interleaved coronal sections showing the lateral half-OB subjected to triple IHC for VGLUT2 (blue), Olfr1507 (red) and GFP (green). GFP-immunoreactive glomeruli were tracked by comparison of interleaved sections. A glomerulus is immunoreactive for GFP (dashed circle) (A1). Axons immunoreactive for GFP are visualized (arrow) next to the dashed circle. A second GFP-immunoreactive glomerulus is located more dorsally (A2). The Olfr1507-immunoreactive glomerulus is visible at the most ventral position. Axons immunoreactive for GFP are visualized (arrow) next to the dashed circle. A more dorsal GFP-immunoreactive glomerulus is visible as observed in A2 (A3). Axons immunoreactive for GFP are visualized (arrow) next to the dashed circle.

The most dorsally GFP-immunoreactive glomerulus is visible as observed in A3 (A4). GFP-immunoreactive axons are visible (arrow) and GFP-immunoreactive axons innervate a small glomerulus next to the Olfr1507-immunoreactive glomerulus (dashed circle) (A5). DAPI served as nuclear stain. Data were obtained from three mice.

3.12 The ΔOlfr1507-GFP strain

In the well-established ΔOR paradigm, the coding region of an OR gene is replaced by gene targeting with a marker such as GFP (Feinstein and Mombaerts, 2004; Shykind et al., 2004; Bozza et al., 2009; Fuss et al., 2013). This paradigm has been instrumental in understanding aspects of the mechanisms of OR gene choice.

To further assess the specificity of the Olfr1507 antibody, I made use of a novel, C57BL/6 inbred, gene-targeted ΔOlfr1507-GFP mouse strain. In this strain with a so-called knockout mutation, OSNs that express the ΔOlfr1507 allele do not express the Olfr1507 protein but instead express GFP. The prediction is the complete absence of immunoreactivity for the Olfr1507 antibody.

I subjected MOE sections of homozygous ΔOlfr1507-GFP mice at PD21 to triple IHC with antibodies against OMP, Olfr1507, and GFP. As expected, there is no Olfr1507-immunoreactive signal in the MOE of ΔOlfr1507-GFP mice (Figure 3.21 A2). There are plenty of GFP-immunoreactive OSNs (Figure 3.21 A1). This result validates the specificity of the antibody for Olfr1507 at the level of the MOE. Furthermore, I subjected coronal sections of the OB of homozygous ΔOlfr1507-GFP mice at PD21 to triple IHC with VGLUT2, Olfr1507, and GFP. Once again, no Olfr1507-immunoreactive signal is detectable in the OB, validating the specificity of this antibody at the level of the OB. (Figure 3.21 C2). I found that the GFP immunoreactive axons project to multiple glomeruli in the medial half-OB and lateral half-OB and that the positions of these axons are close to those of the Olfr1507 glomeruli in mice with intact *Olfr1507* loci (Figure 3.21 B, C1). Consistent with the finding that ΔOR OSNs do not coalesce into a few homogeneous glomeruli but spread diffusely over a wide domain of the OB and enter many glomeruli (Bozza et al., 2009; Feinstein and Mombaerts, 2004; Zapiec and Mombaerts, 2020).

Additionally, I conducted triple IHC in sections of the MOE of homozygous ΔOlfr1507-GFP mice at PD21 with antibodies against NQO1, OCAM, and GFP. I found that GFP-immunoreactive OSNs are also OCAM-immunoreactive but not NQO1-immunoreactive and they are located in the dorsolateral and ventromedial areas of the MOE (Figure 3.22 A, B), similar to that of GFP-immunoreactive cells in

Olfr1507-IRES-tauGFP, Olfr1508-IRES-tauGFP, or Olfr1509-IRES-tauGFP mice (compare to Figure 3.2). I subjected coronal sections of the OB of homozygous ΔOlfr1507-GFP mice at PD21 to triple IHC with NQO1, OCAM, and GFP. The GFP-immunoreactive axons project to multiple glomeruli, which are located in the ventral, OCAM-immunoreactive domain of the OB but not in the dorsal, NQO1-immunoreactive domain of the OB (Figure 3.22 C, D).

To estimate the number of glomeruli that receive axons of ΔOlfr1507-GFP OSNs and possibly may be innervated by these axons, I analyzed every third OB section of one homozygous ΔOlfr1507-GFP mouse at PD21. In the medial half-OB and lateral half-OB, I identified numerous glomeruli with different types of innervation (Figure 3.23 A1 – A7, C, D). I classified the different degrees of (presumed) innervation into four categories: (1) barely, (2) sparsely, (3) intermediately, and (4) strongly (Figure 3.23 B), based on the approach of Fuss et al., 2013. In the left OB, I counted 35 of the barely type, 29 sparsely, 26 intermediately, and 24 strongly, for a total of 114 glomeruli. In the right OB of the same mouse, I counted 32 of the barely type, 31 sparsely, 29 intermediately, and 16 strongly, for a total of 108 glomeruli. Assuming that these GFP-immunoreactive OSN axons indeed synapse within the glomeruli and in view of the internal symmetry of the OB, I tentatively conclude that ΔOlfr1507 OSNs may coexpress one of as many as 54-57 other OR genes.

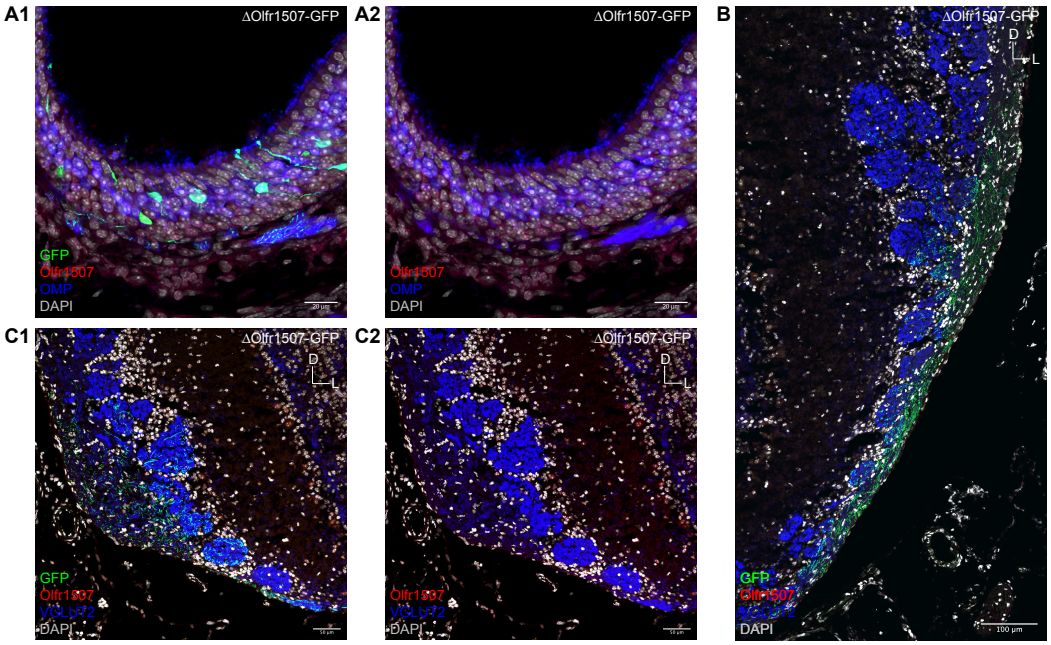


Figure 3.21. Olfr1507-immunoreactivity in homozygous ΔOlfr1507-GFP mice at PD21.

(A1 – C2) Confocal images of coronal sections of the MOE or the OB subjected to triple IHC for VGLUT2 or OMP (blue), Olfr1507 (red) and GFP (green). There are plenty of GFP-immunoreactive OSNs in the MOE (A1). There is no immunoreactive signal for Olfr1507 in the MOE (A2). GFP-immunoreactive axons project diffusely to multiple glomeruli medially (B) and laterally (C1), in an area of the OB where the Olfr1507, Olfr1508, and Olfr1509 glomeruli reside. There is no immunoreactive signal for Olfr1507 in the OB (C2). DAPI served as nuclear stain. Data were obtained from three mice.

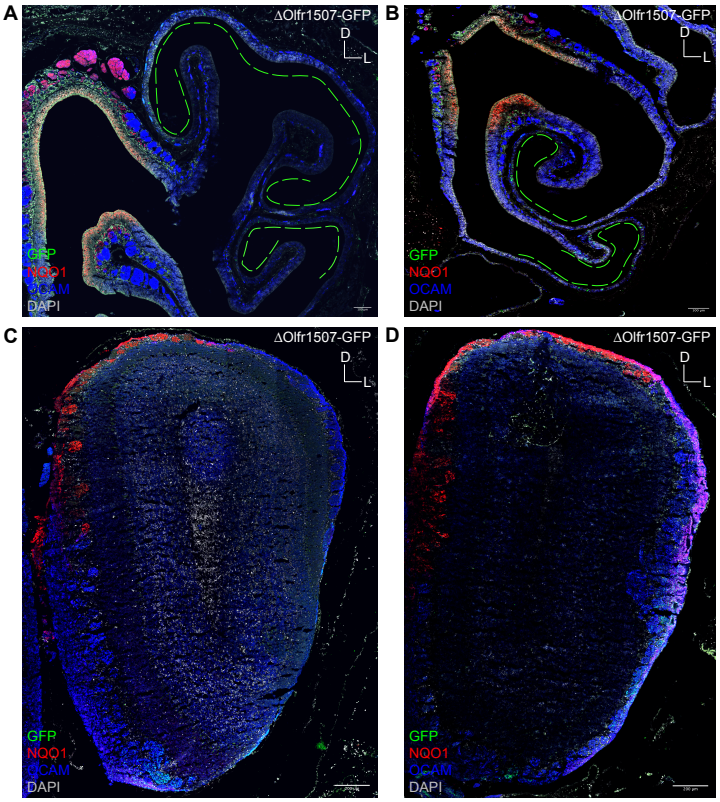


Figure 3.22. Location and axonal projections of ΔOlfr1507 OSNs in homozygous ΔOlfr1507-GFP mice at PD21.

Confocal images at low magnification of coronal sections subjected to triple IHC for OCAM (blue), NQO1 (red), and GFP (green) showing the dorsolateral part of the MOE (A), and the ventromedial part of the MOE (B) where the GFP-immunoreactive cells reside in the OCAM-immunoreactive region but not in the NQO-immunoreactive region. GFP-immunoreactive axons project to multiple glomeruli in the OCAM-immunoreactive domain but not in the NQO1-immunoreactive domain of the medial half-OB (C) and lateral half-OB (D). The green-dashed line indicates the areas of the MOE in which GFP-immunoreactive OSNs (green) reside. DAPI served as nuclear stain. Data were obtained from two mice.

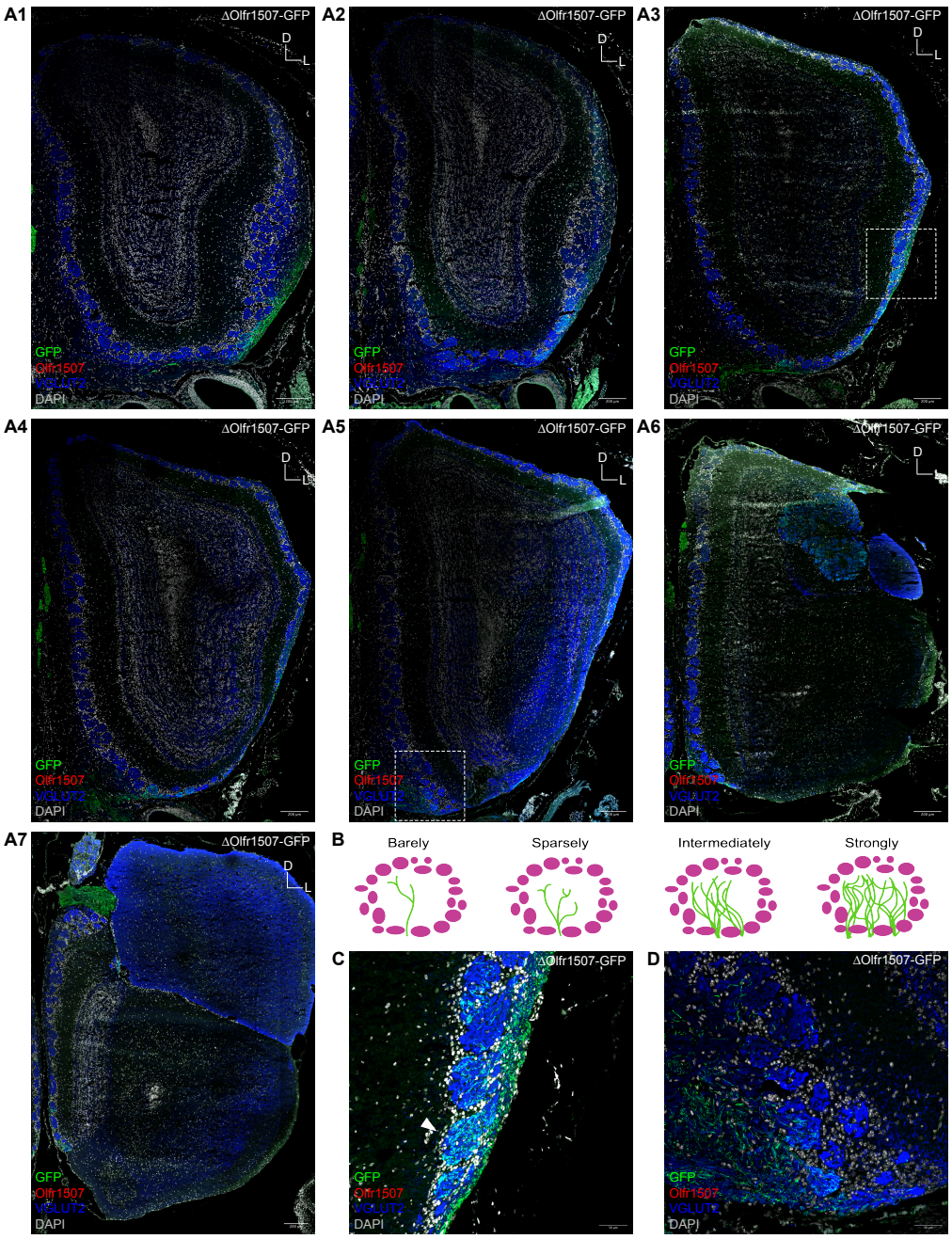


Figure 3.23. Different degrees of aparent innervation by GFP-immunoreactive axons in the olfactory bulbs of a homozygous ΔOlfr1507-GFP mouse at PD21.

(A1 – A7) Confocal images at low magnification of 7 interleaved coronal sections showing the right OB subjected to triple IHC for VGLUT2 (blue), Olfr1507 (red), and GFP (green). Individual GFP-immunoreactive glomeruli were tracked by comparison of every third section. The degree of innervation of each glomerulus was scored according to four categories (B). The dashed square in (A3) is the area magnified in (C).The arrowhead indicates a strongly innervated glomerulus in the lateral half-OB. The dashed square in (A5) is the area magnified in (D). DAPI served as nuclear stain. Data were obtained from one mouse.

3.13 The septal organ of Olfr1509-IRES-tauGFP mice

The SO is a patch of sensory mucosa that is separated from the MOE by respiratory mucosa. Similar to the MOE, the olfactory epithelium of the septal organ comprises OSNs, basal cells, and sustentacular cells. SO-OSNs respond to a broad range of odorant stimuli, as do some OSNs in the MOE (Marshall and Maruniak, 1986). Expression of ~50 class II OR genes has been identified in the mouse SO (Kaluza et al., 2004; Tian and Ma, 2008). OR genes are expressed in very different numbers of SO-OSNs. The two most frequently expressed OR genes are *Olfr370* and *Olfr1509*. Of interest here, *Olfr1509* was reported to be expressed in a range from 370 to 1,300 cells per SO (Kaluza et al., 2004; Tian and Ma, 2008; Fuss et al., 2013).

I subjected sections of the SO of homozygous Olfr1509-IRES-tauGFP mice at PD21 to triple IHC with antibodies for OMP, Olfr1507, and GFP. I confirmed that Olfr1509 is expressed abundantly in SO-OSNs (Figure 3.24 A). There is no Olfr1507-immunoreactive signal in SO-OSNs of Olfr1509-IRES-tauGFP mice (Figure 3.24 B, C). I examined the number of GFP-immunoreactive cells in both SOs in each of seven Olfr1509-IRES-tauGFP mice, for a total of 14 SOs. The average number of GFP-immunoreactive cells in one SO is 247 $\pm$ 68 and the range of cells in a SO is between 102 and 604. These numbers are similar to the average reported by Kaluza et al., 2004 and Tian and Ma, 2008, counting Olfr1509-expressing OSNs in the SO by ISH.

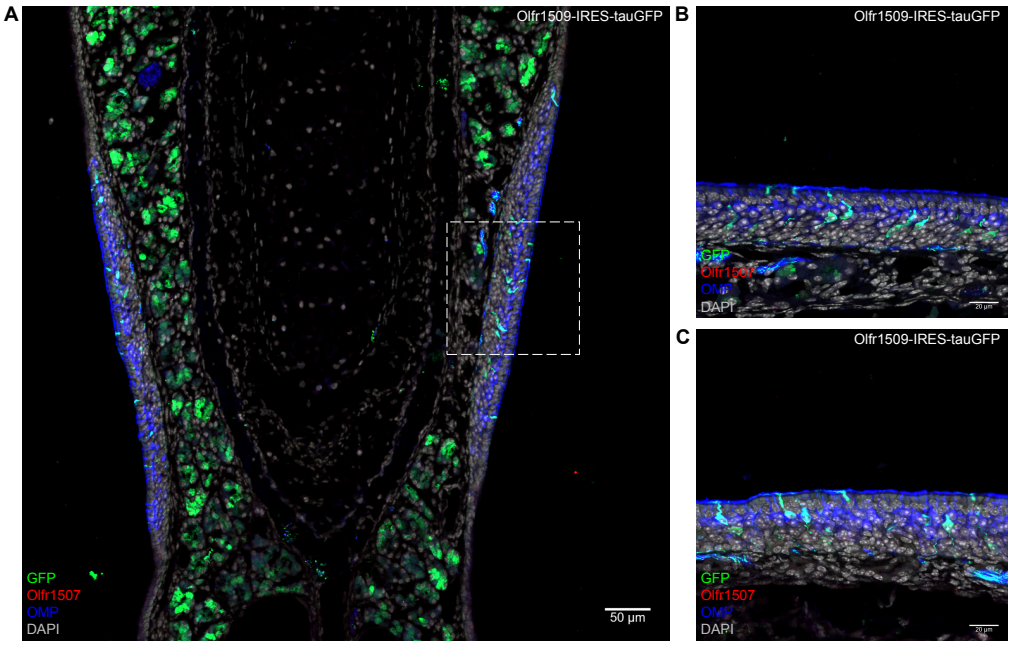


Figure 3.24. GFP-immunoreactive OSNs in the septal organ of homozygous Olfr1509-IRES-tauGFP mice at PD21.

Confocal images of coronal sections subjected to triple IHC for OMP (blue), Olfr1507 (red), and GFP (green). (A) Low magnification through the anterior region of the nose showing the septal organs on both sides of the nasal septum. Plenty of OMP-immunoreactive SO-OSNs are GFP-immunoreactive and none are Olfr1507-immunoreactive. Note that the green signal in the lamina propria is background IHC staining. The dashed square in (A) is imaged at higher magnification in (B). (C) Another coronal section. DAPI served as nuclear stain. Data were obtained from seven mice.

3.14 Atypical trajectories of GFP-immunoreactive axons in Olfr1508-IRES-tauGFP mice

Homotypic fasciculation has been proposed as a mechanism of glomerular coalescence of OSN axons (Feinstein and Mombaerts, 2004). Analyses of the trajectory of single axons expressing GFP in M72-IRES-tauGFP, M71-IRES-tauGFP, and P2-IRES-tauGFP mice showed that in the periphery, the majority of axons course individually or in small fascicles, whereas, as axons approach the target glomerulus, they enter within the inner olfactory nerve layer into larger axon bundles (Treloar et al., 2002). Fascicles of OSN axons follow variable pathways before entering the glomerulus. Diverse and complex trajectories can be interpreted that multiple guidance mechanisms are used for axon targeting (Potter et al., 2001; Treloar et al., 2002). Despite the contorted trajectories of single OSN axons, the synapses within the cognate glomeruli are highly precise, with a high level of homogeneous composition observed at the electron microscopic level (Treloar et al., 2002).

I subjected sections of the OB of homozygous Olfr1508-IRES-tauGFP mice at PD21 to triple IHC with antibodies against VGLUT2, Olfr1507, and GFP. I observed Olfr1507-immunoreactive signal in axon termini coalescing into a single homogeneous glomerulus (Figure 3.25). GFP-immunoreactive OSN axons terminate into a more dorsally located homogeneous glomerulus, as I reported earlier in this thesis. Interestingly, I observed individual GFP-immunoreactive axons traveling in trajectories that are different from the large GFP-immunoreactive axon fascicles (Figure 3.25 A1 – A3, arrowheads). These GFP-immunoreactive axons entered the glomerular layer in various paths before coalescing into the single homogeneous GFP-immunoreactive glomerulus (Figure 3.25 B, arrowheads). I performed the same IHC on consecutive sections of the OB of homozygous Olfr1508-IRES-tauGFP mice at PD56 and observed single GFP-immunoreactive axons traveling throughout the glomerular layer (Figure 3.26). These GFP-immunoreactive axons can be tracked in a consecutive series of confocal images but no additional immunoreactive glomeruli could be detected. Note that Olfr1507-immunoreactive axons are not observed in the olfactory nerve layer, possibly because the signal is below detection threshold.

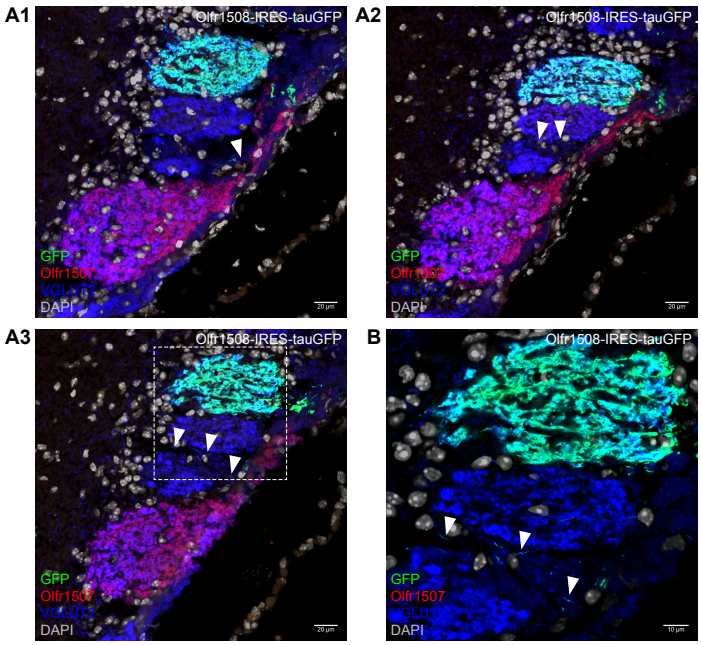


Figure 3.25. Atypical trajectories of GFP-immunoreactive axons in the olfactory bulb of homozygous Olfr1508-IRES-tauGFP mice at PD21.

Confocal images showing the lateral half-OB. Triple IHC for VGLUT2 (blue), Olfr1507 (red), and GFP (green). (A1 – A3) The projections of GFP-immunoreactive axons were followed in three consecutive OB sections. Two distinct homogeneous glomeruli are immunoreactive for either Olfr1507 (red) or GFP (green). Single GFP-immunoreactive axons enter the glomerular layer at lower magnification (arrowheads). Single GFP-immunoreactive axons traveling within the glomerular layer entering from regions other than the apposed outer nerve layer (arrowheads). The dashed square in (A3) is the area magnified in (B). These GFP-immunoreactive axons followed many distinct trajectories and appear to target their cognate glomerulus. DAPI served as nuclear stain. Data were obtained from three mice.

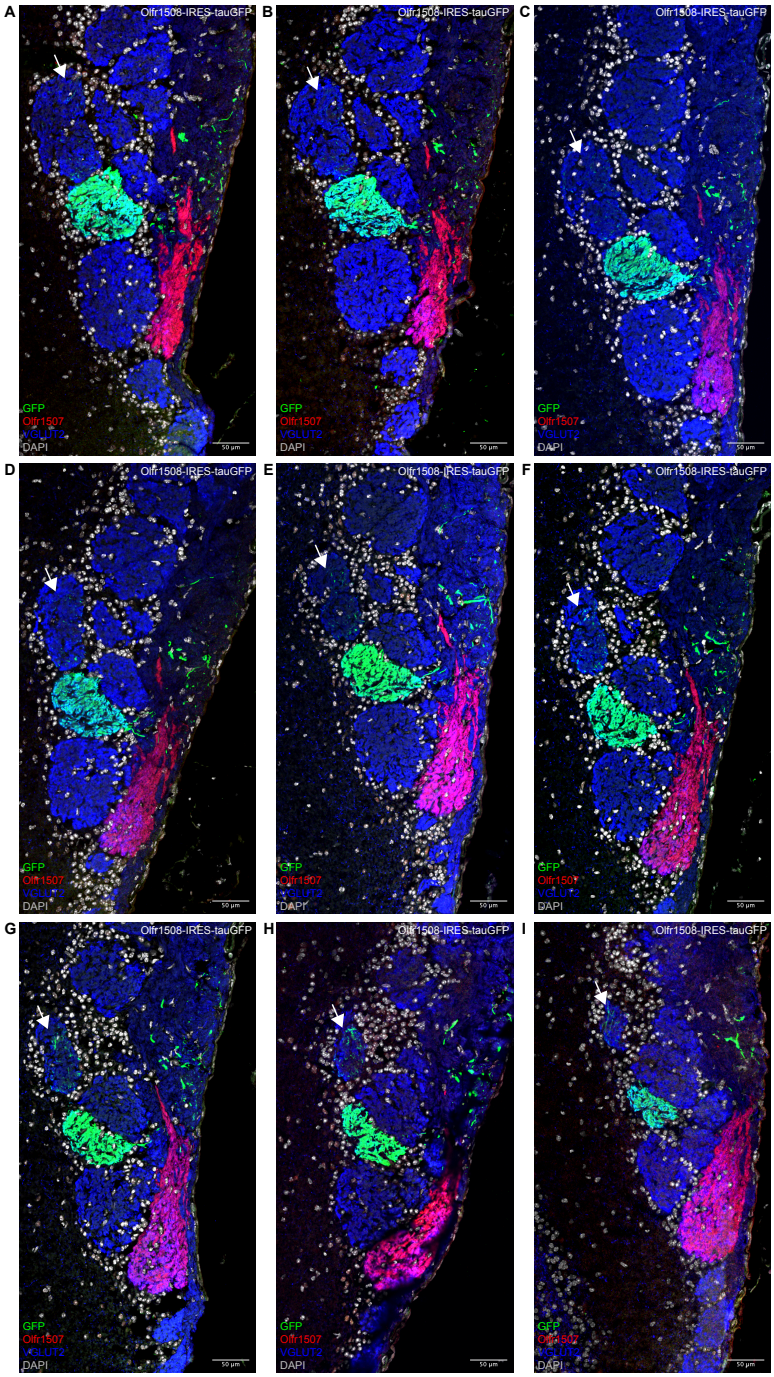


Figure 3.26. GFP-immunoreactive axons follow different routes in the lateral half-olfactory bulb of homozygous Olfr1508-IRES-tauGFP mice at PD56.

Confocal images of nine consecutive OB sections. Triple IHC for VGLUT2 (blue), Olfr1507 (red), and GFP (green). (A – E) One GFP-immunoreactive glomerulus is visualized. Axons are immunoreactive either for Olfr1507 or GFP in the outer nerve layer. Single GFP-immunoreactive axons are observed (arrows). (E – I) Two distinct homogeneous glomeruli are immunoreactive for either Olfr1507 or GFP. Individual GFP-immunoreactive axons enter from regions other than the apposed outer nerve layer (arrows). These GFP-immunoreactive axons followed many distinct trajectories and appear to target their cognate glomerulus. DAPI served as nuclear stain. Data were obtained from three mice.

4 Discussion

I have characterized novel inbred C57BL/6 mouse strains with various gene-targeted mutations in *Olfr1507*, *Olfr1508*, or *Olfr1509*. The expression of these OR genes is confined to the OCAM-immunoreactive dorsal region of the MOE. I demonstrated that the commercial antibody against the mouse Olfr1507 is specific. The Olfr1507-immunoreactive OSNs show complete concordance with GFP-immunoreactive OSNs in homozygous Olfr1507-IRES-tauGFP mice and in homozygous Olfr1507-IRES-gapGFP mice, and with LacZ-immunoreactive OSNs in homozygous Olfr1507-IRES-tauLacZ mice. The absence of double Olfr1507-immunoreactive and GFP-immunoreactive OSNs in Olfr1508-IRES-tauGFP or Olfr1509-IRES-tauGFP mice rules out cross-reactivity of the Olfr1507 antibody against Olfr1508 or Olfr1509. I observed fewer LacZ-immunoreactive OSNs in homozygous Olfr1507-IRES-tauLacZ mice. I found that Olfr1507 is expressed in 4-fold more OSNs than Olfr1508 and three-fold more than Olfr1509. The number of OSNs was reduced to half after performing the Abercrombie correction factor. I observed the abundant presence of GFP-immunoreactive OSNs in the SO of Olfr1509-IRES-tauGFP mice and no GFP-immunoreactive OSNs in the SO of homozygous Olfr1507-IRES-tauGFP mice or Olfr1508-IRES-tauGFP mice.

I characterized the positions of the corresponding glomeruli at PD21 and PD56 and computed the total glomerular volume. I found that the glomerular positions of the Olfr1507, Olfr1508, or Olfr1509 are consistent among mice. The Olfr1507 glomeruli are located ventrally, the Olfr1509 glomeruli dorsally, and the Olfr1508 glomeruli occupy an intermediate position. I also validated the specificity of the Olfr1507 antibody at the level of the OB. To compute the total glomerular volume per mouse, I developed a pipeline computing the glomerular area of each optical section from a z-stack obtained under a confocal microscope. Olfr1507-IRES-tauGFP mice exhibited the largest total glomerular volume, followed by Olfr1509-IRES-tauGFP and then Olfr1508-IRES-tauGFP.

I characterized the relative positions of these glomeruli in double heterozygous Olfr1508-IRES-tauGFP x Olfr1509-IRES-tauGFP mice. I found little or no variability in the relative positions of the Olfr1507, Olfr1508, or Olfr1509 glomeruli. I observed atypical trajectories of single GFP-immunoreactive axons, which I believe are from Olfr1508-expressing OSNs.

A convincing validation of the specificity of the Olfr1507 antibody is the absence of immunoreactive signal in a novel C57BL/6 inbred knockout strain, carrying a ΔOlfr1507-GFP gene-targeted mutation. ΔOlfr1507 OSNs reside within the OCAM-immunoreactive region and project their axons to multiple glomeruli within a restricted OCAM-immunoreactive domain of the OB and remain located to the OCAM-immunoreactive region. ΔOlfr1507 OSNs appear to express a subset of >50 intact OR genes for second choice.

4.1 The Olfr1507 antibody is specific for Olfr1507

To rigorously test the specificity of the Olfr1507 antibody from Osenses, I performed IHC on coronal sections of the MOE of mice homozygous for either of five gene-targeted mutations: Olfr1507-IRES-tauGFP, Olfr1507-IRES-gapGFP, Olfr1507-IRES-tauLacZ, Olfr1508-IRES-tauGFP, or Olfr1509-IRES-tauGFP mice. This antibody had previously been characterized in MOE and OB of the MOR28-IRES-gap-GFP strain from the Sakano laboratory (Low and Mombaerts, 2017). The MOR28-IRES-gap-GFP strain is in a mixed genetic background and displays multiple glomeruli, together with compartmentalization for heterozygous mice (Zapiec and Mombaerts, 2015; Low and Mombaerts, 2017). Immunoreactivity can be affected by high sequence homology between ORs, by post-translational modifications, by protein folding, by protein-protein interactions, and by fixation crosslinking. Due to the high homology between Olfr1507, Olfr1508, and Olfr1509 OR genes, it was necessary to exclude cross-reactivity, even weak cross-reactivity.

Importantly, the Olfr1507-immunoreactive signal shows complete concordance with the GFP-immunoreactive signal in homozygous Olfr1507-IRES-tauGFP mice, both at the level of the MOE and of the OB; with the GFP-immunoreactive signal in the MOE of homozygous Olfr1507-IRES-gapGFP mice; and with the LacZ-immunoreactive signal in the MOE of homozygous Olfr1507-IRES-lacZ mice. In the course of these analyses, it came to my attention that there are fewer Olfr1507-expressing OSNs in Olfr1507-IRES-tauLacZ mice compared to in mice with the same type of gen-targeted mutation expressing tauGFP or gapGFP. The reasons are not clear. This lower cell number may reflect a lower stability or translational efficiency of the Olfr1507-IRES-tauLacZ transcripts. GFP may afford a higher degree of sensitivity of detection compared to LacZ (Fuss et al., 2013).

I documented the absence of cross-reactivity of the Olfr1507 antibody against Olfr1508 or Olfr1509 by demonstrating the absence of colocalization of Olfr1507-immunoreactive signal with GFP-immunoreactive signal in OSNs of homozygous Olfr1508-IRES-tauGFP or Olfr1509-IRES-tauGFP mice. Despite the high similarity in the amino acid sequences of Olfr1507, Olfr1508, or Olfr1509, the Olfr1507-peptide with which the rabbits were immunized gave rise to a polyclonal serum that is specific

for Olfr1507. I conclude that this commercially available Olfr1507 antibody is a valuable tool for investigating the distribution of the OR protein and to characterize Olfr1507-specific glomeruli in the OB of wild-type mice.

4.2 *Olfr1507* is the highest expressed OR gene

The scarcity of reports on the numbers of OSNs expressing a given OR gene is probably related to the labor-intensive nature of such counting efforts. Two papers from the Mombaerts laboratory reported cell counts in strains with a gene-targeted mutation in an OR gene that generates a fluorescent protein (Bressel et al., 2016; Low and Mombaerts, 2017). Bressel et al., 2016 reported counts for a set of strains with and OR-IRES-marker mutation in 11 OR genes and found that P3-IRES-tauGFP to be the smallest OSN population (2,236 ± 247 cells per mouse at PD21) and the MOR256-17-IRES-tauGFP the largest OSN population (37,023 ± 6,318 per mouse at PD21); they did not report cell counts for Olfr1507, Olfr1508, or Olfr1509. Low and Mombaerts, 2017 report counts of Olfr1507-immunoreactive OSNs for each allele in MOR28-IRES-gap-GFP +/- mice (Serizawa et al., 2000) where one of the alleles, the wild-type allele, was either from a C57BL6/N or a 129S6/SvEvTac genetic backgrounds. They obtained a total of 31,657 ± 2305 cells for homozygous MOR28-IRES-gap-GFP mice (Serizawa et al., 2000) and a total of 41,988 ± 3142 Olfr1507-immunoreactive cells for heterozygous MOR28-IRES-gap-GFP mice. Note that the expression of gap-GFP reporter is driven by a 129-derived promoter sequence in the gene-targeted mutation. In my Ph.D. thesis, I reported the number of OSNs expressing Olfr1507, Olfr1508, or Olfr1509 at PD21 for inbred C57BL/6 mice. My results showed that the highest OR expressed is Olfr1507, four-fold more than Olfr1508 and 3-fold more than Olfr1509.

The counting approaches differ in several ways. In cell counting studies, a correction factor must be implemented to avoid overcounting of cells and a very popular formula is that of Abercrombie. The Abercrombie correction factor has been widely used in biology to prevent overcounting of cells, but the formula considers thick sections, typically vibratome sections, and measures the cell nucleus diameter in the z-plane, considering depth, instead of x and y-planes. My approach to obtain the cell counts was to collect every third section from cryosectioning, I used 6 µm sections, and to count manually from scanned slides, with Panoramic viewer software (3D Histech), all GFP-immunoreactive cells from every collected section from the whole set of IHC slides. I then applied the Abercrombie correction factor. For the extrapolation, I measured the average nucleus diameter in the x and y planes with the Slide Viewer

or ZEN Blue software. Bressel et al., 2016 manually counted every cell from every 12 µm section of the MOE under a confocal microscope. Low and Mombaerts, 2017 counted cells in every fifth 12 µm section using the cell counter plugin in Fiji ImageJ. Bressel et al., 2016 measured the nucleus diameter of OSNs in the z-plane. Low and Mombaerts, 2017 measured the nucleus diameter with Panoramic viewer software (3D Histech) in the x and y-planes. My total cell counts, without employing the Abercrombie correction, are similar to the counts obtained after correction by Low and Mombaerts, 2017 for Olfr1507-immunoreactive OSNs in homozygous MOR28-IRES-gap-GFP mice.

Low and Mombaerts, 2017 counted Olfr1507-immunoreactive cells but not GFP-immunoreactive cells; the section thickness and the interleaved sampling are different, as well as the software used to count OSNs; and the mice were not inbred. These factors could explain the differences in cell counts. A caveat of my approach of counting every third section assumes a uniform distribution of OSNs expressing Olfr1507, Olfr1508, or Olfr1509 across the MOE. But the intervening sections may have more, less, or no labeled OSNs. In future studies, I advocate counting all labeled OSNs in every consecutive section in addition to performing cell counting using a semi-automated pipeline that recognizes every labeled OSN.

4.3 Characterization of the positions of the glomeruli for Olfr1507, Olfr1508, or Olfr1509

OSNs expressing homologous OR genes within a cluster tend to project their axons to glomeruli that are closely juxtaposed in the OB (Tsuboi et al., 1999; Strotmann et al., 2000). My work confirms and extends the concept of glomerular convergence demonstrating that axons expressing Olf1507, Olfr1508, or Olfr1509 coalesce into unique glomeruli in Olfr1507-IRES-tauGFP, Olfr1507-IRES-gapGFP, Olfr1507-IRES-tauLacZ, Olfr1508-IRES-tauGFP, or Olfr1509-IRES-tauGFP gene-targeted strains. Using the OR-IRES-marker genetic approach (Mombaerts et al., 1996) permitted the visualization of glomeruli for expressing Olfr1507, Olfr1508, or Olfr1509 in novel C57BL/6 inbred gene-targeted strains. The comparison between the positions of the GFP-immunoreactive glomeruli in homozygous Olfr1508-IRES-tauGFP or Olfr1509-IRES-tauGFP mice was facilitated by the ability to visualize the Olfr1507 glomeruli on the basis of the Olfr1507-immunoreactive signal. I found that axons expressing either Olfr1507, Olfr1508, or Olfr1509 coalesce into a single pair of glomeruli in each OB, for a total of four glomeruli per mouse. I validated the specificity of the Olfr1507 antibody by demonstrating colocalization of the GFP-immunoreactive or LacZ-immunoreactive signal with the Olfr1507-immunoreactive signal in Olfr1507-IRES-marker strains. I did not observe Olfr1507 signal in neighboring glomeruli.

I observed little or no variability in the relative glomerular positions for Olfr1507, Olfr1508, or Olfr1509, both at PD21 (the standard age used in the Mombaerts laboratory) and at PD56 (an age that is typically used in neuroanatomical studies). In Olfr1508-IRES-tauGFP mice, the GFP-immunoreactive glomeruli reside dorsally to the Olfr1507-immunoreactive glomeruli, one glomerulus width away. In Olfr1509-IRES-tauGFP mice, the GFP-immunoreactive glomeruli are located dorsally to the Olfr1507-immunoreactive glomeruli, three to four glomerular widths away. Olfr1507 glomeruli occupy are at the most ventral position, the Olfr1509 glomeruli have the most dorsal position, and the Olfr1508 glomeruli occupy an intermediate position. The absence of variability in the relative glomerular positions may reflect the use of mice in an inbred background. I conclude that inbred OR-IRES-tauGFP mice represent a reliable approach to characterize OR-specific glomeruli.

4.4 The Olfr1507 glomeruli in the MOR28-IRES-gap-GFP strain

The multiple Olfr1507 glomeruli in the MOR28-IRES-gap-GFP strain of the Sakano laboratory raise the question whether they can be considered as transient phenomena or persist in aged mice. The Olfr1507 glomerular positions are extremely ventral, making it challenging to image in whole mounts. Using an antibody for VGLUT2 to observe all glomeruli, I corroborated the presence of multiple Olfr1507 glomeruli. I studied this published MOR28-IRES-gap-GFP strain mainly with the aim to compare it to the inbred Olfr1507-IRES-tauGFP, Olfr1507-IRES-gapGFP, and Olfr1507-IRES-tauLacZ strains.

4.5 Total glomerular volume in homozygous OR-IRES-marker mice

I measured the total glomerular volume (TGV) in homozygous Olfr1507-IRES-tauGFP, Olfr1508-IRES-tauGFP, or Olfr1509-IRES-tauGFP mice. Studies to quantify the glomerular volume for a given OR gene are scarce (Bressel et al., 2016) and methods to reconstruct the glomerular volume from cryosections must be developed according to the experimental conditions used. I developed a pipeline using CellProfiler in collaboration with Ph.D. student Yu Weng based on the analysis of a study in which the total glomerular volume was measured in 11 OR-gene-targeted strains (Bressel et al., 2016). I included three measures in order to compute the glomerular volume in my project. The first measure is the use of the VGLUT2 antibody as a marker to delineate the glomerular structures, allowing me to exclude the outer nerve layer during image processing and to obtain a more accurate area value during image segmentation. A second measure is the inclusion of every optical section in the analysis, acknowledging that glomeruli are not structures with perfect spherical shapes; I acquired z-stacks from 6 µm OB sections with constant intervals of 1 µm between optical planes. The third measure is the development of a semi-automated pipeline for assessing the cross-sectional area of each glomerular section, as opposed to manual measurements by an observer. This choice was driven by the unique shapes of glomeruli, and the program excels in recognizing the boundaries of GFP-immunoreactive glomeruli better than a human eye. Note that cryosectioning sometimes rips the lateral glomeruli because they are very exposed and the only protecting structure is the skull. Instead, the medial glomeruli remain intact because they are protected by the brain. The collection of images captured were analyzed in the CellProfiler pipeline to create a 3D representation of the glomerular volume. The total glomerular volume does not differ significantly between Olfr1507 and Olfr1509. I did not perform a correlation analysis between the numbers of Olfr1507 and Olfr1509 OSNs and the total volume of the corresponding glomeruli.

In Bressel et al., 2016, the linear correlation estimates that the number of OSNs is approximately one tenth of the computed TGV. For instance, the largest TGV per mouse was found for MOR256-17 (Olfr15) with a glomerular volume of ~3,000,000 μm^3 for a total of 37,023 $\pm$ 6,318 cells per mouse. Similarly, for the lowest OR expressed, P3 (Olfr713), the TGV was ~250,000 μm^3 for a total of 2,236 $\pm$ 247 cells.

The magnitudes of the TGV I computed range from 3 to 5 times that of the volume represented by MOR256-17. Why are my TGV values much larger than the ones reported by Bressel et al., 2016? The methods differ, starting from sample collection to the computation of the glomerular area. Three differences may account for the larger TGV values that I computed. The first is that I measured the cross-sectional area from every optical section acquired under the confocal microscope vs. measuring one cross-sectional area only at the middle of the optical section. The second is the use of VGLUT2 antibody is to outline glomerular shapes together with the GFP antibody. The third is the delineation of the glomerular area from every section using the pipeline instead of manually. I argue that the automated process to define the area containing a glomerulus is more accurate than to execute it manually by an observer, because a glomerulus is not always a perfect sphere.

4.6 Glomeruli in double heterozygous Olfr1508-IRES-tauGFP x Olfr1509-IRES-tauGFP mice

I generated double heterozygous Olfr1508-IRES-tauGFP x Olfr1509-IRES-tauGFP mice to determine the relative positions of the Olfr1507, Olfr1508, or Olfr1509 glomeruli. Note that because the Olfr1508 and Olfr1509 genes are linked, it is not possible to generate mice that are homozygous for Olfr1508-IRES-tauGFP and/or Olfr1509-IRES-tauGFP. Although it is not possible to distinguish the two types of GFP-immunoreactive axons, I inferred the identity of the Olfr1508 or Olfr1509 glomeruli based on my previous characterizations in homozygous mice. In these double heterozygous mice, both *Olfr1507* alleles are wild-type and axons of Olfr1507-expressing OSNs can be visualized on the basis of their Olfr1507-immunoreactive signal. I observed two distinct GFP-immunoreactive glomeruli per half-OB, consistent with Olfr1508 or Olfr1509 having their own glomeruli. Due to monoallelic expression of the *Olfr1508* or *Olfr1509* genes, glomeruli are not homogeneous for GFP immunoreactivity and appear as partially innervated.

I did not observe local permutations (Strotmann et al., 2000) in the positions of the Olfr1507, Olfr1508, or Olfr1509 glomeruli in these double heterozygous mice.

4.7 GFP-immunoreactive axons in double heterozygous mice

While characterizing the glomerular positions in the double heterozygous Olfr1508-IRES-tauGFP x Olfr1509-IRES-tauGFP mice, I observed GFP-immunoreactive axons traveling close to the presumptive Olfr1508 glomerulus in the lateral half-OB. Axons expressing a given OR can take different trajectories before terminating in the cognate glomerulus. My analyses did not allow me to distinguish whether GFP-immunoreactive axons are just “passing by” or they actually terminate and synapse in that glomerular location - which could be assessed with 3D reconstructions of whole-mount samples such as reported by Potter et al., 2001. The Olfr1507, Olfr1508, or Olfr1509 glomerular positions are located very posteriorly and ventrally in the OB, which makes them challenging to image in whole mounts. Although the identity of the single GFP-immunoreactive axons cannot be identified unambiguously in the double heterozygous mice, I believe that these axons are from OSNs expressing the Olfr1508-IRES-tauGFP allele. The reason is that I observed such axons uniquely near the presumptive Olfr1508 glomerulus in the lateral half-OB. An alternate approach to discover whether GFP-immunoreactive axons are passing by or terminate in nearby glomeruli is to stain for synaptic vesicle markers present in OSNs such as synaptophysin and bassoon (Marcucci et al., 2009; Thyssen et al., 2010).

4.8 GFP-immunoreactivity in the main olfactory epithelium of ΔOlfr1507-GFP mice

The final test to validate specificity of the Olfr1507 antibody was performing IHC in a novel inbred knock-out strain, ΔOlfr1507-GFP, in which the coding region of Olfr1507 is replaced with the reporter GFP. There are plenty of GFP-immunoreactive OSNs in homozygous ΔOlfr1507 mice, showing that this mutant allele can be chosen for expression, stably transcribed, and translated. The absence of Olfr1507-immunoreactive signal in the MOE and OB is powerful evidence that the antibody is specific for Olfr1507.

Over the past quarter of a century, the ΔOR paradigm has been applied to several OR genes and by several groups, and has provided novel insights into aspects of the mechanisms of OR gene choice (Wang et al., 1998; Serizawa et al., 2003; Feinstein et al., 2004; Lewcock and Reed, 2004; Shykind et al., 2004; Bozza et al., 2009; Grosmaitre et al., 2009; Fuss et al., 2013; Zapiec and Mombaerts, 2020). The fate of ΔOlfr1507-expressing OSNs may be one or a combination of the following: these cells may have a reduced life span, undergo extinction of ΔOlfr1507 expression, or coexpress an intact OR gene. The coexpression of an intact OR gene by individual ΔOlfr1507 OSNs is classically interpreted by a cell-autonomous mechanism and as the consequence of the lack of negative feedback signaling within these cells. Further exploration of the ΔOlfr1507-GFP strain should be performed to identify OSNs that have turned off transcription of the ΔOlfr1507 allele and proceeded to express an intact OR gene; to identify OSNs that contain RNA of the ΔOlfr1507 allele and an intact OR gene; to identify the time window during which this coexpression occurs; to determine the ratio between OSNs expressing an intact Olfr1507 OR protein and OSNs expressing ΔOlfr1507; and finally, to identify OSNs that coexpress two OR loci permanently, the ΔOlfr1507 allele and an intact OR gene.

ΔOlfr1507 OSNs reside within the dorsolateral and ventromedial areas of the MOE, where normally OSNs expressing Olfr1507 reside. This observation suggests that ΔOlfr1507-OSNs may coexpress an intact OR gene that is normally also expressed in this area.

4.9 GFP-immunoreactivity in the olfactory bulb of ΔOlfr1507-GFP mice

Whereas axons of OSNs that express a given OR gene coalesce into one or a few glomeruli on each the medial half-OB and lateral half-OB, axons of ΔOR OSNs project diffusely over a wide domain of the OB and enter many glomeruli (Wang et al., 1998; Serizawa et al., 2003; Feinstein et al., 2004; Shykind et al., 2004; Bozza et al., 2009; Fuss et al., 2013; Zapiec and Mombaerts, 2020). This phenotype correlates with the coexpression of multiple OR genes across the population of ΔOR OSNs.

I found that GFP-immunoreactive axons in homozygous ΔOlfr1507-GFP mice project diffusely across the ventral aspect of the OCAM-immunoreactive domain of the OB. A popular interpretation of this phenotype is that these axons are from OSNs that express an intact OR gene and project to the cognate glomerulus. The negative feedback hypothesis assumes that the ΔOR allele is the first choice to occur in a temporal sequence. However, to prove the hypothesis is technically difficult as individual ΔOR OSNs cannot be followed over time (Fuss et al., 2013).

The total number of (apparently) innervated glomeruli can give an estimate on how many OR genes are coexpressed. I observed that GFP-immunoreactive OSNs axons of homozygous ΔOlfr1507 mice project to >100 glomeruli in both the medial and lateral half-OB, suggesting that there may be >50 OR gene candidates for coexpression/second choice in these OSNs. I analyzed only one mouse, at PD21. It will be interesting to analyze older mice, as glomerular projections may undergo a refinement process. In older mice, ΔOlfr1507 OSNs that succeed in expressing an intact OR may send their axons to their cognate glomeruli in the OB thus exhibiting a phenotype with fewer innervated glomeruli than in PD21 mice. Conversely, axons of ΔOlfr1507 OSNs that do not succeed in co-expressing a functional OR will not make or maintain synaptic connections in glomeruli.

4.10 Olfr1509-expressing OSNs in the septal organ

A small subset of OR genes are also expressed in the SO. Axons of SO-OSNs project to so-called septal glomeruli residing in the ventromedial aspect of the OB (Fuss et al., 2013). I observed GFP-immunoreactive OSNs in the SO of homozygous Olfr1509-IRES-tauGFP mice but not in homozygous Olfr1507-IRES-tauGFP or Olfr1508-IRES-tauGFP mice. It appears that Olfr1509-expressing SO-OSNs send their axons to the same pair of glomeruli where Olfr1509 OSNs that originate from the MOE converge, as I observed only a single immunoreactive glomerulus per half-OB. Alternatively, the low number of Olfr1509-expressing SO-OSNs may not be sufficient to form additional glomeruli that are stable. It is not possible to distinguish Olfr1509-expressing SO-OSNs from Olfr1509-expressing OSNs in the MOE.

4.11 Olfr1508 axons follow atypical trajectories in Olfr1508-IRES-tauGFP mice

An axonal mechanism that axons may use to target glomeruli is homotypic fasciculation. Axons from OSNs expressing the same OR would fasciculate en route from the MOE to the OB and then innervate the same glomerulus. However, a small proportion of axons target their glomeruli by anomalous routes through the glomerular layer (Treloar et al., 2002). I observed single GFP-immunoreactive axons of homozygous Olfr1508-IRES-tauGFP mice at PD21 and PD56 traveling around and along neighboring glomeruli before entering the cognate glomerulus. It is unlikely that these axons terminate in adjacent glomeruli because I did not observe the formation of additional GFP-immunoreactive glomeruli in the medial and lateral half-OB. I speculate that homotypic fasciculation between axons is not a prerequisite for correct axonal targeting but can facilitate the coalescence into glomeruli. It is not clear whether GFP-immunoreactive axons make synapses there or whether these are axons that are simply passing through and will eventually terminate in the cognate glomerulus. The apparent absence of stable homotypic fasciculation does not exclude the possibility that transient periods of fasciculation may be necessary for correct glomerular targeting.

4.12 Concluding remarks

In my thesis, I have shown that employing C57BL/6 inbred gene-targeted strains provides consistent and reliable data. I examined the expression in the MOE and glomerular patterns associated with Olfr1507, Olfr1508, or Olfr1509 utilizing a commercially available antibody for Olfr1507. I validated the specificity of the Olfr1507 antibody using several novel OR-IRES-marker knockin strains and the ΔOlfr1507 knockout strain. I showed that in knockin strains, the relative positions of the Olfr1507, Olfr1508, or Olfr1509 glomeruli are consistent and do not show overt glomerular permutations. ΔOlfr1507-expressing OSNs reside in the same area of MOE as Olfr1507-expressing OSNs and project their axons to >100 glomeruli per OB with different degrees of apparent innervation, suggesting that ~50 OR genes are co-expressed with ΔOlfr1507.

5 Literature

Abercrombie, M. (1946). Estimation of nuclear population from microtome sections. Anat. Rec. *94*, 239–247.

Au, W. W., Treloar, H. B., and Greer, C. A. (2002). Sublaminar organization of the mouse olfactory bulb nerve layer. J. Comp. Neurol. *446*, 68–80.

Barnea G., O'Donnell S., Mancia F., Sun X., Nemes A., Mendelsohn M., and Axel R. (2004). Odorant receptors on axon termini in the brain. Science *304*, 1468.

Barnes, I.H.A., Ibarra-Soria, X., Fitzgerald, S., Gonzalez, J.M., Davidson, C., Hardy, M.P., … Frankish, A. (2020). Expert curation of the human and mouse olfactory receptor gene repertoires identifies conserved coding regions split across two exons. BMC Genomics *21*, 196.

Barrios, A.W., Núñez, G., Sánchez Quinteiro, P., and Salazar, I. (2014). Anatomy, histochemistry, and immunohistochemistry of the olfactory subsystems in mice. Front. Neuroanat. *8*, 63.

Bozza, T., Feinstein, P., Zheng, C., Mombaerts, P. (2002). Odorant receptor expression defines functional units in the mouse olfactory system. J. Neurosci. 22, 3033–3043.

Bozza, T., Vassalli, A., Fuss, S., Zhang, J.J., Weiland, B., Pacifico, R., Feinstein, P., and Mombaerts, P. (2009). Mapping of class I and class II odorant receptors to glomerular domains by two distinct types of olfactory sensory neurons in the mouse. Neuron *29*, 220–233.

Bressel, O.C., Khan, M., and Mombaerts, P. (2016). Linear correlation between the number of olfactory sensory neurons expressing a given mouse odorant receptor gene and the total volume of the corresponding glomeruli in the olfactory bulb. J. Comp. Neurol. *524*, 199–209.

Buck, L., and Axel, R. (1991). A novel multigene family may encode odorant receptors: a molecular basis for odor recognition. Cell *65*, 175–187.

Carpenter, A. E., Jones, T. R., Lamprecht, M. R., Clarke, C., Kang, I. H., Friman, O. (2006). CellProfiler: image analysis software for identifying and quantifying cell phenotypes. Genome Biol. 7: R100.

Chess A, Simon I, Cedar H, and Axel R. (1994). Allelic inactivation regulates olfactory receptor gene expression. Cell *78*, 823–834.

Døving, K. B., and Trotier, D. (1998). Structure and function of the vomeronasal organ. J. Exp. Biol. *201*, 2913–2925.

Emoto, K. (2005). Mechanisms of heat-induced antigen retrieval: does pH or ionic strength of the solution play a role for refolding antigens? J Histochem. Cytochem. *53*, 1311–1321.

Feinstein, P., and Mombaerts, P. (2004). A contextual model for axonal sorting into glomeruli in the mouse olfactory system. Cell, *117*, 817–831.

Feinstein, P., Bozza, T., Rodriguez, I., Vassalli, A., and Mombaerts, P. (2004). Axon guidance of mouse olfactory sensory neurons by odorant receptors and the β2 adrenergic receptor. Cell *117*, 833–846.

Fuss, S.H., Omura, M., and Mombaerts, P. (2007). Local and cis effects of the H element on expression of odorant receptor genes in mouse. Cell *130*, 373–384.

Fuss, S.H., Zhu, Y., and Mombaerts, P. (2013). Odorant receptor gene choice and axonal wiring in mice with deletion mutations in the odorant receptor gene SR1. Mol. Cell. Neurosci. *56*, 212–224.

Graziadei, P.P.C. (1971). The Olfactory Mucosa of Vertebrates BT - Olfaction. In J.E. Amoore, M.G.J. Beets, J.T. Davies, T. Engen, J. Garcia, R.C. Gesteland, … L.M. Beidler (Eds.) (pp. 27–58). Berlin, Heidelberg: Springer Berlin Heidelberg.

Grosmaitre, X., Fuss, S.H., Lee, A.C., Adipietro, K.A., Matsunami, H., Mombaerts, P., and Ma, M. (2009). SR1, a mouse odorant receptor with an unusually broad response profile. J. Neurosci. *29*, 14545–14552.

Grüneberg H. (1973). A ganglion probably belonging to the N. terminalis system in the nasal mucosa of the mouse. Z. Anat. Entwicklungsgesch. *140*, 39–52.

Gussing, F., and Bohm, S. (2004). NQO1 activity in the main and the accessory olfactory systems correlates with the zonal topography of projection maps. Eur. J. Neurosci. *19*, 2511–2518.

He, L., Li, Y., Li, Y., Pu, W., Huang, X., Tian, X., … and Zhou, B. (2017). Enhancing the precision of genetic lineage tracing using dual recombinases. Nature Med. *23*, 1488–1498.

Ibarra-Soria, X., Nakahara, T.S., Lilue, J., Jiang, Y., Trimmer, C., Souza, M.A., Netto, P., Ikegami, K., Murphy, N.R., Kusma, M., Kirton, A., Saraiva, L.R., Keane, T.M., Matsunami, H., Mainland, J., Papes, F., and Logan, D.W. (2017). Variation in olfactory neuron repertoires is genetically controlled and environmentally modulated. eLife 6: e21476.

Imai, T., Suzuki, M., and Sakano, H. (2006). Odorant receptor-derived cAMP signals direct axonal targeting. Science *314*, 657–661.

Ishii, T., Serizawa, S., Kohda, A., Nakatani, H., Shiroishi, T., Okumura, K., … and Sakano, H. (2001). Monoallelic expresion of the odourant receptor gene and axonal projection of olfactory sensory neurones. Genes Cells *6*, 71–78.

Iwema, C.L., Fang, H., Kurtz, D.B., Youngentob, S.L., and Schwob, J.E. (2004). OR expression patterns are restored in lesion-recovered rat olfactory epithelium. J. Neurosci. *24*, 356–369.

Kaluza, J.F., Gussing, F., Bohm, S., Breer, H., and Strotmann, J. Olfactory receptors in the mouse septal organ. (2004). J. Neurosci. Res. *76*, 442-452.

Kawagishi, K., Ando, M., Yokouchi, K., Sumitomo, N., Karasawa, M. Fukushima, N, and Moriizumi, T. (2014). Stereological quantification of olfactory receptor neurons in mice. Neuroscience *272*, 29–33.

Khan, M., Vaes, E., and Mombaerts, P. (2011). Regulation of the probability of mouse odorant receptor gene choice. Cell *147*, 907–921.

Klenoff, J.R., and Greer, C.A. (1998). Postnatal development of olfactory receptor cell axonal arbors. J. Comp. Neurol., *390*, 256–267.

Koshimoto, H., Katoh, K., Yoshihara, Y., Nemoto, Y., and Mori, K. (1994). Immunohistochemical demonstration of embryonic expression of an odor receptor protein and its zonal distribution in the rat olfactory epithelium. Neurosci. Lett. *169*, 73–76.

Lee, A.C., Tian, H., Grosmaitre, X., and Ma, M. (2009). Expression patterns of odorant receptors and response properties of olfactory sensory neurons in aged mice. Chem. Senses *34*, 695–703.

Lledo, P.M., Gheusi, G., and Vincent, J.D. (2005). Information processing in the mammalian olfactory system. Physiol. Rev. *85*, 281–317.

Lewcock, J.W. and Reed, R.R. (2004). A feedback mechanism regulates monoallelic odorant receptor expression. Proc. Natl. Acad. Sci. U.S.A. *101*, 1069–1074.

Low, V. F., and Mombaerts, P. (2017). Odorant receptor proteins in the mouse main olfactory epithelium and olfactory bulb. Neurosci. *344*, 167–177.

Ma, M., Grosmaitre, X., Iwema, C.L., Baker, H., Greer, C.A., and Shepherd, G.M. (2003). Olfactory signal transduction in the mouse septal organ. J. Neurosci. *23*, 317–324.

Madisen, L., Zwingman, T. A., Sunkin, S. M., Oh, S. W., Zariwala, H. A., Gu, H., … and Zeng, H. (2010). A robust and high-throughput Cre reporting and characterization system for the whole mouse brain. Nat. Neurosci. *13*, 133–140.

Malnic, B., Hirono, J., Sato, T., and Buck, L.B. (1999). Combinatorial receptor codes for odors. Cell *96*, 713–723.

Marcucci, F., Zou, D.-J. and Firestein, S. (2009), Sequential onset of presynaptic molecules during olfactory sensory neuron maturation. J. Comp. Neurol., 516: 187-198.

Marshall, D.A., and Maruniak, J.A. (1986). Masera's organ responds to odorants. Brain Research. *366*, 329-332.

Menco, B.P.M., Cunningham, A.M., Qasba, P., Levy, N., and Reed, R.R. (1997). Putative odour receptors localize in cilia of olfactory receptor cells in rat and mouse: a freeze-substitution ultrastructural study. J. Neurocytol. *26*, 297–312.

Miyamichi, K., Serizawa, S., Kimura, H.M., and Sakano, H. (2005). Continuous and overlapping expression domains of odorant receptor genes in the olfactory epithelium determine the dorsal/ventral positioning of glomeruli in the olfactory bulb. J. Neurosci. *25*, 3586–3592.

Mombaerts, P., Wang, F., Dulac, C., Chao, S.K., Nemes, A., Mendelsohn, M., Edmondson, J., and Axel, R. (1996). Visualizing an olfactory sensory map. Cell *87*, 675–686.

Mombaerts, P. (1999). Seven-transmembrane proteins as odorant and chemosensory receptors. Science *286*, 707–711.

Mombaerts, P. (2004). OR gene choice in OSNs: the one receptor–one neuron hypothesis revisited. Curr. Opin. Neurobiol. *14*, 31–36.

Mombaerts, P. (2006). Axonal wiring in the mouse olfactory system. Annu. Rev. Cell Dev. Biol. *22*, 713–73

Mori, K., Kishi, K., and Ojima, H. (1983). Distribution of dendrites of mitral, displaced mitral, tufted, and granule cells in the rabbit olfactory bulb. J. Comp. Neurol. *219*, 339–355.

Mosimann, C., Kaufman, C. K., Li, P., Pugach, E. K., Tamplin, O. J., and Zon, L. I. (2011). Ubiquitous transgene expression and Cre-based recombination driven by the ubiquitin promoter in zebrafish. Development *138*, 169–177.

Muzumdar, M. D., Tasic, B., Miyamichi, K., Li, L., and Luo, L. (2007). A global double-fluorescent Cre reporter mouse. Genesis *45*, 593–605.

Nagayama, S., Takahashi, Y. K., Yoshihara, Y., and Mori, K. (2004). Mitral and tufted cells differ in the decoding manner of odor maps in the rat olfactory bulb. J. Neurophysiol. *91*, 2532–2540.

Nagy, A. (2000). Cre recombinase: The universal reagent for genome tailoring. Genesis *26*, 99–109.

Oka, Y., Katada, S., Omura, M., Suwa, M., Yoshihara, Y., and Touhara, K. (2006). Odorant receptor map in the mouse olfactory bulb: in vivo sensitivity and specificity of receptor-defined glomeruli. Neuron *52*, 857–869.

Orona, E., Scott, J.W., and Rainer, E.C. (1983). Different granule cell populations innervate superficial and deep regions of the external plexiform layer in rat olfactory bulb. J. Comp. Neurol. *217*, 227–232.

Parrish-Aungst, S., Shipley, M.T., Erdelyi, F., Szabo, G., and Puche, A.C. (2007). Quantitative analysis of neuronal diversity in the mouse olfactory bulb. J. Comp. Neurol. *501*, 825–836.

Pinching, A.J., and Powell, T.P. (1971). The neuron types of the glomerular layer of the olfactory bulb. J. Cell. Sci. *9*, 305–345.

Potter, S.M., Zheng, C., Koos, D.S., Feinstein, P., Fraser, S.E., and Mombaerts, P., (2001). Structure and emergence of specific olfactory glomeruli in the mouse. J. Neurosci. *21*, 9713–9723.

Price, J.L., and Powell, T.P. (1970). An electron-microscopic study of the termination of the afferent fibres to the olfactory bulb from the cerebral hemisphere. J. Cell Sci. *7*, 157–87.

Ressler, K.J., Sullivan, S.L., and Buck, L.B. (1993). A zonal organization of odorant receptor gene expression in the olfactory epithelium. Cell *73*, 597–609.

Richard, M.B., Taylor, S.R., and Greer, C.A. (2010). Age-induced disruption of selective olfactory bulb synaptic circuits. Proc. Natl. Acad. Sci. U.S.A. *107*, 15613–15618.

Rodriguez-Gil, D.J., Bartel, D.L., Jaspers, A.W., Mobley, A.S., Imamura, F., and Greer, C.A. (2015). Odorant receptors regulate the final glomerular coalescence of olfactory sensory neuron axons. Proc. Natl. Acad. Sci. U.S.A. *112*, 5821–5826.

Royal, S.J., and Key, B. (1999). Development of P2 olfactory glomeruli in P2 internal ribosome entry site taulacZ transgenic mice. J. Neurosci. *19*, 9856–9864.

Ruiz Tejada Segura, M.L., Abou Moussa, E., Garabello, E., Nakahara, T.S., Makhlouf, M., Mathew, L.S., … and Saraiva, L.R. (2022). A 3D transcriptomics atlas of the mouse nose sheds light on the anatomical logic of smell. Cell Reports *38*, 110547.

Saraiva, L.R., Ibarra-Soria, X., Khan, M., Omura, M., Scialdone, A., Mombaerts, P., … and Logan, D.W. (2015). Hierarchical deconstruction of mouse OSNs: from whole mucosa to single-cell RNA-seq. Sci. Rep. *5*, 18178.

Serizawa, S., Ishii, T., Matsuda, Y., Nagawa, F., and Sakano, H. (1999). Olfactory neurons expressing closely linked and homologous odorant receptor genes tend to project their axons to neighboring glomeruli on the olfactory bulb. J. Neurosci. *19*, 8409–8418.

Serizawa, S., Ishii, T., Nakatani, H., Tsuboi, A., Nagawa, F., Asano, M., … and Sakano, H. (2000). Mutually exclusive expression of odorant receptor transgenes. Nat. Neurosci. *3*, 687–693.

Serizawa, S., Miyamichi, K., Nakatani, H., Suzuki, M., Saito, M., Yoshihara, Y., & Sakano, H. (2003). Negative feedback regulation ensures the one receptor-one olfactory neuron rule in mouse. Science *302*, 2088–2094.

Shepherd, G.M. (2004) The human sense of smell: Are we better than we think? PLoS Biol 2(5): e146.

Shi, S.R., Cote, R.J., and Taylor, C.R. (2001). Antigen retrieval techniques: current perspectives. J. Histochem. Cytochem. *49*, 931–937.

Shykind, B.M., Rohani, S.C., O'Donnell, S., Nemes, A., Mendelsohn, M., Sun, Y., Axel, R., and Barnea, G. (2004). Gene switching and the stability of odorant receptor gene choice. Cell *117*, 801–815.

Soucy, E.R., Albeanu, D.F., Fantana, A.L., Murthy, V.N., and Meister, M. (2009). Precision and diversity in an odor map on the olfactory bulb. Nat. Neurosci. *12*, 210–220.

Strotmann, J., Wanner, I., Krieger, J., Raming, K., and Breer, H. (1992). Expression of odorant receptors in spatially restricted subsets of chemosensory neurones. *Neuroreport 3*, 1053–1056.

Strotmann, J., Wanner, I., Helfrich, T., Beck, A., Meinken, C., Kubick, S., and Breer, H. (1994). Olfactory neurones expressing distinct odorant receptor subtypes are spatially segregated in the nasal neuroepithelium. Cell Tissue Res. *276*, 429-438.

Strotmann, J., Conzelmann, S., Beck, A., Feinstein, P., Breer, H., and Mombaerts, P., (2000). Local permutations in the glomerular array of the mouse olfactory bulb. J. Neurosci. *20*, 6927–6938.

Strotmann, J., Levai, O., Fleischer, J., Schwarzenbacher, K., and Breer, H. (2004). Olfactory receptor proteins in axonal processes of chemosensory neurons. J. Neurosci. *24*, 7754–7761.

Sullivan, S.L., Adamson, M.C., Ressler, K.J., Kozak, C.A., and Buck, L.B. (1996). The chromosomal distribution of mouse odorant receptor genes. Proc. Natl. Acad. Sci. USA *93*, 884–888.

Takahashi, H., Yoshihara, S., Nishizumi, H., & Tsuboi, A. (2010). Neuropilin-2 is required for the proper targeting of ventral glomeruli in the mouse olfactory bulb. Mol. Cell. Neurosci, *44*, 233–245.

Tian, H., and Ma, M. (2004). Molecular organization of the olfactory septal organ. J. Neurosci. *24,* 8383–8390.

Tian, H. and Ma, M. (2008). Differential development of odorant receptor expression patterns in the olfactory epithelium: A quantitative analysis in the mouse septal organ. Dev. Neurobio. 68, 476-486.

Thyssen, A., Hirnet, D., Wolburg, H., Schmalzing, G., Deitmer, J. W., & Lohr, C. (2010). Ectopic vesicular neurotransmitter release along sensory axons mediates neurovascular coupling via glial calcium signaling. Proc. Natl. Acad. Sci. *107*, 15258–15263.

Treloar, H.B., Feinstein, P., Mombaerts, P., and Greer, C.A. (2002). Specificity of glomerular targeting by olfactory sensory axons. J. Neurosci. *22*, 2469–2477.

Tsuboi, A., Yoshihara, S., Yamazaki, N., Kasai, H., Asai-Tsuboi, H., Komatsu, M., … Sakano, H. (1999). Olfactory Neurons Expressing Closely Linked and Homologous Odorant Receptor Genes Tend to Project Their Axons to Neighboring Glomeruli on the Olfactory Bulb. J. Neurosci*. 19*, 8409 LP – 8418.

Vassalli, A., Rothman, A., Feinstein, P., Zapotocky, M., and Mombaerts, P. (2002). Minigenes impart odorant receptor-specific axon guidance in the olfactory bulb. Neuron *35*, 681–696.

Vassalli, A., Feinstein, P., Mombaerts, P. (2011). Homeodomain binding motifs modulate the probability of odorant receptor gene choice in transgenic mice. Mol. Cell. Neurosci, *46*, 381–396.

Vassar, R., Ngai, J., and Axel, R. (1993). Spatial segregation of odorant expression in the mammalian olfactory epithelium. Cell *74*, 309–318.

Wang, F., Nemes, A., Mendelsohn, M., and Axel, R. (1998). Odorant receptors govern the formation of a precise topographic map. Cell *93*, 47–60.

Wilson, R.I., and Mainen, Z.F. (2006). Early events in olfactory processing. Annu. Rev. Neurosc. *29*, 163–201.

Yoshihara, Y., Kawasaki, M., Tamada, A., Fujita, H., Hayashi, H., Kagamiyama, H., and Mori, K. (1997). OCAM: a new member of the neural cell adhesión molecule family related to zone-to-zone projection of olfactory and vomeronasal axons. J. Neurosci. *17*, 5830–5842.

Young, J.M., Shykind, B.M., Lane, R.P., Tonnes-Priddy, L., Ross, J.A., Walker, M., Williams, E.M., and Trask, B.J. (2003). Odorant receptor expressed sequence tags demonstrate olfactory expression of over 400 genes, extensive alternate splicing and unequal expression levels. Genome Biol. *4*, R71.

Zapiec, B., and Mombaerts, P. (2015). Multiplex assessment of the positions of OR-specific glomeruli in the mouse olfactory bulb by serial two-photon tomography. Proc. Natl. Acad. Sci. USA *112*, E5873–E5882.

Zapiec, B., and Mombaerts, P. (2020). The zonal organization of odorant receptor gene choice in the main olfactory epithelium of the mouse. Cell Reports *30*, 4220-4234.e5.

Zhang, X., and Firestein, S. (2002). The olfactory receptor gene superfamily of the mouse. Nat. Neurosci. *5*, 124–133.

Zheng, C., Feinstein, P., Bozza, T., Rodriguez, I., and Mombaerts, P. (2000). Pheripheral olfactory projections are differentially affected in mice deficient in a cyclic nucleotide-gated channel subunit. Neuron, *26*, 81–91.